Removal and Immobilization of Arsenic in Water, Ion Exchange Brine, and Soil Using a New Class of Ion Exchangers and Nanoparticles

by

Byungryul An

A dissertation submitted to the Graduate Faculty of
Auburn University
in partial fulfillment of the
requirements for the Degree of
Doctor of Philosophy

Auburn, Alabama
December 13, 2010

Keywords: Arsenic, ion exchange, magnetite,
nanoparticles, oxidation, immobilization

Approved by

Dongye Zhao, Chair, Associate Professor of Civil Engineering
T. Prabhakar Clement, Professor of Civil Engineering
Mark O. Barnett, Professor of Civil Engineering
Ahjeong Son, Assistant Professor of Civil Engineering
John P. Blake, Professor of Poultry Science

Abstract

Removal of arsenic, As(III) and As(V), in water and soils is one of the most challenging environmental issues. Six polymeric ligand exchangers (PLEs) were synthesized by functionalizing various polymeric matrices (known as XAD resins) with 2-picolylamine or di(2-picolyl) amine functional groups and by immobilizing Cu(II) ions onto the functional groups. The six PLEs were extensively tested for arsenate removal from a simulated groundwater water. The PLE's displayed greater affinity toward arsenate than for sulfate. The binary arsenate-sulfate separation factor ($\alpha_{As/S}$) ranged from 5.1 to 10. Bench-scale column breakthrough tests confirmed the greater selectivity for arsenate over other common anions (sulfate, bicarbonate, and chloride). A new class of starch-bridged magnetite nanoparticles was prepared for removal of arsenate from spent ion exchange brine. A low-cost, "green" starch was used as a stabilizer to prevent the nanoparticles from agglomerating and as a bridging agent allowing the nanoparticles to flocculate and precipitate while maintaining their high arsenic sorption capacity. The starch (0.049 wt.%)-bridged Fe_3O_4 nanoparticles had a mean diameter of 26.6 ± 4.8. The starch-bridged nanoparticles removed 5 times more arsenic than bare magnetite particles under otherwise identical conditions, yet the bridged nanoparticles can be easily separated from water by gravity. The optimum pH range was determined to be from 5 to 6. Based on FTIR results showing one single band for arsenate adsorption, inner-sphere complexation is the predominant mechanism.

Stabilized Fe-Mn nanoparticles were prepared using carboxymethyl cellulose (CMC) as a stabilizer and were tested to remove both As(III) and As(V) from contaminated water and soil.

The presence of $MnO_{2(s)}$ was able to enhance the sorption capacity of As(III). High sorption capacity was observed in the pH range from 6 to 7 for As(III) and less than 3 for As(V). Stabilized Fe-Mn nanoparticles can be delivered in a sandy soil. Batch tests showed that when an As-laden sandy soil was treated with CMC-stabilized Fe-Mn at an Fe-to-As molar ratio of 6.5 the leached arsenic concentration was reduced by 91%. FTIR results indicated a shift from 3444 to 3400 cm^{-1} can be attributed to the increased strength of intermolecular hydrogen bonds between the stabilizers and surface of the Fe-Mn particles. The toxicity characteristic leaching procedure (TCLP) leaching tests performed on the nanoparticle amended soil indicated that the leachability of arsenic was reduced by 94 and 90% for samples treated with CMC and starch-stabilized Fe-Mn, respectively.

Acknowledgements

First of all, I would like to acknowledge my dissertation advisor Dr. Dongye Zhao for all the support, patience, and encouragement. He taught me what I am doing now on my research and gave me complete academic freedom to explore on my own and at the same time offered watchful guidance whenever required. These tremendous efforts let me to pursue a PhD. I gratefully acknowledge all the members of my committee, Dr. T. Prabhakar Clement, Dr. Mark O. Barnett, Dr. Ahjeong Son, and Dr. John P. Blake, and dissertation outside reader Dr. Yucheng Feng, who have given their time to read this dissertation, and who have also offered valuable advice and provided instrumentation helps during my graduate study at Auburn. I appreciate Jinling Zhuang, lab instructor, for teaching and assisting during experiment. I also thank my former and current lab mates, Dr. Fu, Dr. Joo, Dr. Xu, Dr. Liu, Mr. Steinwinder, Dr. Yi, Dr. He, Dr. Xiong, as well as other members of AU environmental engineering program. I want to memorialize my friend, Jungwoo Oh who left us in 2009 and I am missing you. I also thank my two friends, Boha Kim and Changsoo Park.

Finally, I really appreciate my mother and father who devoted their life to me, and my mother and father-in-law, Boksun Park and Bokho Son who carefully and lovely brought up my wife. Bukyong Son, my wife, has given everything up to support me. Every day, I can feel I am very happy because of her infinite love for me. I thank and love Bukyung Son.

Table of Contents

List of Tables

List of Figures

Chapter 1. General Introduction

1.1 Arsenic contaminant

Arsenic is a metallic element that occurs naturally in the earth's surface at 1.5 to 2 ppm, mostly in inorganic form (National Academy of Sciences, 1977). It generally exists in low concentrations in many rock types but is frequently associated with metal ore deposits (Au, Ag, Cu, and Fe). In the United State the largest occurrence of arsenic is near Au mines in northern Nevada (Bowell and Parshley, 2001). It can be further released into the environment through natural activities such as volcanic action, erosion of rocks and forest fires. Another source into the environment is through human actions. Approximately 90 percent of industrial arsenic in the U.S. is currently used as a wood preservative, but arsenic is also used in paints, dyes, metals, drugs, soaps and semi-conductors. High arsenic levels can also come from certain fertilizers and animal feeding operations. Industry practices such as copper smelting, mining and coal burning also contribute to arsenic in our environment. Typical concentration of arsenic in natural waters is; rain water (0.02-16 μg/L), river water (<0.02-21,800 μg/L), lake water (<0.2-1,000 μg/L), estuarine water (0.7-16 μg/L), seawater (0.7-3.7μg/L), groundwater (<0.5-50,000 μg/L), industrial waters, such as mine drainage (<1-850,000 μg/L), oilfield and related brine (230-243,000 μg/L), (Marquez et al. 2005; Smedley and Kinniburgh, 2002).

The presence of arsenic (As) in U.S. waters is widespread. It was estimated that ~16.4% of groundwater sources exceeded 5 μg/L in various regions of the country (Chwirka at al., 2000). The US EPA estimates that approximately 2% of the U.S. population receives drinking water

containing > 10 μg/L As (Holm, 2002), and the Natural Resources Defense Council estimates that ~56 million people in the U.S. drinking water with As at unsafe levels. Arsenic has been associated with various cancerous and non-cancerous health effects. According to a recent report by the National Academy of Science (NAS) and National Research Council (NRC), even at 3 μg/L of As, the risk of bladder and lung cancer is between 4 and 7 deaths per 10,000 people. At 10 μg/L, the risk increases to between 12 and 23 deaths per 10,000 people. In addition, As can cause high blood pressure and diabetes. Triggered by the risk concern, the U.S. EPA announced its ruling in October 2001 to lower the Maximum Contaminate Level (MCL) from current 50 μg/L (established in 1942) to 10 μg/L with a compliance date of January 22, 2006. This ruling poses tremendous impacts on water utilities. Approximately 4,100 water utilities serving ~13 million people are affected by the law (Gilles and Mathis, 2002). The compliance cost has been estimated to be ~$600 million per year using current treatment technologies (Frey et al., 2000). For instance, almost half of the wells in Albuquerque, NM, will require additional treatment to meet the new standard (German, 2001). In the State of Maine, 12% of community water systems will need additional treatment.

1.2 Arsenic chemistry

Arsenic is a semimetal and occurs in natural groundwater mostly occurring as oxyanions as trivalent arsenic or pentavalent arsenic. The occurrence of organic arsenic compounds, especially methylated species is only reported from surface water (Anderson and Bruland, 1991) but they rarely, if ever occur in ground water. Arsenic chemistry in the aquatic environment is quite complicated because inorganic arsenic can be formed and stable in four oxidation states: +5, +3, 0, and -3 under different redox conditions. However, two forms are common in natural water. At

the high Eh value encountered in oxygenated waters, arsenic acid species (H_3AsO_4, $H_2AsO_4^-$, $HAsO_4^{2-}$, and AsO_4^{3-}) referred to arsenic(V) or pentavalent are stable whereas under mild reducing conditions arsenous acid species (H_3AsO_3, $H_2AsO_3^-$, $HAsO_3^{2-}$, and AsO_3^{3-}) become stable in Fig.1-1 (Ferguson and Gavis, 1972). The equilibrium for both As(V) and As(III) is given below equations along with their respective acid disassociation constants (O'Neill, 1990).

Arsenate, As(V)

$$H_3AsO_4 + H_2O \leftrightarrow H_2AsO_4^- + H_3O^+ \qquad pK_a=2.20 \qquad (1\text{-}1)$$

$$H_2AsO_4^- + H_2O \leftrightarrow HAsO_4^{2-} + H_3O^+ \qquad pK_a=6.97 \qquad (1\text{-}2)$$

$$HAsO_4^{2-} + H_2O \leftrightarrow AsO_4^{3-} + H_3O^+ \qquad pK_a=11.53 \qquad (1\text{-}3)$$

Arsenite, As(III)

$$H_3AsO_3 + H_2O \leftrightarrow H_2AsO_3^- + H_3O^+ \qquad pK_a=9.22 \qquad (1\text{-}4)$$

$$H_2AsO_3^- + H_2O \leftrightarrow HAsO_3^{2-} + H_3O^+ \qquad pK_a=12.13 \qquad (1\text{-}5)$$

$$HAsO_3^{2-} + H_2O \leftrightarrow AsO_3^{3-} + H_3O^+ \qquad pK_a=13.4 \qquad (1\text{-}6)$$

Fig. 1-2 is As(V) and As(III) species as a function of pH. As shown in Fig. 1-2 in the typical pH range (6-8) of natural waters, the most thermodynamically stable compounds of As(V) are present as $H_2AsO_4^-$ and $HAsO_4^{2-}$ and As(III) is found mostly as the uncharged species, H_3AsO_3 while AsO_4^{3-} and $H_2AsO_3^-$ is the dominate ionic form in alkalinity pH.

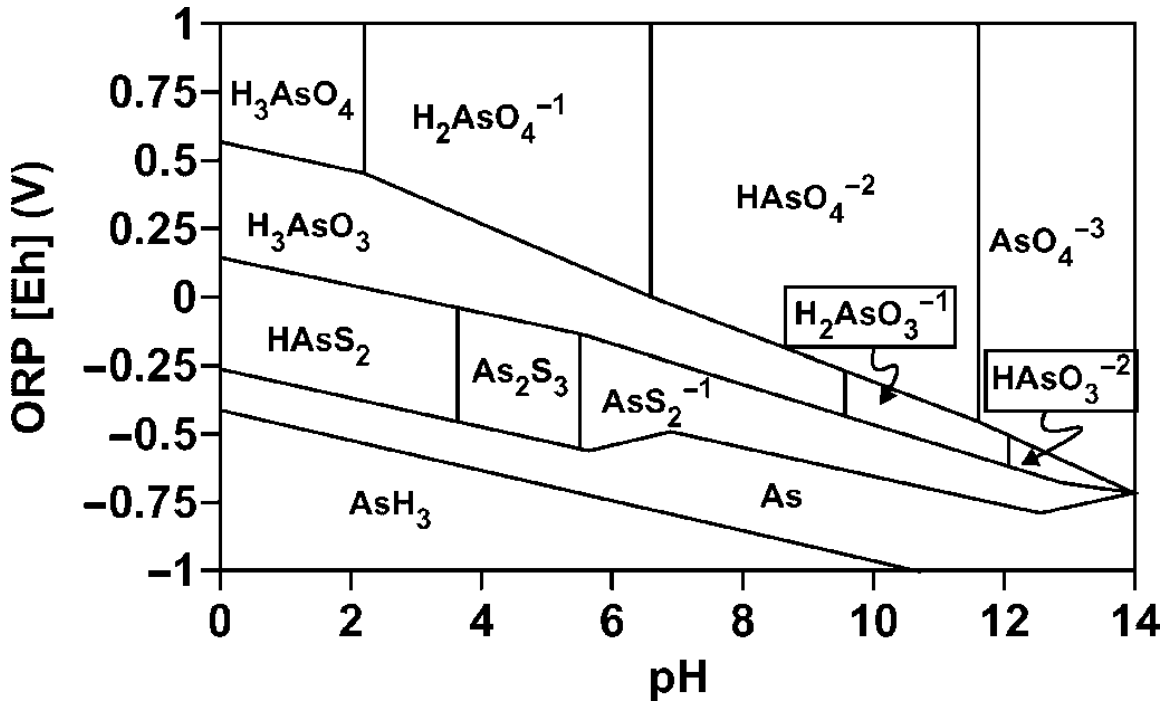

Fig. 1-1. The Eh–pH diagram for arsenic at 25 ℃ and 1 atmosphere with total arsenic 10^{-5} mol/L and total sulfur 10^{-3} mol /L. (Ferguson and Gavis, 1972).

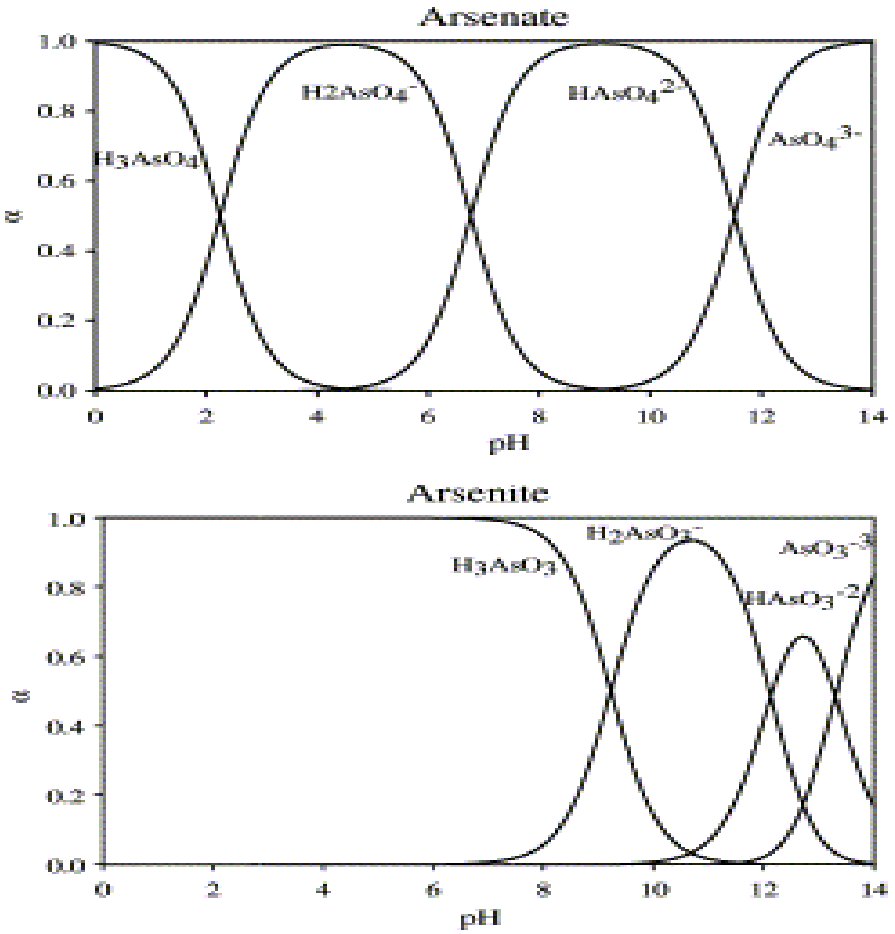

Fig. 1-2. Arsenate, As(V) and Arsenite, As(III) species as a function of pH. (Ghimire et al., 2003).

1.3 Arsenic treatment technologies

Several treatment technologies have been examined to remove arsenic from drinking water under both laboratory and field conditions. Promising technologies which are currently applied are shown below (USEPA, 2000a):

(I) Technologies based on adsorption reactions:

- Coagulation with iron or alum coagulants
- Adsorption on activated alumina
- Adsorption on iron oxide based adsorbants

(II) Other technologies:

- Ion exchange
- Membrane processes, i.e. reverse osmosis and nanofiltration

Coagulation, followed by precipitation and filtration is a widely used treatment, not only for As, but especially for the removal of colloidal substances. The insoluble oxides produced by the hydrolysis by adding alum, ferric chloride, or ferric sulfate rely on the dosing of alum or iron salts to form precipitates of iron hydroxide which takes up arsenate by adsorption. Coagulation and precipitation for arsenic removal from water depend upon the co-precipitation of both water insoluble arsenates and iron or aluminum oxides. Ferric salts can be used over a wider pH range, whereas the use of alum is limited at neutral pH.

Ion exchange can be used in small-scale systems because of ease of handing and sludge free operation. Strong base anion exchange can effectively remove arsenic. However, high treatment cost in large-scale systems is required and less selectivity for arsenic reduce the arsenic capacity than sulfate and other anions. Current commercial SBA resins suffer from poor selectivity for arsenic. Due to the strong competition from some ubiquitous anions such as

sulfate, the arsenic capacity of SBA resins is prohibitively retarded (Clifford, 1999). For example, the binary arsenate/sulfate separation factor for a typical SBA resin is 0.1~0.5 (a separation factor of less than 1 indicates the resin's preference toward the competing ions). As a result, the As breakthrough occurs before sulfate, and chromatographic peaking of As, i.e. effluent concentration exceeds influent concentration, is often observed (Kim et al., 2003a). IX does not show removal of As(III) in natural pH range because As(III) exists as a form of H_3AsO_3 (no charge) in less than pH 9.

In order to purify brackish water or seawater for use as drinking water, membrane methods have been developed and primarily applied, which are not selective to arsenic and other toxic contaminants. This process can remove arsenic through filtration, electric repulsion, and adsorption of arsenic-bearing compounds. The capacity for arsenic removal is highly dependent on the size distribution of arsenic-bearing particles in the source water.

Activated alumina does not produce backwash sludge but needs regeneration due to the restricted lifetime of the media until exhaustion. The treatment pH for arsenic removal is optimized around 6.

Adsorption using iron oxides such as oxyhydroxides and hydroxides, including amorphous hydrous ferric oxide (FeOOH), goethite (α-FeOOH) and hematite (α-Fe_2O_3), were introduced and they are promising adsorbents for removing both As(III) and As(V) from water (Wilkie, 1996). Such iron oxides have been studied in column or batch experiments for potential use in drinking water treatment. There are other studies using other kinds of iron oxides including granular ferric hydroxide (GFH) (Badruzzaman et al., 2004), activated carbon-based iron oxide-containing sorbents (Gu et al., 2005), iron oxide-coated sand (Benjamin et al., 1996), and nanostructured hydrous iron oxide-coated polymeric beads (Sylvester et al., 2007). The

significantly improved adsorption capacity for arsenic removal in water treatment is due to the higher surface area and affinity for arsenic.

1.4 Objectives

The overall goal of this research is to develop a new technology for the removal of arsenic and optimize arsenic removal using water treatment. The specific objectives are to:

1) Develop a new class of chelating resins using commercially available polystyrene/divinylbenzene (PS-DVB) copolymers and acrylic copolymers and then prepare a new polymeric ligand exchanger (PLE).

- Determine the arsenate sorption capacity and breakthrough behavior
- Test regeneration using 6% NaCl

(2) Prepare starch-bridged magnetite (Fe_3O_4) for the removal of arsenic from spent brine solution.

- prepare and characterize the starch-bridged magnetite particles
- determine arsenic sorption and desorption performances of the bridged nanoparticles
- elucidate arsenic binding mechanisms in terms of particle surface chemistry and binding modes

(3) Develop stabilized Fe-Mn oxide nanoparticles using carboxymethyl cellulose (CMC) and starch for the feasibility of such as *in-situ* remediation process for immobilization of As(III) and As(V) in contaminated soils using a new class of stabilized Fe-Mn oxide nanoparticles

- prepare and characterize a new class of stabilized Fe-Mn nanoparticles
- determine the effectiveness of the stabilized nanoparticels for As(III) and As(V) removal from water

- examine mobility of the stabilized Fe-Mn nanoparticles in a model soil, and test effectiveness of the stabilized Fe-Mn nanoparticles for immobilizing As(III) in a contaminated soil

Chapter 2. Synthesis and Characterization of a New Class of Polymeric Ligand Exchagners for Selective Removal of Arsenate from Drinking Water

This chapter studies removal of arsenate, As(V), from drinking water using six new chelating resins which are prepared by functionalizing three commercially available XAD resins of various matrix properties, including XAD1180, XAD16 and XAD7HP. To evaluate capacity of arsenate uptake and compare the behavior of each prepared polymeric ligand exchangers (PLEs), isotherm test, kinetic test, and column test are conducted.

2.1 Introduction

Arsenic (*As*) in drinking water has been known to cause serious cancerous and non-cancerous heath effects and high blood pressure and diabetes. For example, even at an *As* levels of 5 μg/L, the lifetime risk of lung and bladder cancer is 6 deaths per 10,000 people (NRC, 2001). Both anthropogenic activities and natural erosion can lead to arsenic contamination of drinking water (Berg et al., 2001; Chatterjee et al., 1995; Nriagu, 1994). According to a British Geological Survey study in 1998, in 61 of the 64 districts in Bangladesh, 46% of the samples were above 0.01 mg/L and 27% were above 0.05 mg/L (BGS, 2000). In the western United States, it is estimated by the US EPA in 2001 (EPA, 2001) that some 13 million of the population are exposed to arsenic in drinking water at 0.01 mg/L or higher. To mitigate the human ingestion of arsenic, the Safe Drinking Water Act in 1996 required EPA to issue a new drinking water stand for arsenic. Later, as more detailed risk data associated with arsenic became available, EPA

ruled in October 2001 to lower the previous maximum contaminant level (MCL) of *As* from 50 µg/L to 10 µg/L effective January 22, 2006. The revised MCL is affecting more than four thousands of water utilities in the U.S.

Although this 10 µg/L MCL had been recommended by the World Health Organization (WHO) and adopted by the European Union for years (Badruzzaman, 2004), water utilities have been challenged by the tremendous treatment cost with current technologies for arsenic removal. It was estimated that the compliance cost can be more than $600 million per year using current treatment technologies (Frey, 2000).

The following technologies have been well studied for arsenic removal: Ion exchange (IX), Activated alumina (AA), Reverse osmosis (RO), Modified coagulation/filtration, Modified lime softening, Electrodialysis, and Oxidation/Filtration (US EPA, 2000b). Although the treatment cost of Modified Conventional Treatment (MCT) is less than that of RO (Chen, et al., 1999), it is extremely difficult to meet the new MCL. Consequently, additional treatment such as microfiltration is often required (Ghurye et al., 2004). Among these methods, IX is considered by EPA as one of the best available technologies (BAT) because of its ability to remove arsenic, simple operation, and the long lifetime of the resin (EPA, 2000a). However, conventional standard IX resins are not selective toward arsenic. For example, the following selectivity sequence has been observed for strong base anion (SBA) exchangers (EPA, 2000a):

$$SO4^{2-} > HAsO4^{2-} > Cl^- > (H2PO4^-, H2AsO4^-, HCO3^-) > OH^- \quad (2\text{-}1)$$

For instance, the binary arsenate/sulfate separation factor for two commonly used SBA resins (IRA 900 and IRA 958) has been reported to be 0.20 and 0.10, respectively, (An et al., 2005) indicating the resins' strong preference for sulfate over arsenate. As a result, the presence of high concentrations of sulfate can dramatically inhibit the uptake of arsenate and can also induce

significant chromatographic peaking of arsenate. Moreover, the lack of arsenate selectivity leads to frequent regeneration, which not only consumes large volumes of regenerant brine, but also produces large volumes of process waste residuals.

The concept of ligand exchange chromatography was first introduced by Helfferich (Helfferich, 1962). Later, Chanda et al. (1988) reported a new Polymeric Ligand Exchanger (PLE) prepared by loading ferric ions onto a chelating resin for selective removal of arsenic. Later, Ramana and SenGupta (1992) prepared a PLE by loading Cu^{2+} onto a weak base chelating resin with 2 picolylamine groups per functional group (Ramana and SenGupta, 1992). To increase copper loading, Zhao and SenGupta developed and characterized another PLE, referred to as DOW 3N-Cu, prepared by loading Cu^{2+} ions onto a chelating resin with 3-picolylamine groups per functional group to remove phosphate (Ramana and SenGupta, 1992; Zhao, 1997). They reported that DOW 3N-Cu can remove phosphate highly selectively. An et al. (2005) further tested Dow 3N-Cu for arsenic removal in the presence of strong competing anions such as sulfate. Fig. 2-1 shows a schematic illustration of the binding mechanisms of arsenate onto such a PLE.

As these PLE's have demonstrated tremendous promise for selective arsenic removal, there have been very limited choices in selecting the appropriate parent chelating resins for preparing PLE's. In fact, little is known pertaining to the effect of the matrix type, structure, and porosity of the metal-hosting resins on the performance of the resultant PLE's.

The overall goal of this study was to explore new ways and to synthesize new chelating resin templates for preparing various types of PLE's geared toward selective arsenate removal. The specific objectives were to: 1) develop a new class of chelating resins using commercially available polystyrene/divinylbenzene (DVB) copolymers and acrylic copolymers, and then

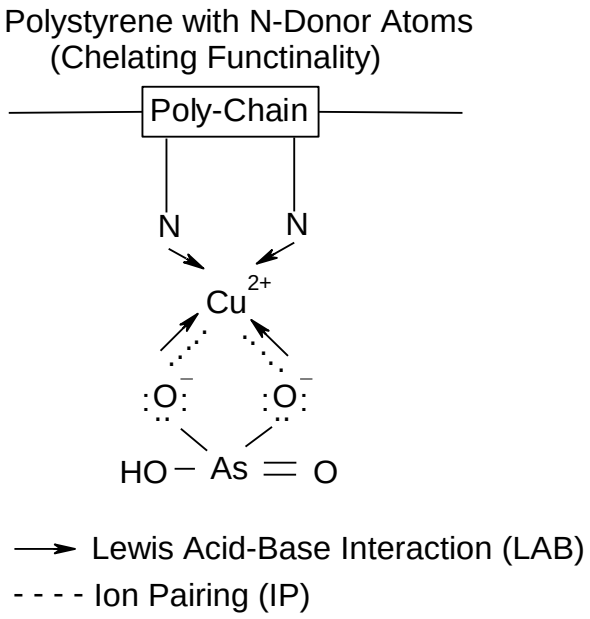

Fig. 2-1. Schematic illustration of functionality of a PLE and binding mechanisms of arsenic onto an XAD-based PLE.

prepare a class of new PLE's based thereon; 2) determine the arsenate sorption equilibrium and kinetics for each of the new PLE's; 3) test arsenate breakthrough behaviors with the PLE's in multi-component systems; and 4) test the regenerability of the arsenate-exhausted PLE's.

2.2 Materials and Methods

2.2.1 Materials

All resins, solvents, and other chemicals are from Sigma Aldrich (Milwaukee, WI, USA), including Amberlite® XAD16, XAD1180, XAD7HP, choromethyl methyl ether, $FeCl_3$, $SnCl_4$, dimethoxy methane, thionyl chloride, acetone, toluene, methylene chloride, ethanol, methanol, di(2-picolyl)amine, 2,2'-dipyridylamine, 1-(2-pyridyl)piperazine, 1-(2-pyrimidyl)piperazine dihydrogenchloride, 2,4-diamino-6-methyl-1,3,5-triazine, and guanidine hydrochloride. Poly(4-vinylpyridine) (crosslinked, methyl chloride quaternary salt) was also purchased from Sigma Aldrich for a test of copper chelating ability.

Before functionalizing, the XAD resins were cleaned and dried according to the following procedure: the resin was first dispersed in DI water and 0.1N HCl was added to adjust the pH of the water to about 4. The resin slurry was stirred and then washed three more times with plenty amounts of DI water. Finally the resin was washed with methanol and air dried first, followed by oven-dry at 70°C until the weight no longer changed.

2.2.2 Synthesis of parent chelating resins

To explore effects of matrix properties on the behaviors of the resultant PLE's, six new chelating resins were prepared based on three non-functionalized macroporous polymeric sorbents, designated as XAD1180, XAD16, and XAD7HP. Table 2-1 shows the properties of these

polymeric matrices. XAD1180 and XAD16 are composed of polystyrene (PS) copolymers crosslinked with DVB, while XAD7HP is composed of poly(methyl methacrylate) also known as polyacrylic polymer, which is characterized of being much more hydrophilic than the PS/DVB matrix. In general, these polymer matrices provide large surface areas, well-controlled particle size and porosity, and narrow pore size distribution. These characteristics will be beneficial for fast ion exchange kinetics and high selectivity of the resultant functionalized resins. Furthermore, starting with commercialized materials will guarantee a reliable source for potential large-scale production of the chelating resins. Functionalization of the PS-DVB copolymers (XAD16 and XAD1180) involved two steps of reactions: chloromethylation of available aromatic rings in the copolymer, and then, immobilization of nitrogen-containing functional (chelating) groups by the reaction between the chloromethyl groups on the polymer and amine groups of selected ligand compounds.

Chloromethylation of XAD16 and XAD1180 was carried out by two different methods. In Method (a) (Prepper et al., 1953), the polymer beads were soaked in chloromethyl methyl ether (5 ml per gram of resin) at room temperature for 30 minutes. Anhydrous $SnCl_4$ (0.2 ml per gram of resin) was then added while stirring. The reaction flask was then set in an oil bath with temperature set in the range of 35 to 55 ℃. The reaction mixture was stirred for 1 to 5 hours. At the end of the reaction, the mixture was quenched by dropwise addition of methanol under stirring until the mixture was cooled down, the liquid was then separated from the resin, and the resin was washed with acetone, DI water, and methanol sequentially. In Method (b) (Grinstead and Nasutavicus, 1977), instead of using chloromethyl methyl ether directly, a mixture of thionyl chloride and dimethoxymethane (5:6 v/v) was used as the reagents for *in-situ* generation of chloromethyl methyl ether, and anhydrous $SnCl_4$ was used as a catalyst. The reagent mixture and

Table 2-1. Salient properties of various ion exchange resins used in this study.

Sorbent	XAD1180	XAD16	XAD7HP
Manufacturer	Rohm and Haas, Philadelphia, PA	Rohm and Haas, Philadelphia, PA	Rohm and Haas, Philadelphia, PA
Matrix	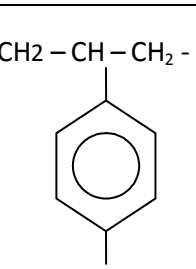 Polystyrene, Macroporous	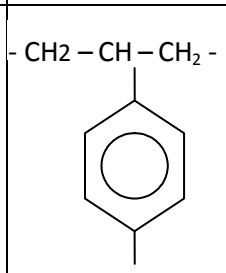 Polystyrene, Macroporous	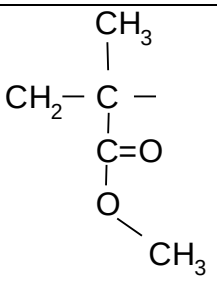 Polyacrylic, Macroporous
Functional Group: 2N	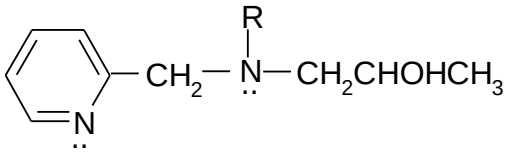		
Functional Group: 3N	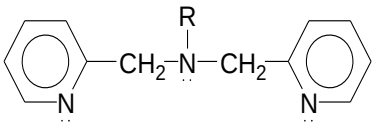		
Particle Size(mm)	0.35-0.60	0.56-0.71	0.56-0.71
Surface Area(m2/g)	≥500	≥800	≥380
Porosity(ml/ml)	0.60	0.55	0.50
Medium Pore Size(mm)/Distribution	45/narrow		35/narrow

catalyst amounts were kept at 8 ml and 0.2 ml per gram of resin, respectively. The resin was first soaked with reagent mixture for 20 minutes, and then $SnCl_4$ was added dropwise while the resin and reagent mixture was under stirring and cooling, keeping the reaction temperature below 40 ℃. When all the catalyst was added, the reaction vessel was set into a 35 ℃ or 40 ℃ oil bath; the reaction mixture was then stirred for a predetermined period of time (0.5 to 5 hours). After the reaction, the mixture was quenched by dropwise addition of methanol under stirring until the mixture was cooled down, the liquid was then separated from the resin, and the resin was washed with acetone, DI water, and methanol, sequentially. In both methods, the chloromethylated resin was air-dried and then oven-dried at 70 ℃. The resin weight was compared to the pre-reaction weight, with the weight gain indicating the degree of chloromethylation. Based on the results of chloromethylation and the subsequent ligand functionalization, both methods showed quite similar effectiveness. However, Method (b) avoids direct use of chloromethyl methyl ether, which is a known potent carcinogen, and thus, is considered "greener". Consequently, Method (b) was employed as the main method of chloromethylation in this study. Immobilization of the ligand functional groups on the chloromethylated XAD resins was carried out by reacting the chloromethylated polymer beads with 2-picolylamine or di(2-picolyl)amine. The aminations were carried out using a mixture of toluene and dimethylformamide (DMF) (2:1 v/v) as solvent. The molar ratio of the ligand compound and chloromethyl groups was kept at 2:1. The resin, ligand compounds, and solvents were mixed in a dry Erlenmeyer flask connected with a condenser, and all the reactions were carried out in 95 ℃ oil bath for 24 hours under gentle stirring. The functionalized resins were thoroughly washed with acetone and methanol, rinsed with DI water, and then air-dried for testing.

Functionalization of the acrylic copolymer (XAD7HP) was carried out through the aminolysis of the ester groups in the polymer backbone by the amine group of the 2-picolylamine or di(2-picolyl)amine, which resulted in two chelating resins, designated as XAD7HP-2N and XAD7HP-3N, respectively. The reactions were carried out using dimethyl sulfoxide (DMSO) as solvent. The ligand and polymer ratio was set at 1:1 (w/w), and 5 ml of DMSO was used per gram of polymer. The resin, ligand compounds, and solvent were loaded in a dry Erlenmeyer flask and purged with nitrogen; the reaction mixture was then heated in an oil bath under stirring and nitrogen purging; the bath temperature was gradually raised from room temperature to 170 ℃ during the first hour of the reaction; then the reaction was kept at 170 ℃ for 4 hours. The reactor was then cooled down, and the resin was washed with plenty amounts of DI water, and then with 0.1N HCl aqueous solution ten times and finally washed with DI water.

2.2.3 Copper loading and copper sorption capacity measurement

As mentioned before, the PLE's in this work use immobilized Cu(II) ions as the center ions (functional groups) that can bind with target ligands such as arsenate in the solution phase. To complete the preparation of the PLE's, the functionalized chelating resins were loaded with Cu(II) by mixing each of the resin with 0.1% (w/w) copper solution prepared by $CuCl_2$ at pH 3.5-4.0 for two weeks.

To measure the maximum copper loading capacity for each of the new chelating resins, ~0.12 gram of a copper-loaded resin was mixed with 15 mL of ammonium hydroxide solution (4 wt. % of NH_3), and the mixture was shaken for one day to completely strip off the loaded copper from the resin. The desorbed copper in the solution was then measured using UV-Vis spectrometer (Hewlett Packer UN-Vis 8453) at a wavelength of 630 nm, and then copper uptake was calculated through mass balance calculations.

2.2.4 Isotherm tests

Sorption isotherm tests were carried out for the six PLE resins to test their sorption capacity for *As*(V) (q_e) in the presence of the competing anion sulfate. A solution with an initial concentration of 10 mg/L as *As* and 100 mg/L as SO_4^{2-} was prepared with DI water. Isotherm tests were then initiated by mixing 50 mL of the solution with known amounts (ranging from 0.004g to 0.15g) of each of the six PLE resins in 60 mL glass vials. The mixtures were then equilibrated for 7 days under shaking with a rotating tumbler. Separate kinetic tests indicated that the equilibration time was sufficient to ensure equilibrium. The initial pH of the solution was set at ~7.5, which was kept at 7.0 to 7.5 through intermittent adjustment using 0.1 M NaOH or HCl on a daily basis. All tests were conducted at room temperature (21 ℃).

2.2.5 Fixed-bed column tests

Fixed-bed column tests were carried out to test arsenate breakthrough behaviors of the newly prepared PLE's. The column test setup included a Plexiglass column (11 mm in diameter and 250mm in length), an Accuflow Series II high-pressure liquid chromatography stainless steel pump, and an Eldex automatic fraction collector. For each column run, 3 mL of each PLE was packed into column with a thin (~5 mm) layer of glass wool placed underneath the resin bed. The influent solution contained: 97 µg/L of arsenate as *As*(V), 47 mg/L of sulfate, 82 mg/L of chloride, and 35 mg/L of bicarbonate, and the pH of the influent was kept at 7.5. The influent was passed through the packed column in the down-flow mode with a constant flow rate of 1.2 mL/min, which translates into an empty bed contact time (EBCT) of 4.1 min, or a superficial liquid velocity (SLV) of 3.0 m/hr. All tests were performed at room temperature (~21 ℃). The influent compositions and operating conditions were kept identical for the three column tests

with XAD1180-3N-Cu, XAD16-3N-Cu, and XAD7HP-3N. The effluent was automatically collected in 22 mL glass tubes and stored in refrigerator (4℃) until analysis.

2.2.6 Kinetic tests

Batch kinetic tests were conducted with the three PLE's to determine the sorption rates and the intraparticle diffusion coefficients. The tests were carried out with 2 L glass bottles, each containing 2 L of a solution containing 5 mg/L as *As* and 100 mg/L as SO_4^{2-}. The tests were initiated by adding ~0.95g of a PLE into a mixture. Then, the mixtures were intensively agitated on the shaker to eliminate the possible film diffusion limitation on the mass transfer process. The solution pH was kept in the rage of 7.0-7.6 (adjusted hourly) during the kinetic tests. At pre-determined time intervals, 2 mL samples were taken from the solution phase and analyzed for *As* remaining in the solution. The *As* uptake at various times was then determined through mass balance calculations.

2.2.7 Regeneration of As-laden PLE's

As-laden PLE's (XAD1180-3N, XAD16-3N and XAD7HP-3N) were regenerated using the same column configuration as in the service breakthrough runs. Before the regeneration tests, 5 mL of a fresh PLE was equilibrated with a 2 L solution containing 10 mg/L of *As* and 100 mg/L of SO_4^{2-} at a pH of 7.5-7.0. The *As*-laden PLE's were then packed in the column and regenerated under a variety of conditions (regenerant brine concentration = 4%~8% w/w and pH = 9-10) in the down-flow mode. In all cases, the hydrodynamic conditions, EBCT and SLV, were kept identical at 22 min and 1.4 m/hr, respectively.

2.2.8 Chemical analyses

A Perkin Elmer Atomic Adsorption Spectrophotometer was used for *As* analyses. Sulfate and chloride were analyzed using a Dionex Ion Chromatography (Model DX-120). Bicarbonate was analyzed with a UV-Persulfate TOC Analyzer (Phoenix 8000). The solution pH was measured with an Orion pH meter (Model 520A).

2.3 Results and discussion

2.3.1 Screening of chelating compounds for amination of XAD resins

Table 2-2 lists the six compounds that were tested for their chelating abilities with Cu(II). They were selected for the following considerations: a) at least one primary or secondary amine group is needed for the grafting reaction with the chloromethyl group (for the PS/DVB resins), and b) they contain multiple nitrogen donor atoms, especially preferred are those with pyridine nitrogens; or they are reported to be used as copper chelating groups in the literature.

Among the six compounds tested, only No. 1 Di(2-picolyl)amine showed strong blue/green color when mixed with the Cu(II) solution, both in the solution-phase and as grafted ligand on PS/DVB surface. No. 4 and No. 6 only showed very light blue/green color, and there was no apparent color change with No. 3, indicating little interactions between Cu(II) and these ligand compounds. Ligand No. 5 is an aromatic amine, but it is not soluble in either aqueous solution or in organic solvents (tested with toluene, methanol, and acetone), and thus, was excluded for further consideration for its potential inability to react with the chloromethyl group.

Table 2-2. Ligand compounds tested for complexing with Cu(II). (Color Test 1: Color change or metal-ligand complexation in homogeneous solution phase; Color Test 2: Color change of the resin beads upon Cu(II) loading).

No	Name	Structure	Color Test 1 (500ppm Cu^{2+})	Color Test 2 (500ppm Cu^{2+})
1	Di(2-picolyl)amine	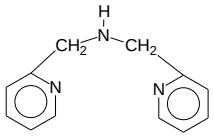	Strong blue/green	Dark green
2	2,2'-dipyridylamine	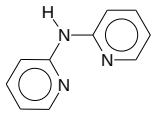	Light blue/green	No change
3	1-(2-pyridyl) piperazine	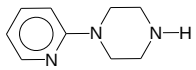		No change
4	(2-pyrimidyl) piperazine	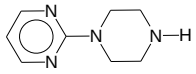		Very light green
5	2,4-diamino-6-methyl-1,3,5-triazine	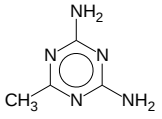	Not soluble	
6	guanidine	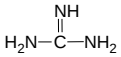	Light blue	Light green

Table 2-3 shows some other ligand structures reported in the literature that showed remarkable Cu(II) uptakes are shown. The alkyl (2-picolyl) amine (structure No. 7) (Grinstead and Nasutavicus, 1977; Warshawsky, 1986) is represented by the DOW 2N resin, with copper uptaking capacity of ~0.70 mmole/g; a resin grafted with pyridyl-imidazolyl group (structure No.8) had a capacity of 0.83 mmole/g (Warshawsky, 1986) and a polystyrene resin grafted with polyethylenimine (polyamine) (structure No. 9) also showed similar levels of copper capacity (Warshawsky, 1986). Based on our knowledge, a Cu(II) binding capacity of 0.7 – 0.8 mmole/g is still not quite comparable to that of the Di(2-picolyl)amine grafted polymer (such as DOW 3N) (Grinstead and Nasutavicus, 1977; Zhao and SenGupta, 1998). The reported structure No. 10 (Melby, 1975) had a capacity of 1.70 mmole/g which is comparable to DOW 3N (No. 11). Ligand No. 10 has four nitrogen atoms and may take up four coordinating positions for chelating with each copper atom, which is good for a tight anchoring of the metal ions, but may also leave fewer coordinating positions for the resultant PLE to bind with ligands (such as arsenate) from the aqueous phase.

Another group of structures for copper uptake include No. 12 (polyamidoxime) (Lufor et al., 2000), No. 13 (8-hydroxyquinoline grafted polymer) (Warshawsky, 1986), and the most common type of chelating group—imidodiacetate (No.14) (such as the commonly used chelating resin IRA-718). In these structures, oxygen anions, together with nitrogen, take part in the chelation with Cu^{2+}. Consequently, the positive charges of the copper atom are neutralized and the electrostatic interactions for anion exchange will disappear. The very low capacity of arsenate uptake of the copper-loaded IRA-718 or Purolite® S-910 (tested by B. An) has proven this assertion.

Table 2-3. Chelating resins reported in the literature or by manufacturers used for Cu(II) binding.

No.	Name	Structure	Copper Loading Capacity (mmole/g)	Ref.
7	Alkyl (2-picolyl)amine grafted on PS/DVB	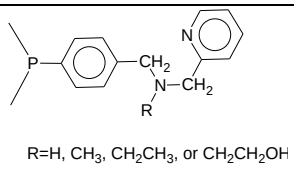	0.6 – 0.7	[18,19]
8	Pyridyl imidazolyl grafted on PS/DVB	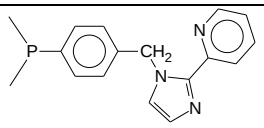	0.83	[19]
9	Polyethylenimine on PS/DVB	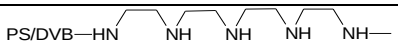	0.73	[19]
10	4N ligand on PS/DVB	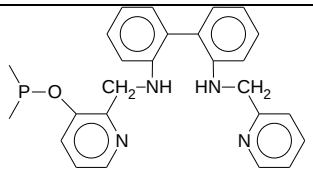	1.70	[21]
11	Dow 3N	Ligand No.1 grafted on PS/DVB	1.5	[20]
12	Polyamidoxime from polyacrylonitrile	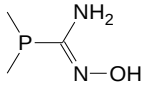	1-3	[22]
13	Hydroxyquinoline polymer	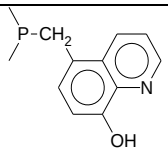	0.51	[19]
14	Imidodiacetate functionalized PS/DVB (Amberite IRA-718)	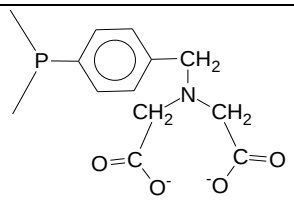		Rohm and Haas

Based on the preliminary structure screening test and the available information about the other chelating groups, di(2-picolyl)amine and 2-picolylamine were considered the most promising ligands for grafting onto the polymer matrices, and thus, were focused in this work.

2.3.2 Functionalization of XAD16 and XAD1180

Fig. 2-2 depicts the two-step reactions (chloromethylation followed by amination) responsible for the functionalization of the PS/DVB XAD resins. The chloromethylation of the aromatic rings in styrenic polymers follows the Friedel-Crafts alkylation mechanism (Prepper, et al., 1953; Camps et al., 1982; Frechetand and Farrall, 1977). While linear polystyrene and low-crosslinking polystyrene (with 1-2% divinylbenzene) can be chloromethylated to a greater degree (chloromethylation of more of the benzene rings), it is expected that increasing the degree of crosslinkage (DVB) will hinder the degree of chloromethylation. This is because more benzene rings on the polymer backbone are sterically hindered for the chemical reaction at a greater crosslinkages. Previous study (Hubbard et al., 1998) has shown that, using chloromethyl methyl ether and $SnCl_4$, the chloromethylation of styrene-divinylbenzene copolymers with 5, 20, and 40% of divinylbenzene gave a functionalization result of 6.0, 3.5, and 1.1 mmol Cl/g of resin, respectively. The crosslinkage of XAD16 and XAD1180 was not disclosed by the manufacture, however, some study showed that the crosslikage for these commercial resins is quite high (~40%) (Greig and Sherrington, 1979), which partially accounted for the high surface area of these sorbents. Our experimental results showed that, after the chloromethylation, XAD16 and XAD1180 resins gained 20 to 30% of weight, which correspond to 3.3 to 4.6 mmol Cl/g of resin (assuming that side reactions are insignificant), indicating that chloromethylation of XAD16 and XAD1180 to medium-high levels was achieved. Note that the larger pore structures of these polymer beads, compared to the smaller-pore or non-pore structures of low crosslinking

Chloromethylation:

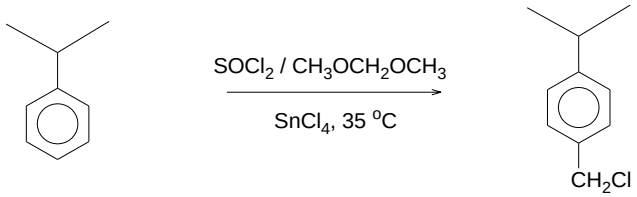

Amination:

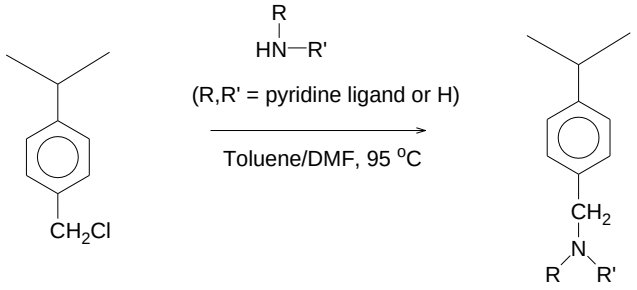

Fig. 2-2. Chloromethylation of XAD16 and XAD1180 (PS/DVB copolymers) and functionalization with pyridine ligands.

analogues, offer advantages with respect to mass transfer and ion exchange kinetics of the resultant PLE's.

To maximize the degree of amination, we studied the effect of chloromethylation conditions on the final degree of ligand grafting. The XAD1180 resin was chloromethylated under various reaction conditions, and the chloromethylated samples were then aminated with di(2-picolyl)amine under a fixed set of reaction conditions (using toluene/DMF as the solvent, reacted at 95 ℃ for 24 hours). The maximum copper loading capacities of these samples were measured and are used to characterize the degree of functionalization. Table 2-4 shows the experimental results. As we can see, after about 1 hour of reaction, the chloromethylation weight gain kept increasing slowly as the reaction time and temperature increased. However, maximum copper chelation was not achieved at the most intensive chloromethylation condition (40 ℃, 5 hours); instead, mild reaction conditions (35 ℃, 1 to 2 hours) gave the best functionalization results. As the reaction time and the concentration of chloromethyl groups in the polymer increases, it is quite possible that a side reaction will occur: the reaction of a chloromethyl group on one benzene ring of the polymer reacts with a neighboring benzene ring in the polymer to creat a $–CH_2-$ crosslinkage (Prepper et al., 1953). This side reaction consumes some chloromethyl groups and further increases the crosslinking density of the polymer, both having adverse effect on the second-step functionalization. The high crosslinkage of the original XAD polymers makes the polymer beads hard to swell, and thus, very likely renders the side reaction to occur earlier compared with the low-crosslinkage analogues.

The second step of the functionalization was finished by the amination of chlormethylated XAD16 and XAD1180 with 2-picolylamine or di(2-picolyl)amine. The optimal reaction condition was found to be using a mixture of toluene and DMF (2:1 v/v) as the solvent

Table 2-4. Effect of chloromethylation conditions on maximum copper loading of di(2-picolyl)amine-functionalized XAD1180.

Chloromethylation Condition	35 ℃, 0.5 hour	35 ℃, 1 hour	35 ℃, 1.5 hours	35 ℃, 2 hours	40 ℃, 5 hours
Weight Gain after Chloromethylaton (%)	18	20	21	22	24
Max. Cu-Loading (mg/g resin)	30	35	39	33	26

and reacting at 95 ℃ for 24 hours. The use of DMF increased the solubility of the HCl salts of the excess amines, which would be phase-separated and clog the pores of the beads during the reaction if only toluene were used. Based on the weight gains, the degrees of functionalization were about 1.2 mmol/g and 0.7 mmol/g for the 2-picolylamine and di(2-picolyl)amine functionalized XAD polymers, respectively. The difference between XAD16 and XAD1180 was very small, with XAD16 giving slightly higher degrees of functionalization. This result indicates that not all the chloromethyl groups were reacted; the bulky molecular sizes of the ligand compounds, especially for di(2-picolyl)amine, prohibit their reaction with the chloromethyl groups located in a sterically hindered places of the highly crosslinked polymer network. Table 2-5 gives the maximum Cu(II) loading on these newly synthesized chelating resins. Comparing the maximum copper loading and the ligand-grafting density of these chelating polymers, it is shown that in the di(2-picolyl)amine-functionalized XAD16 and XAD1180 resins, the Cu/ligand molar ratio is about 1:1, while in the 2-picolylamine functionalized resins, the Cu/ligand ratio is about 1:1.5 to 1:2.

2.3.3 Functionalization of XAD7HP

XAD7HP is a crosslinked methyl methacrylate copolymer (macroporous beads). Functionalization of XAD7HP was achieved by directly reacting with 2-picolylamine and di(2-picolyl)amine utilizing the aminolysis reaction of the amines with the ester groups on the polymer, as depicted by Fig. 2-3.

The maximum copper loading of the resultant chelating resins are shown in Table 2-6. The functionalization was a one-step reaction, and a high degree of functionalization was achieved with 2-picolylamine. The relatively low degree of functionalization with di(2-

Table 2-5. Maximum copper loading of the newly prepared chelating resins.

Chelating Resin	Functional group	Maximum Cu-Loading Capacity (mg/g)
XAD1180-2N	2-Picolylamine	40
XAD1180-3N	Di(2-picolyl)amine	39
XAD16-2N	2-Picolylamine	43
XAD16-3N	Di(2-picolyl)amine	40
XAD7HP-2N	2-Picolylamine	44
XAD7HP-3N	Di(2-picolyl)amine	26

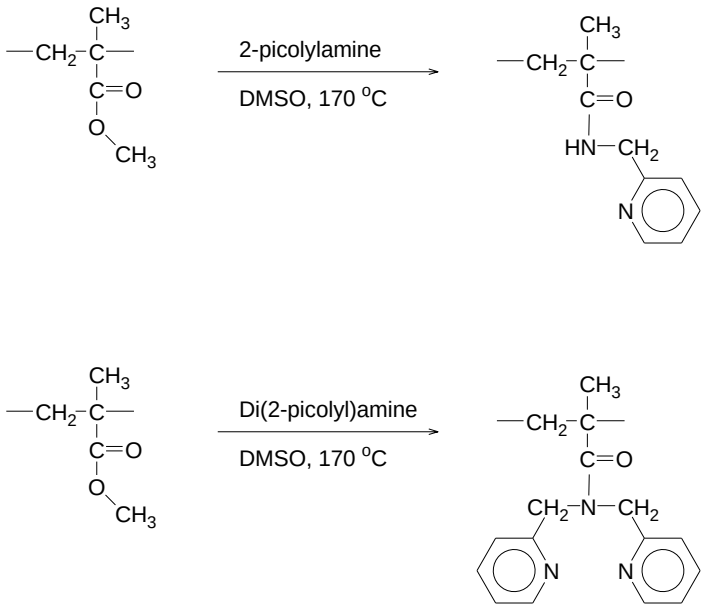

Fig. 2-3. Functionalization of XAD7HP (crosslinked acrylic copolymer) with pyridine ligands.

Table 2-6. The values of model-fitted Langmuir parameters (*Q, b*) and the mean arsenate/sulfate separation factors ($\alpha_{As/S}$).

Resin	*Q*(Standard Error) (mg/g)	*b* (Standard Error) (L/mg)	$\alpha_{As/S}$ (Standard deviation)
XAD1180-2N-Cu	20(1.9)	0.37(0.089)	8.5(3.8)
XAD1180-3N-Cu	26(6.4)	0.11(0.050)	7.4(2.0)
XAD16-2N-Cu	15(2.6)	0.23(0.074)	7.5(0.74)
XAD16-3N-Cu	18(1.7)	0.19(0.43)	10(2.1)
XAD7HP-3N-Cu	19(4.1)	0.13(0.051)	4.9(0.84)

picolyl)amine was probably due to both the low reactivity of its secondary amine group and the bulky molecular size.

To our knowledge, the direct functionalization of acrylic polymers via aminolysis reaction to synthesis of pyridine-containing chelating polymers has not been reported in the literature. The synthesis route is rather straightforward, and as shown in Table 2-4, with the 2-picolylamine-functionalized XAD7HP, the combination of pyridine nitrogen and amide nitrogen gives amazing chelating result for copper, possibly also good for other transitional metals. Compared with regular amine groups, both the pyridine and amide nitrogen donor atoms will remain non-protonized down to very low pH (<3), which grants the resins a broad pH range for effective metal complexation. When the crosslinkage of the acrylic polymer matrix is optimized, it is very likely that chelating polymers with even higher metal-binding capacities can be synthesized with this approach.

2.3.4 Copper loading and PLE functionality

As shown in Table 2-5, six PLE's were prepared based on the chelating resins functionalized with the two types of pyridinyl functional groups. Five of the PLE resins have copper loading capacities at about 0.7 mmol/g.

As illustrated in Fig. 2-1, the removal of *As* from water involves formation of tertiary complexes between the hosting chelating resins, the central metal ions and the target ligands. Apparently, the key functional groups of a PLE are the central metal ions, i.e. Cu(II). Consequently, the Cu(II) capacity of the hosting chelating resin will govern the resin's capacity for the target arsenate uptake. The Cu(II) loading capacity in Table 2-5 indicates that despite the considerable differences in the matrix properties (polymer type, surface area and number of nitrogen donor atoms) of the parent polymers, the resultant chelating resins do not significantly

differ in their copper capacity, except for XAD7HP-3N. This observation suggests that the copper sorption capacity of the XAD-based chelating resins may be confined by the extremely high crosslinkage (~40%) of these polymer matrices. Although high crosslinkage increases the surface area of the resins, it reduces the size of the pores, rendering the sorption sites less accessible. The observed copper capacity shown in Table 2-5 was 2 to 2.5 times lower compared to another commercial chelating resin DOW 3N, which has a much smaller surface area (~139 m^2/g), but larger mean pore size (~250 Å).

2.3.5 Arsenate sorption isotherms

As stated earlier, standard SBA resins such as IRA 900 and IRA 958 prefer sulfate to arsenate, which often results in low arsenate sorption capacity in the presence of sulfate, greater regeneration needs and production of larger volumes of process waste residuals (An et al., 2005; Zhao and SenGupta, 2000). In contrast, because the copper-loaded PLE's take up arsenate thorough concurrent Lewis acid-base and electrostatic interactions (Fig. 2-1), the arsenate selectivity is expected to be greatly in favor of arsenate over sulfate, thereby overcoming the drawbacks associated with the standard SBA resins.

Fig. 2-4 shows the isotherms of arsenate sorption for five of the PLE's. Based on the isotherm data, the arsenate-to-sulfate binary separation factor ($\alpha_{As/S}$) was calculated to compare the relative affinity of the PLE's toward these two competing ligands. The arsenate/sulfate separation factor was defined as follows:

$$\alpha_{As/S} = \frac{q_{As} C_S}{C_{As} q_S} \tag{2-2}$$

where, q_{As} and q_S are the concentrations of arsenate and sulfate, respectively, in the solid phase; C_{As} and C_S are the concentrations arsenate and sulfate in the solution, respectively. As a rule, a

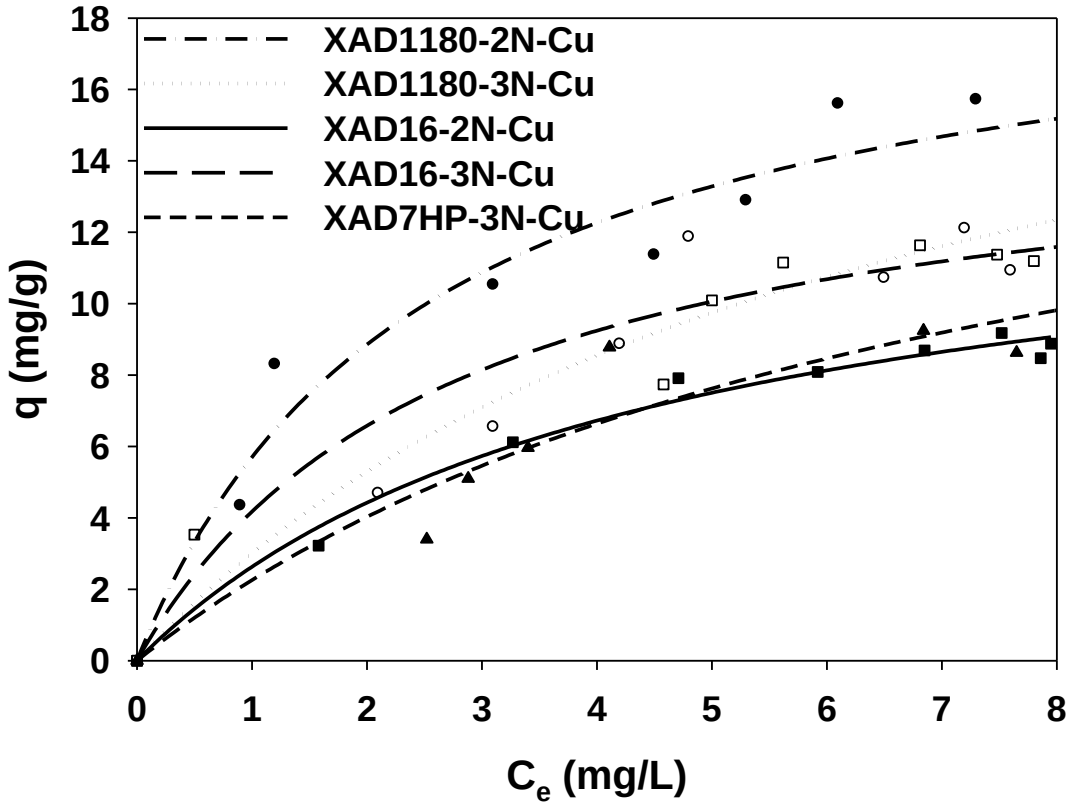

Fig. 2-4. Arsenate sorption isotherms for various XAD resins in the presence of competing sulfate ion (97-100 mg/L). (observed data: ●-XAD1180-2N-Cu,○XAD1180-3N-Cu, ■-XAD16-2N-Cu, □-XAD16-3N-Cu, ▲-XAD7HP-3N-Cu, lines: Langmuir model fits).

separation factor value of greater than one indicates greater selectivity for arsenate than sulfate. The values of $\alpha_{As/S}$ shown in Table 2-6 range from 5.1 (XAD7HP-3N-Cu) to 10 (XAD16-3N-Cu), clearly indicating that all the PLE's are highly selective for arsenate over sulfate. In contrast, for standard SBA resins, the $\alpha_{As/S}$ values are reported to be 0.2 for IRA 900 and 0.1 for IRA 958 (An et al., 2005). The greatly enhanced arsenate selectivity of the PLE's is attributed to the much stronger ligand strength of arsenate over sulfate. As noted earlier, for the PLE's, arsenate is taken up synergistically through concurrent Lewis acid-base (LAB) and electrostatic interactions, while for SBA resins, only electrostatic interactions are operative. In other words, the PLE's take advantage of the stronger ligand strength of arsenate, which results in a much greater LAB interaction. Note that pH of the aqueous phase ranged from 7.0 to 7.5, where arsenate was present predominantly as a bidentate, divalent ligand ($HAsO_4^{2-}$).

To experimental isotherm data were interpreted with the classical Langmuir model:

$$q_e = \frac{bQC_e}{1+bC_e} \tag{2-3}$$

where q_e is the equilibrium *As* uptake (mg/g), C_e is the equilibrium concentration of *As* in aqueous phase (mg/L), Q is the maximum capacity for arsenate, and b is the Langmuir affinity coefficient. The non-linear fitting was performed using the SigmaPlot8.0 package. Table 2-6 lists the values of the model-fitted b and Q values. The range of Q values is from 15 to 26 for XAD16-2N-Cu and XAD1180-3N-Cu, respectively, whereas for standard SBA, the Q values of 5.5 and 4.5 were reported for IRA 958 and IRA 900, respectively (An et al., 2005).

It should be noted that although the values of $\alpha_{As/S}$ and the Langmuir parameters (Q and b) for XAD-based PLE's far exceed those for standard SBA resins, these values are lower than for DOW 3N-Cu ($\alpha_{As/S}$=12 and Q=92 mg/g). Again, given the much greater surface area of the XAD resins compared to DOW 3N, this quite counter-intuitive finding reveals that high surface area

alone does not guarantee greater copper loading capacity, and the greater copper and arsenate capacities of DOW 3N-Cu are attributed to the lower crosslinkage (typically <10% for chelating resins compared to 40% for the

XAD resins). In other words, the high crosslinkage of the XAD resins limited the copper loading during the PLE's preparation.

2.3.6 Breakthrough behaviors

Fixed bed column tests were carried out to investigate the breakthrough profiles of sulfate, chloride, bicarbonate and arsenate with the XAD-based PLE's. Fig. 2-5 shows breakthrough histories of arsenate and other competing anions (bicarbonate, sulfate and chloride) for XAD1180-3N-Cu. The influent concentrations and hydrodynamic conditions (EBCT and SLV) are also provided in Fig. 2-5. All three competing anions, including sulfate, immediately broke through within 50 bed volumes (BV) and chromatographic peaking was observed for chloride and sulfate. The breakthrough sequence indicates the following affinity sequence of this PLE:

$$HAsO_4^{2-} > HCO_3^- > SO_4^{2-} > Cl^- \quad (2\text{-}4)$$

Taking the 10 µg/L MCL as the breakthrough point for arsenic, more than 900 BV of the synthetic water can be treated per service run. This treatment capacity is about two times that of typical SBA resins (An et al., 2005; Clifford, 1999), for which sulfate is the most preferred anion. Similar breakthrough sequence and profiles were also observed for other XAD-based PLE's prepared in this work (data not shown).

Fig. 2-6 shows arsenic breakthrough curves obtained with three of the XAD-based PLE's (XAD1180-3N-Cu, XAD16-3N-Cu, and XAD7HP-3N-Cu) under otherwise identical conditions. The breakthrough BV ranged from 780 BV for XAD7HP-3N-Cu to 920 for XAD1180-3N-Cu. The lower treatment capacity of XAD7HP-3N-Cu is attributed to its lower copper capacity

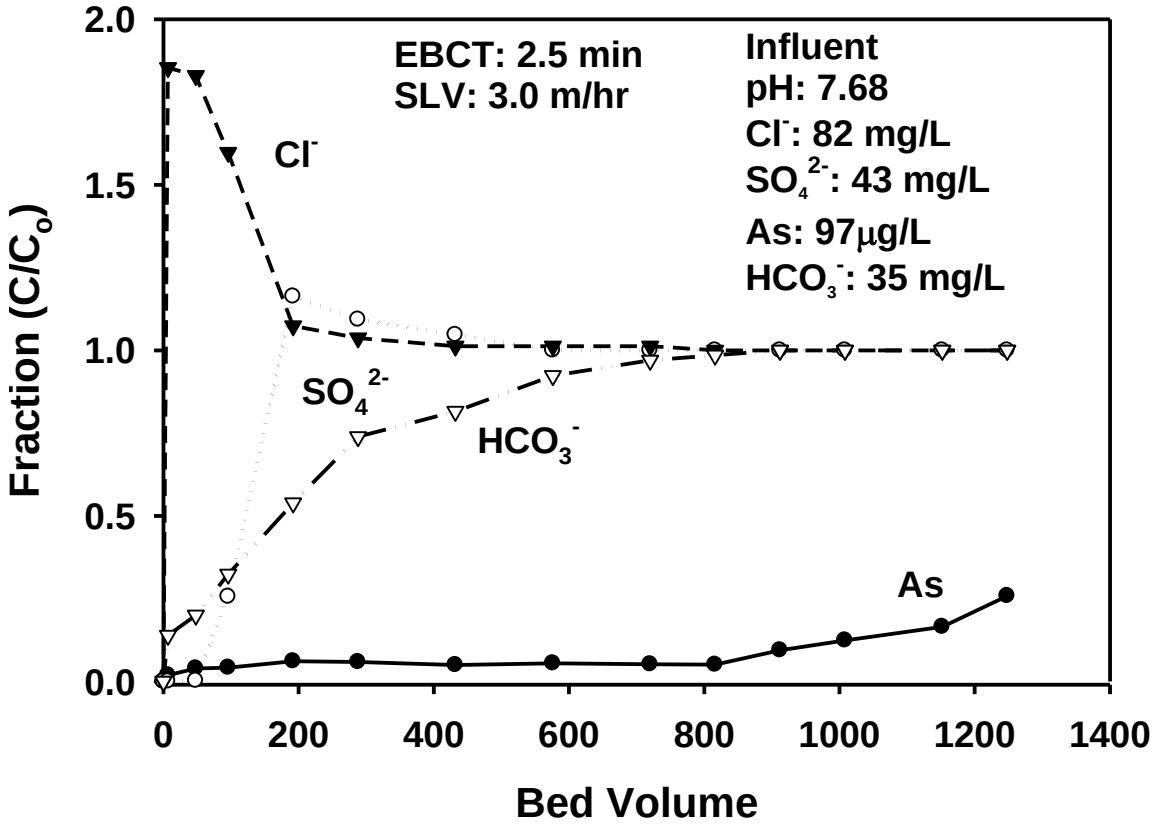

Fig. 2-5. Breakthrough histories of arsenate and competing anions in a multi-component system using a XAD1180-3N-Cu.

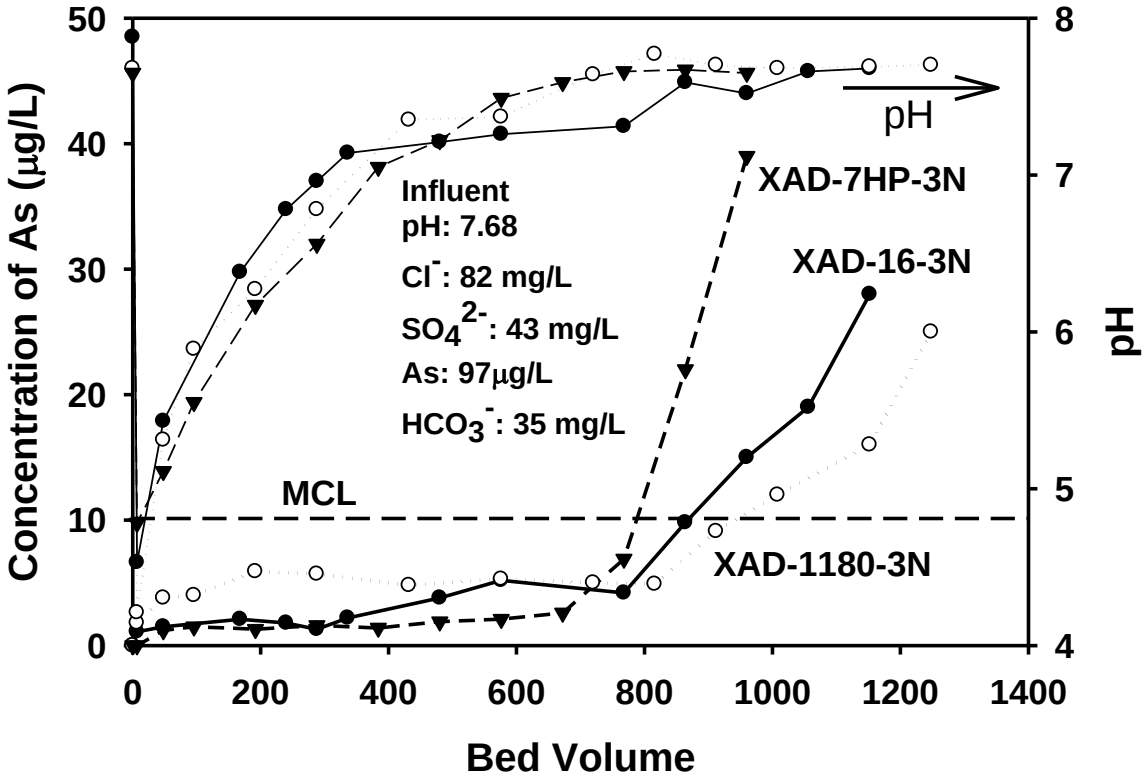

Fig. 2-6. Breakthrough histories and pH for three types of sorbents under identical condition.

(Table 2-5) associated with its lower surface area and porosity (Table 2-1). However, because of its hydrophilic matrix, this PLE is expected to be more resistant to organic fouling, and thus, may be advantageous where high concentrations of organic compounds are present.

The pH histories during the three column runs generally coincided (Fig. 2-6). It is characterized with an abrupt drop of pH to <5, and followed by gradual recovery to the initial pH of ~7.5. The initial pH drop can be attributed to 1) uptake of hydroxyl anions (OH^-) by the fresh PLE bed; and 2) uptake of bicarbonate and arsenate. As the column is gradually exhausted, a fraction of sorbed hydroxyl and bicarbonate ions can be eluted by arsenate, which accounts for the gradual rise in pH as the column runs progressed.

2.3.7 Kinetic tests

In previous work, Zhao and SenGupta (2000) observed an intraparticle diffusivity of 1.0 x 10^{-8} cm^2/s for phosphate sorption by DOW 3N-Cu, and An et al. (2005) obtained a *D* value of 1.0 x 10^{-7} cm^2/s for arsenate sorption by DOW 3N-Cu. In both cases, they confirmed that intraparticle diffusion is the rate-limiting step. Given the similar nature of the PLE resins, the sorption kinetics is interpreted following the similar modeling procedure as described in (An et al., 2005). For an intraparticle-diffusion-controlled process, sorption rates can be modeled by the Fick's second law. For spherical beads, the governing equation is (Crank, 1975)

$$\frac{\partial q}{\partial t} = D\left(\frac{\partial^2 q}{\partial r^2} + \frac{2}{r}\frac{\partial q}{\partial r}\right) \tag{2-5}$$

where r is the radial coordinate and $q(t, r)$ is the solid-phase arsenic concentration at time t. Under the experimental conditions, the following initial and boundary conditions apply:

$$q(0) = 0 \quad \text{at} \quad 0 \le r \le a \tag{2-6}$$

$$\partial q/\partial r = 0 \quad \text{at} \quad r = 0 \tag{2-7}$$

$(\partial q/\partial r)(3D\,M/a) = -V\,(\partial C/\partial t)$ at $r = a$ (2-8)

where a is the mean radius of the resin beads, which was determined to be 0.24 mm for XAD1180 and 0.32 mm for XAD16 and XAD7HP, M is the mass of the resin added, and V is the solution volume, which is considered constant during the course of the experiment.

The above system conforms to the scenario where diffusion takes place in a well-stirred solution of limited volume (Clifford, 1999). The solution given by Crank (1975) as the fractional attainment of equilibrium (F),

$$F = \frac{q(t)}{q_\infty} = 1 - \sum_{n=1}^{\infty} \frac{6\alpha(\alpha+1)\exp(-Dq_n^2 t/a^2)}{9 + 9\alpha + q_n^2\alpha^2} \tag{2-9}$$

where q_∞ is the arsenate uptake by DOW 3N-Cu at infinite time (i.e. at equilibrium), the parameter α is expressed in terms of the final fractional uptake of arsenate as

$$\frac{Mq_\infty}{V_o C_o} = \frac{1}{1+\alpha} \tag{2-10}$$

where V_o and C_o are initial solution volume and initial arsenate concentration in solution, respectively. The q_n's are the non-zero roots of

$$\tan q_n = \frac{3q_n}{3 + \alpha q_n^2} \tag{2-11}$$

The form of eqn (2-11) allows for convenient bracketing of the roots in well-defined intervals as determined by the tan function, which allows for simple root finding using the method of bisection. The aqueous phase concentration at time t, $C(t)$, was then determined via the following mass-balance equation:

$$Mq(t) = V\,[C_o - C(t)] \tag{2-12}$$

The model was then applied to fit the experimental kinetic data (Fig. 2-7) with *D* being the single fitting parameter.

Fig. 2-7 shows the kinetic data of arsenate sorption by three of the XAD-based PLE's. In all cases, ion exchange equilibrium was reached in 16 hours, suggesting fairly fast mass transfer kinetics. The intraparticle diffusivity was determined to be 2.0 x 10^{-6} cm^2/sec for XAD1180-3N-Cu, 3.0 x 10^{-6} cm^2/sec for XAD16-3N-Cu, and 3.0 x 10^{-6} cm^2/sec for XAD7HP-3N-Cu. These diffusivity values are about one to two orders of magnitude greater than those for the previously tested PLE (DOW 3N-Cu) and for standard SBA resins. Although the sorption capacity of these XAD-based PLE's is lower than the macroporous PLE (DOW 3N-Cu), the arsenate sorption sites of the XAD-based PLEs appears to be much more easily accessible. This kinetic advantage can be of practical significance. For example, these relatively low-capacity PLE's may be more resistant to organic fouling, and thus, may perform better for treating water that contains high strength of dissolved organic matter.

2.3.8 Regeneration

Based on our previous study on DOW 3N-Cu, copper-loaded PLE can be regenerated effectively using (6-10) wt.% NaCl at pH 9-10 and at an EBCT of 17 min (An et al., 2005), and the regeneration effectiveness depends on the salt concentration and pH of the feeding regenerant. Fig. 2-8 shows the arsenic elution histories during regeneration runs using 8 wt.% of NaCl at pH 10. Mass balance calculations indicated that in all cases 100% recovery of arsenic was achieved with 20-30 BVs of the regenerant, where regeneration of the PLE based on polyacrylic XAD matrix was more effective. This quite high regeneration efficiency is in accord with the fast ligand exchange kinetics as demonstrated above.

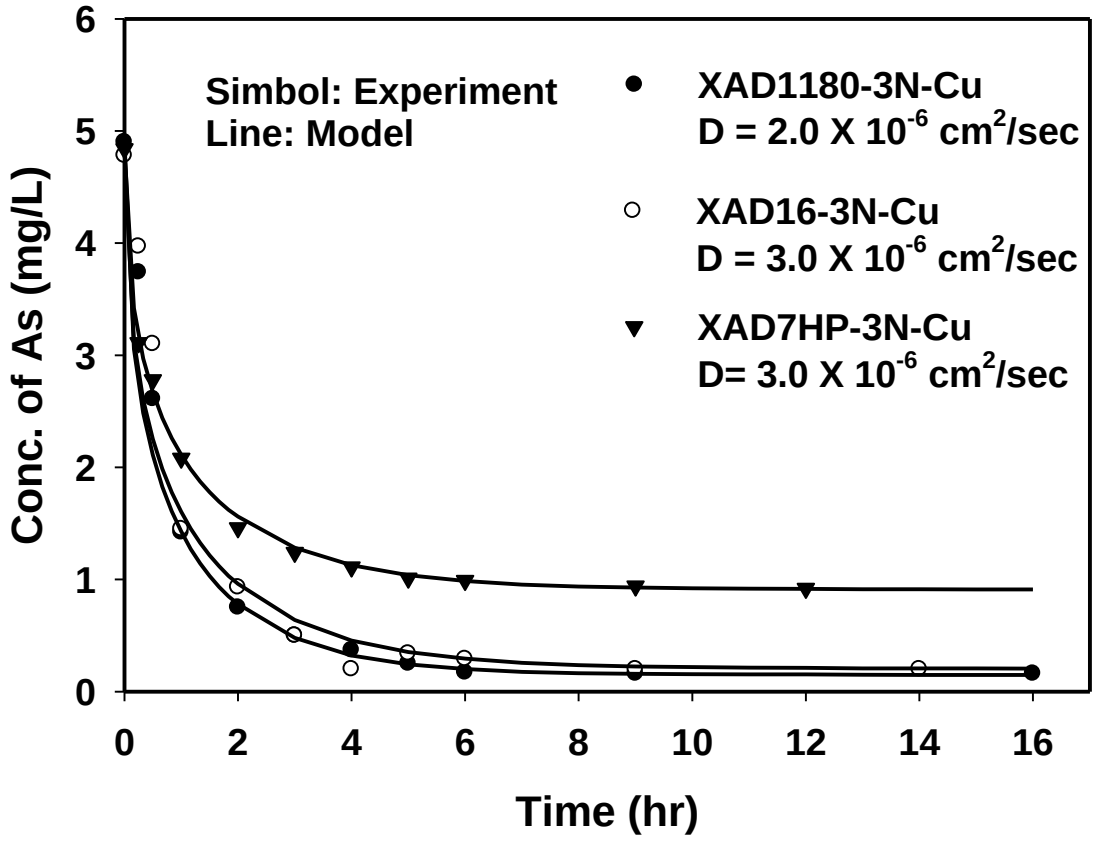

Fig. 2-7. Experimental and model-simulated arsenate sorption kinetics of three types of XAD resins. (symbols: observed data; lines: model simulation).

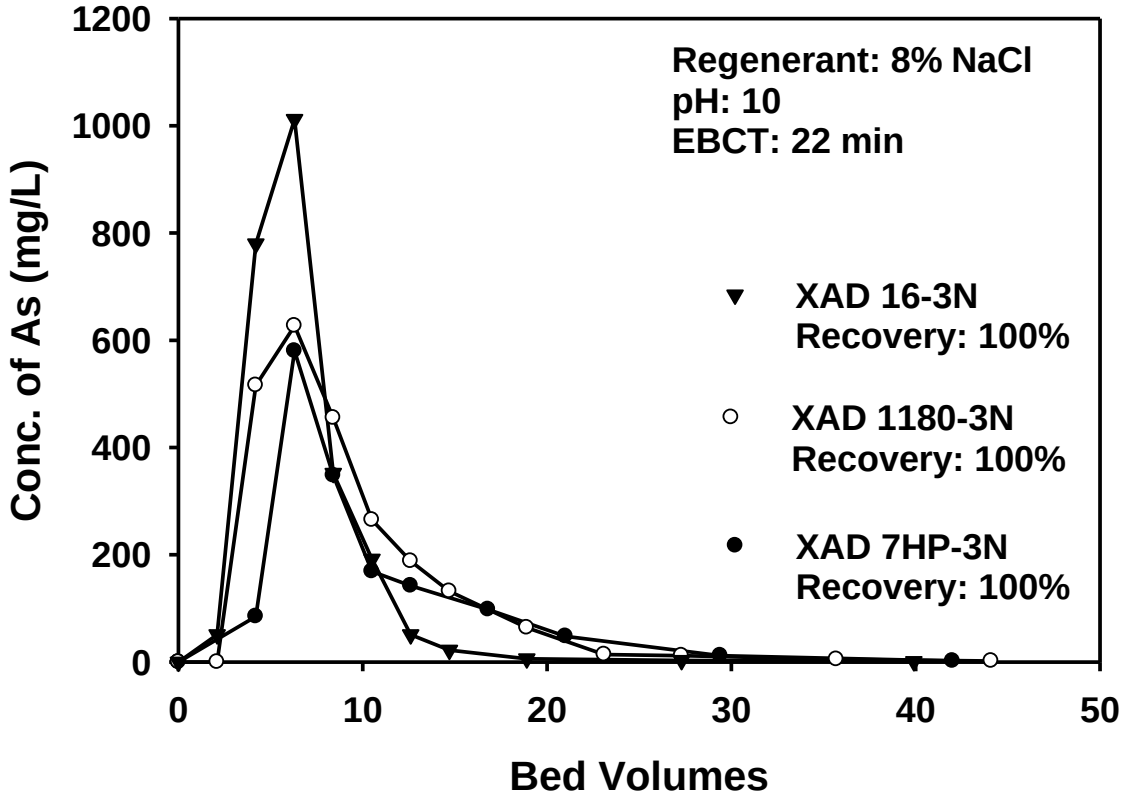

Fig. 2-8. Arsenate elution profiles during regeneration of saturated PLE resins using 8% NaCl (w/w) at pH 10.

Assuming that $HAsO_4^{2-}$ is the predominant arsenic species in the sorbent phase, the regeneration reaction stoichiometry at the alkaline pH can be illustrated as follows:

$$R\text{-}Cu^{2+}HAsO_4^{2-} + Cl^- + OH^- \rightarrow R\text{-}Cu^{2+}(Cl^-)(OH^-) + HAsO_4^{2-} \quad (2\text{-}13)$$

Note that at an elevated pH, OH^- ions, which are a fairly strong ligand, will replace arsenate in the resin phase. As a result, the regenerated PLE's will be converted to the forms of both chloride and hydroxyl anions. In addition, copper bleeding was monitored during the regeneration runs and was found negligible in all cases.

2.4 Conclusions

A new class of polymeric ligand exchangers was synthesized based on the commercially available XAD sorbents. The functionalization of polystyrene/DVB matrices was achieved following the conventional chloromethylation and amination, whereas the acrylic copolymer (XAD7HP) was functionalized through the aminolysis of the ester groups in the polymer backbone by the amine group of 2-picolylamine or di(2-picolyl)amine ligands. There copper-loaded PLE's displayed rather unique selectivity toward arsenate compared to standard SBA resins. Major findings of this research are summarized as follows:

- Despite the very high surface area of the XAD sorbents, the loading capacity of copper ranged from 26 mg/g for the acrylic resin (XAD7HP-3N) and 39-41 mg/g for the other polystyrene/DVB sorbents. This observation suggests that although high crosslinkage (as is the case for the XAD resins) can lead to high surface area and uniform pore size distribution, the actual accessibility of the internal sorption sites, and thus, the sorption capacity, can be greatly discounted. Consequently, matrices with a crosslinkage of <10% and with balanced surface area and pore size would be more advantageous for preparing novel PLE's. In the presence of 100 mg/L of SO_4^{2-}, the PLE's showed much higher

selectivity and arsenate capacity than standard SBA resins. The binary arsenate/sulfate separation factor was determined to be from 5.1 (for XAD7HP-3N-Cu) to 10 (for XAD1180-3N-Cu), which is over one order of magnitude greater than that for standard SBA resins. The maximum Langmuir capacity (*Q*) for the new PLE's ranged from 15 for XAD16-2N-Cu to26 for XAD1180-3N-Cu.

- Among all the ligands with nitrogen as the electron donor atoms, 2-picolylamine and di(2-picolyl)amine are most appropriate for preparing the desired PLE's because of their high copper affinity and neutral (free base) form even at very acidic pH (<3).
- Fixed-bed column tests revealed that despite the different nature of the parent matrices and difference in copper-loading, the XAD-based PLE's were able to treat 780 to 920 BV of arsenic laden water before the breakthrough point of 10 ppb. This treatment capacity is ~30% greater compared to SBA resins. The PLE's also displayed a unique selectivity sequence: arsenate > bicarbonate > sulfate > chloride.
- All the PLEs' offered superior sorption kinetics. The intraparticle diffusivity was determined to be 2.0×10^{-6} cm^2/sec for XAD1180-3N-Cu, 3.0×10^{-6} cm^2/sec for XAD16-3N-Cu, and 3.0×10^{-6} cm^2/sec for XAD7HP-3N-Cu, which are one to two orders of magnitude greater than that for standard commercial macroporous resins.
- All the PLE's are amenable to highly efficient regeneration with brine. Complete arsenate recovery was achieved using 20-30 BVs of 8% NaCl at pH 10 in all cases.
- The new PLE's may be used as an alternative sorbent for ligand separation for their unique selectivity sequence, fast kinetics and resistance to organic fouling. The knowledge gained from this work may guide further studies in controlled synthesis of PLE's of desirable features.

Chapter 3. Removal of Arsenic from Spent from Ion Exchange Brine Using Starch-Bridged Magnetite Nanoparticles

In this chapter, a new class of magnetite nanoparticles was prepared using starch as stabilizer, and used for removal of arsenate from spent ion exchanger brine. The starch-bridged magnetite nanoparticles were successfully prepared and the prepared gnetite nanoparticles were characterized with transmission electron microscope (TEM) and FTIR. A series of batch adsorption tests as a function of pH as well as isotherm test and kinetic test, was carried out to determine the removal of arsenate.

3.1 Introduction

Arsenic contamination of drinking water has been a worldwide challenge (An et al., 2005). Arsenic has been associated with skin, lung, bladder and kidney cancers (NRC, 2001). It was reported that 45-57 million people in Bangladesh and 13 million in the United States have been exposed to unsafe levels of arsenic (WHO, 2006). To mitigate human exposure, the US EPA implemented a revised maximum contaminant level (MCL) of 10 μg/L in 2006, representing a 5 fold decrease from its previous drinking water standard.

Technologies for effective arsenic removal from drinking water have been continuously sought for decades, and the effort has been intensified in the U.S. since the new MCL took effect. Approaches such as enhanced coagulation (Hering et al., 1997), adsorption onto iron oxide (Dixit and Hering, 2003), membrane processes (Ballinas, et al., 2004), and ion exchange (An et al.,

2005; Clifford et al., 2003; Cumbal and SenGupta, 2005; Ramana and SenGupta, 1992) have been extensively studied. Ion exchange is considered by US EPA as one of the best available technologies for removing arsenic from drinking water (EPA, 2000). However, IX processes produce a large volume of arsenic-laden regenerant brine, which is often categorized as hazardous process waste residual and requires costly further treatment, handling and disposal. Therefore, there is a dire need for developing an engineered strategy to minimize the production and arsenic leachability of the process waste residual resulting from IX processes.

Macroscale iron (hydr)oxides have been found effective for removing arsenic from drinking water and have been extensively investigated. Ferguson and Anderson (1974) studied adsorption characteristics of As(III) and As(V) with iron hydroxide. Pierce and Moore (1982) tested amorphous iron hydroxide and found adsorption of arsenic was highly pH-dependent. Hering et al. (1997) utilized bulk iron oxide for arsenic removal and concluded that removal of both As(III) and As(V) was affected by pH and the sorption was influenced by sulfate and dissolved organic matter. Dixit and Hering (2003) studied adsorption of As(III) and As(V) on hydrous ferric oxide (HFO), goethite, and magnetite, all of which were synthesized in the laboratory, and they found that sorption of As(V) onto HFO and goethite was more favorable than that of As(III) below pH 5−6, whereas, above pH 7−8, As(III) had a higher affinity for all of the sorbents. Other types of iron-based materials were also examined for removal of arsenic, including ferrihydrite (Coker et al., 2006; Waychunas et al., 1993), hematite (Aria et al., 2004; Gimenez et al., 2007), goethite (Dixit and Hering, 2003; Fendorf et al., 1997; Gimenez et al., 2007), and zero valent iron (ZVI) (Kanel et al., 2007; Su and Puls, 2001; Yuan and Lien, 2006).

In recent years, nanoscale iron oxides have attracted growing interest in water treatment and environmental remediation (Huber, 2005; Kanel et al., 2006; Yavuz et al., 2006). Iron oxide

nanoparticles offer high adsorption capacities toward a variety of important water contaminants including both As(III) and As(V) (Dixit and Hering, 2003). Magnetite (Fe_3O_4) is a ubiquitous magnetic iron oxide existing in the lithosphere, pedosphere, and biosphere (Cornell and Schwertmann, 2003). The structure of magnetite is a cubic inverse spinal that can be expressed as $FeFe_2O_4$, and it is a face-centered cubic (fcc) structure with Fe ions coordinated to interstitial tetrahedral sites (1/3) occupied by Fe(III) and octahedral sites (2/3) by equal amounts of Fe(III) and Fe(II) (Cornell, 2003). Based on the evidence from extended x-ray absorption fine structure (EXAFS) spectroscopy and Fourier transform infrared (FTIR) spectroscopy (Fendorf et al., 1997; Sun and Doner, 1996; Waychunas et al., 1993), magnetite can adsorb arsenic through inner-sphere bidentate-binuclear complexation.

Various methods have been used to prepare magnetite nanoparticles, including sol-gel (Tang et al., 2004), γ-ray radiation (Wang et al., 1997), hydrothermal technique (Qian et al., 1994), forced hydrolysis (Compean-Jasso et al., 2008), and co-precipitation from a mixture of Fe(III) and Fe(II) salts (Ataie and Heshmati-Manesh, 2001; Ferguson and Anderson, 1974; Jolivet, 2000). The co-precipitation method was first proposed by Anderson (1957) using ferric chloride and ferrous sulfate in a concentrated ammonia solution. In this method, pH of the solution is one of the key factors for controlling the physicochemical properties, such as particle size distribution, of the resultant magnetite particles. The mean particle size of magnetite synthesized by co-precipitation has been found to decrease with increasing final pH. The co-precipitation method has been the most widely employed approach for preparing magnetite particles for its straightforward procedure and the convenience for controlling size and shape.

Typically, this method starts with a solution containing both Fe^{3+} and Fe^{2+} at a molar ratio of Fe^{3+}:Fe^{2+} = 2:1. Upon addition of a base (e.g. NaOH), the Fe^{3+} ions are converted to

FeOOH through the intermediate $Fe(OH)_3$; and Fe^{2+} ions to $Fe(OH)_2$ (Eqns. 1-2). One mole of magnetite is then formed by reacting 2 moles of FeOOH and 1 mole of $Fe(OH)_2$ as shown below:

$$Fe^{3+}+3OH^- \rightarrow Fe(OH)_3 \rightarrow FeOOH + H_2O \quad (3\text{-}1)$$

$$Fe^{2+} + 2OH^- \rightarrow Fe(OH)_2 \quad (3\text{-}2)$$

$$2FeOOH + Fe(OH)_2 \rightarrow Fe_3O_4 + 2H_2O \quad (3\text{-}3)$$

In the presence of dissolved oxygen (DO), magnetite will be oxidized to γ-Fe_2O_3 (maghemite) (Alibeigi and Vaezi, 2008), which constitutes one method for preparing maghemite. High temperatures accelerate the oxidation rate and quantity, and smaller particles of magnetite will be oxidized faster than larger ones due to their shorter diffusion length (Tang et al., 2003).

Because of the high surface energy, magnetite nanoparticles tend to agglomerate into larger aggregates or flocs, which can render loss of specific surface area. Consequently, a stabilizer is often required, which can be sorbed on the nanoparticles and prevent the particles from aggregating thorough the steric and/or electrostatic stabilization mechanisms (He and Zhao, 2005; He and Zhao, 2007; Lee et al., 2002; Nishio et al., 2004; Raveendran et al., 2003; Tamaura et al., 1986; Yokoi and Kantoh, 1993). For examples, Raveendran et al. (2003) used a water soluble starch as a stabilizer for preparing nanoscale Ag particles in aqueous media. He and Zhao (2007) and He et al. (2007) successfully stabilized ZVI nanoparticles with starch and carboxymethyl cellulose (CMC). The use of stabilizers maintained the high specific surface area and high reactivity of the nanoparticles, and enables the nanoparticles to be used for treating contaminated subsurface. For example, CMC-stabilized ZVI nanoparticels can be delivered into subsurface soils for in situ remediation of aquifers contaminated with chlorinated solvents (He et al., 2010). However, when used for water treatment, the particle stabilization can create a problem, i.e. it can be challenging and costly to separate the highly stable nanoparticles from the

product water. Therefore, separation of the spent nanoparticles must be taken into account in preparing the nanoparticles while taking advantage of the novel features (e.g. high specific surface area and high sorption capacity) of the nanoparticles.

For the desired brine treatment, it was desired that the nanoparticles can offer both high sorption capacity and easy separation, and we hypothesized that the desired features can be achieved by use of starch as a bridging agent. Fig. 3-1 presents a conceptualized representation of such bridged nanoparticles. The starch bridging prevents the nanoparticles from aggregating, and thus, maintains their high sorption capacity. On the other hand, the polymeric molecules serve as a flocculating agent, enabling the particles to be flocculated and precipitated by gravity. The primary goal for this study was to develop and test such polymer-bridged magnetite nanoparticles for removal of arsenic from spent IX brine. The specific objectives were to: 1) prepare and characterize the starch-bridged magnetite particles, 2)determine arsenic sorption and desorption performances of the bridged nanoparticles, 3) test the pH effect, 4) elucidate arsenic binding mechanisms in terms of particle surface chemistry and binding modes, and 5) test the leachability of magnetite-bound arsenate in the spent particles (waste sludge).

3.2. Materials and methods

3.2.1. Chemicals

The following chemicals (ACS grade or higher) were purchased from Fisher Scientific (Pittsburgh, PA): Na_2SO_4, $NaHCO_3$, $FeCl_3$, NaOH, and HCl. A hydrolyzed potato starch and $Na_2HAsO_4 \cdot 7H_2O$ were obtained from Sigma-Aldrich (Milwaukee, WI), and $FeSO_4 \cdot 7H_2O$ was from Acros organic (Morris Plains, NJ). All solutions were prepared with ultrapure deionized (DI) (18.2 $M\Omega cm^{-1}$) water.

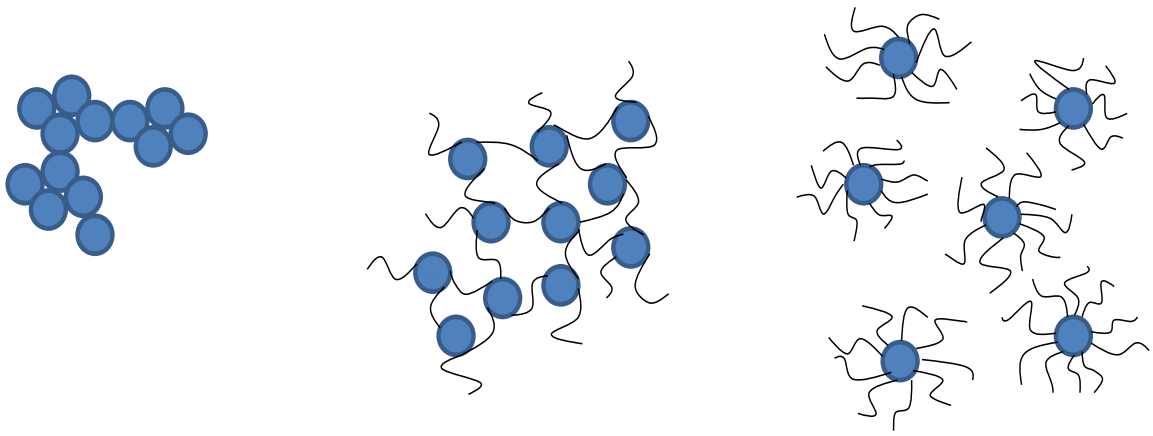

(a) **(b)** **(c)**

Fig. 3-1 A conceptualized illustration of stabilizer effect on particle interactions in aqueous solution: (a) particles aggregate without a stabilizer, (b) particles are bridged and form flocculates in the presence of proper concentrations of a polymeric stabilizer, and (c) particles remain stable in the presence of elevated concentrations of a polymeric stabilizer.

3.2.2. Synthesis of starch-bridged magnetite nanoparticles

The desired magnetite nanoparticles were prepared by modifying the co-precipitation approach in the presence of a suitable concentration of the water soluble starch. First, a solution of Fe^{3+} and Fe^{2+} (from $FeCl_3 \cdot 6H_2O$ and $FeSO_4 \cdot 7H_2O$, respectively) was prepared at a ferric-to-ferrous molar ratio of 2:1 at room temperature (21 ℃). To avoid oxidation during the preparation process, DI water was first deoxygenated by nitrogen purging.

An 0.8 wt.% starch solution was prepared by mixing 8g of the potato starch with 1 L of DI water and heating the mixture to 100℃. Once the starch solution started boiling, heating was removed and the solution was allowed for cooling at room temperature. The cooled starch stock solution was then mixed with the Fe^{3+}/Fe^{2+} solution under N_2 purging at a starch concentration ranging from 0 to 0.13 wt.%. Then, a 4M NaOH solution was added dropwise into the solution under vigorous stirring till a pH of around 11. Note that the change in color from brown to black indicates the formation of the nanoparticles (Schwertmann and Cornell, 2000). Then, the starch-magnetite solution was nitrogen-purged for 20 min. Finally, the suspension was sealed and placed in dark for 48 hrs to allow the magnetite nanoparticles to fully grow. Then the pH was lowered back to 7.0 with HCl, and then the suspension was used within 1hr. For comparison, bare magnetite particles were also prepared in the absence of starch but under otherwise identical conditions.

3.2.3. Physical characterizations

Transmission electron micrograph (TEM) images were taken with a Zeiss EM10 transmission electron microscope (Zeiss, Thornwood, NJ) operated at 40 Kv. The images were then processed using the ImageJ software (National Institute of Mental Health, Bethesda, MD), which gave the

mean size and size distribution of the particles. First, an aliquot of a nanoparticle suspension was diluted 10 times to facilitate the identification of particles and avoid "jamming" of the particles. The diluted suspension has a magnetite concentration of 0.057 g/L as Fe. Then, a single drop of the suspension was deposited on a 300 mesh copper specimen grid and allowed to air dry for at least three days before imaging. Zeta potentials (ζ) of particles in the particle suspension were measured with a Zetasizer nano ZS (Malvern Instruments, UK) at 25°C. A folded-capillary cell filled with 0.75 mL of the nanoparticle suspension was used for the measurements.

3.2.4. Kinetic tests

Batch kinetic tests were carried out to measure arsenate sorption rate for starch-bridged and bare magnetite particles. To determine the effect of starch concentration on arsenate sorption rate, suspensions of magnetite particles were prepared at 0.57 g/L as Fe in a series of vials with various concentrations (0 to 0.081 wt.%) of starch. For each case, 600 mL of the particle suspension was prepared. Under this range of starch concentration, the magnetite particles can be all precipitated by gravity. Then, 500 mL of the supernatant was removed from each vial. Arsenate sorption was then initiated by mixing each of the concentrated particle precipitate with 100 mL of a stock solution of simulated IX brine containing arsenate, sulfate, bicarbonate, and NaCl to yield a 200 mL mixture containing 300 mg/L As(V), 600 mg/L SO_4^{2-}, 305 mg/L HCO_3^-, 6 % (w/w) NaCl, and 1.7 g/L as Fe of magnetite particles (i.e. Fe-to-As molar ratio = 7.6). The reactors were then placed on a shaker and mixed continuously. At predetermined times, selected bottles were taken off the shaker and allowed to settle for 10 min, which was sufficient to remove >98% of the particles. Then, 2 mL of each supernatant was sampled with a pipette. The samples were then further centrifuged for 15 min at 6500 rpm (5857 g of RCF) to remove any remaining particles, and the supernatant was analyzed for arsenic.

3.2.5. Equilibrium sorption tests

A series of batch equilibrium sorption tests were performed with the starch-bridged magnetite nanoparticles. First, the particles were prepared at 0.57 g/L as Fe and with 0.049 wt.% of starch. This recipe offered the most effective removal of As based on kinetic test results. The particles were concentrated by decanting proper volumes of the supernatant, and the concentrated particles were then mixed with a stock solution of the simulated IX, which yielded the following initial concentrations: solution volume = 230 mL, SO_4^{2-} = 600 mg/L, HCO_3^- = 305 mg/L, NaCl = 6 wt.% (w/w), As = 38 ~ 617 mg/L, and magnetite = 1.0 g/L as Fe. The systems were equilibrated under shaking at 200 rpm on platform shaker (New Brunswick Scientific, NJ) for 2 days. The solution pH was kept at either 5.0 or 6.9 through intermittent adjusting using 0.1 M NaOH or 0.1 M HCl. The following mass balance equation was employed to determine the arsenate uptake:

$$q_e = \frac{V(C_o - C_e)}{M} \tag{3-4}$$

where q_e (mg/g) is the equilibrium mass uptake of arsenic, V (L) is the solution volume, C_0 and C_e (mg/L) are the initial and final concentration of arsenic, respectively, and M (g) is the mass of sorbent added calculated as Fe.

3.2.6. FTIR analysis

FTIR was employed to determine arsenate sorption mechanisms and interactions between starch and the magnetite nanoparticles. Three representative samples, namely bare magnetite particles and starch-bridged magnetite nanoparticles before and after the arsenic sorption, were subjected to FTIR and compared. The samples were first vacuum-dried, and then ground in a mortar to fine

powders, which were then mixed with KBr at a sample-to-KBr ratio of 5:95 by weight. The mixtures were pressed at 9 metric tons for 2 min. The specimens were then scanned and characterized using an IR Prestige-21 spectrometer (Shimadzu) over the wave number range from 400 to 4000 $cm^{-1.}$

3.2.7. Leachability tests

In the treatment process, arsenic is co-precipitated with the nanoparticles. As a result, an As-laden process solid waste will be produced. To avert from being categorized as a hazardous waste, the waste must pass a certain leachability test such as TCLP of US EPA and the California waste extraction test (WET). To assess the arsenic leachability in waste sludge, TCLP was carried out according to EPA Method 1311 on air-dried waste sludge samples. The #1 extraction fluid for the TCLP was prepared by adding 5.7 mL glacial CH_3COOH and 64.3 mL of 1 N NaOH to 500 mL DI water, and then adding DI water to 1 L. Solid samples were mixed with the TCLP fluid at a solid-to-liquid ratio of 1:20. The mixtures were then rotated at 30 rpm for 18 hr at room temperature and then centrifuged for 30 min at 6500 rmp (5857 g of RCF). The supernatant was then passed through a 0.45 µm filter and analyzed for arsenic. The leachability tests were performed in duplicate.

3.2.8. Chemical Analysis

Solution or suspension pH was measured using an Oakton pH meter (pH 510 Benchtop Meter, Oakton). Arsenic was analyzed using a Perkin Elmer Atomic Adsorption Spectrophotometer, which has a detection limit of 3 µg/L as As. Dissolved iron was measured using a Flame Atomic Absorption Spectrometer (Varian Spectra 220 FS) (detection limit = 0.05 mg/L). Chloride,

sulfate and bicarbonate were analyzed using a Dionex Ion Chromatograph (Model DX-20) equipped with an AS 14 column.

3.3. Results and discussion

3.3.1. Physical characteristics of starch-bridged magnetite nanoparticles

The physical properties of the starch-bridged magnetite nanoparticles, including their morphology, mean size, and size distribution, were measured by TEM. Fig. 3-2 shows the TEM images of a typical starch-bridged magnetite sample, prepared at 0.57 g/L as Fe with 0.049 wt.% of starch. Based on a total particle count of 176 from this image, a mean particle diameter of 26.6 nm for the sample was obtained, with a standard deviation (SD) of 4.8 nm. The TEM image reveals that the starch-magnetite nanoparticles are nearly spherical in shape and have a relatively narrow size distribution. The histogram shows that 74% of the particles were within the range 21-30 nm. No particles smaller than 10 nm or bigger than 50 nm were observed. The TEM image also suggests that the nanoparticles are inter-bridged yet remain identifiable individual nanoparticles, i.e. the particles did not aggregate into larger solid particles because of the coating of starch on the nanoparticles.

Fig. 3-3 indicated that starch can strongly affect the particle settleability. At relatively low concentrations of stabilizer (e.g. 0.081 wt.% or less starch for 0.57 g/L as Fe of magnetite particles), the nanoparticle surface has sufficient open sites to allow a starch molecule to bind with multiple nanoparticles. As a result, the nanoparticles were bridged and large flocs were formed that precipitated easily. For example, based on the concentration of iron in the supernatant, 99.5 % and 98.2 % of the particles bridged with 0.049 wt.% and 0.081 wt.% starch, respectively, were removed by gravity after 1 hr of settling (Fig. 3-3). At elevated starch

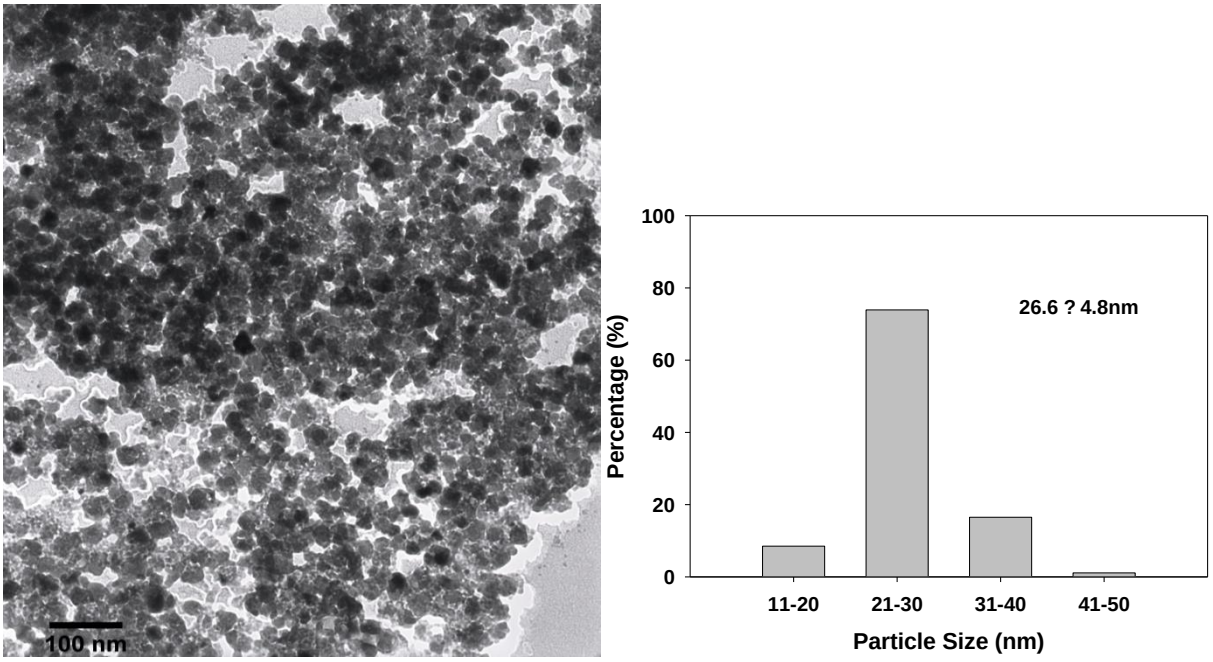

Fig. 3-2 TEM images and size distribution of starch-bridged magnetite nanoparticles prepared at 0.057 g/L as Fe in the presence of 0.049 wt.% starch.

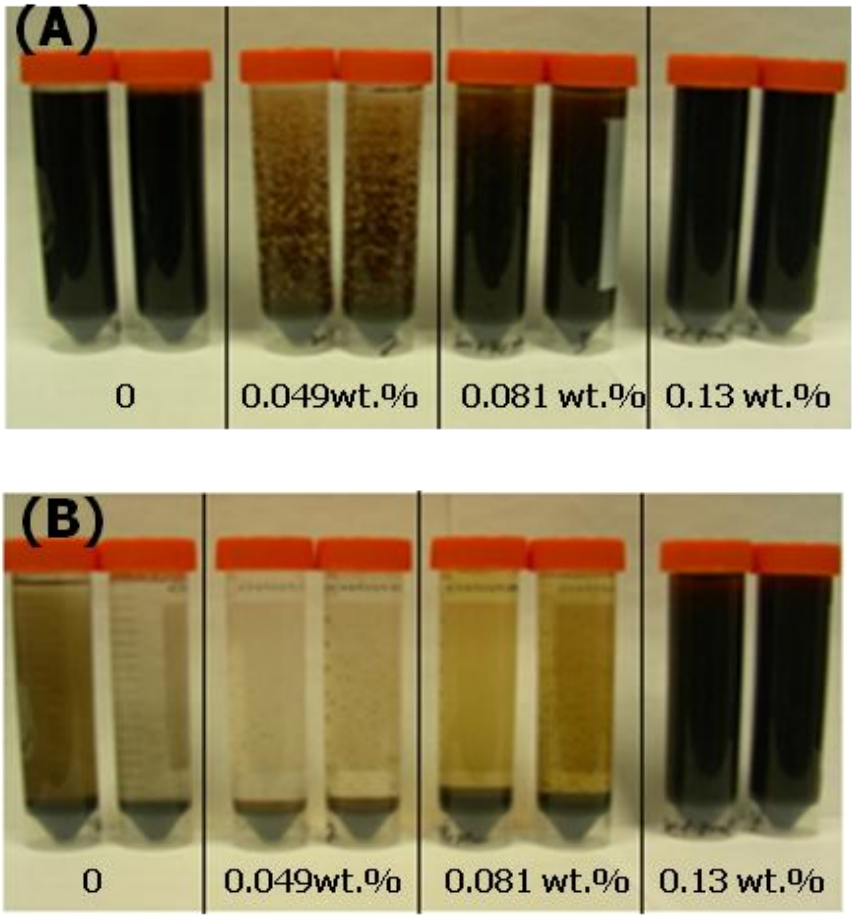

Fig. 3-3 Effect of starch and NaCl on separation of magnetite particles by gravity: (A) immediately after particle preparation, (B) after 1 hr of settling. Numbers under vials refer to starch concentration. For each pair of vials, the left one had no NaCl added, while the right one contained 6% NaCl.

concentrations, the surface of each particle is covered with a denser layer of the stabilizer molecules, which induce a strong steric repulsion force preventing the particles from aggregating or inter-bridging (Fig. 3-1). It is noteworthy that the bridged nanoparticles displayed even better settleability than the bare particles. For instance, the 1-hr particle removal in Fig. 3-3 for the bare particles (without salt addition) was 95.2 %.

The starch stabilizer is a neutral polymer and it stabilizes nanoparticles through steric repulsion arising from the osmotic force when the starch layers overlap as the particles collide. Results from Fig. 3-3 revealed that the presence of 6% NaCl did not affect the settleability of the starch-bridged or starch-stabilized nanoparticles, suggesting strong steric repulsion effect between starched particles. In contrast, the salt addition increased the particle aggregation for the bare magnetite particles, which is in accord with the classical double layer compression theory. More detailed discussion on salt effect is provided in Section 3.4.

3.3.2. Kinetic tests

Fig. 3-4 shows arsenate adsorption rates and removal efficiency at a fixed dosage (1.7 g/L as Fe) of magnetite but various levels of starch ranging from 0 to 0.081 wt.%. In most cases, equilibrium was reached within 4 h with most sorption capacity filled within the first 1 h. This rather fast sorption kinetics supports the assertion that the nanoparticles were present in the form of starch-bridged individual non-porous particles (Figs. 3-1 and 3-2) rather than as aggregated micro-porous sorbents (Cornell, 2003). As the starch concentration increased from 0 to 0.012, 0.024, 0.041, and 0.049 wt.%, the equilibrium arsenic removal increased from ~20% for bare magnetite to 42, 82, 97, and ~99%, respectively. This observation clearly revealed that the presence of starch during particle

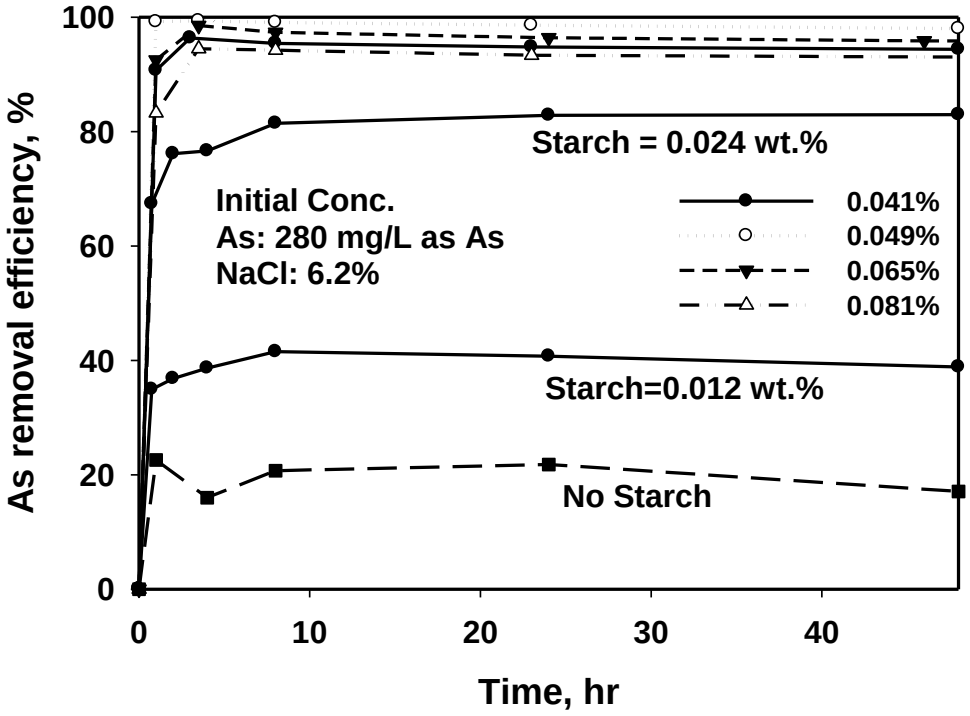

Fig. 3-4 Arsenic removal as a function of time using magnetite particles at various starch levels in a simulated IX brine. Experimental conditions: Fe/As molar ratio = 7.6; starch = 0-0.081 wt.%; Magnetite = 1.7 g/L as Fe (initially prepared at 0.57 g/L); Solution pH was kept at 6.5.

nucleation and growth prevented particle aggregation and resulted in much great specific surface area. In the range of 0.012 to 0.049 wt.%, a higher starch concentration resulted in more loosely bridged particles that are more accessible to arsenic. If the starch concentration is too low, particles are more tightly connected or even aggregated, resulting in greater mass transfer resistance and loss in surface area. However, further increasing starch concentration beyond the critical value of 0.049 wt.% diminished both sorption capacity and kinetics. At elevated starch concentrations, more stabilizer molecules are coated on individual nanoparticles, resulting in steric repulsion between the particles, and thus, the nanoparticles became fully stabilized (Figs. 3-1 and 3-3). Although these well stabilized nanoparticles may offer comparably great specific area, the dense starch layer on the particle surface hinders arsenic uptake both thermodynamically (due to reduced sorption sites and site accessibility) and kinetically (due to increased mass transfer resistance).

Consequently, there exists an optimum starch concentration for a given magnetite concentration to facilitate optimal arsenic removal and yet allow for an easy separation of spent nanoparticles. In this case, 0.049 wt.% appeared to be optimal for preparing 0.57 g/L as Fe of the bridged magnetite nanoparticles.

3.3.3. Isotherm tests and FTIR analysis

Fig. 3-5 shows arsenate sorption isotherms for the starch-bridged magnetite nanoparticles (initially prepared at 0.57 g/L as Fe and with 0.049 wt.% starch) at an equilibrium pH of 5.0±0.1 and 6.9±0.1, respectively. Again, the simulated IX brine was used in the isotherm tests. The classical Langmuir isotherm model, Eq. (3-5), was employed to interpret the

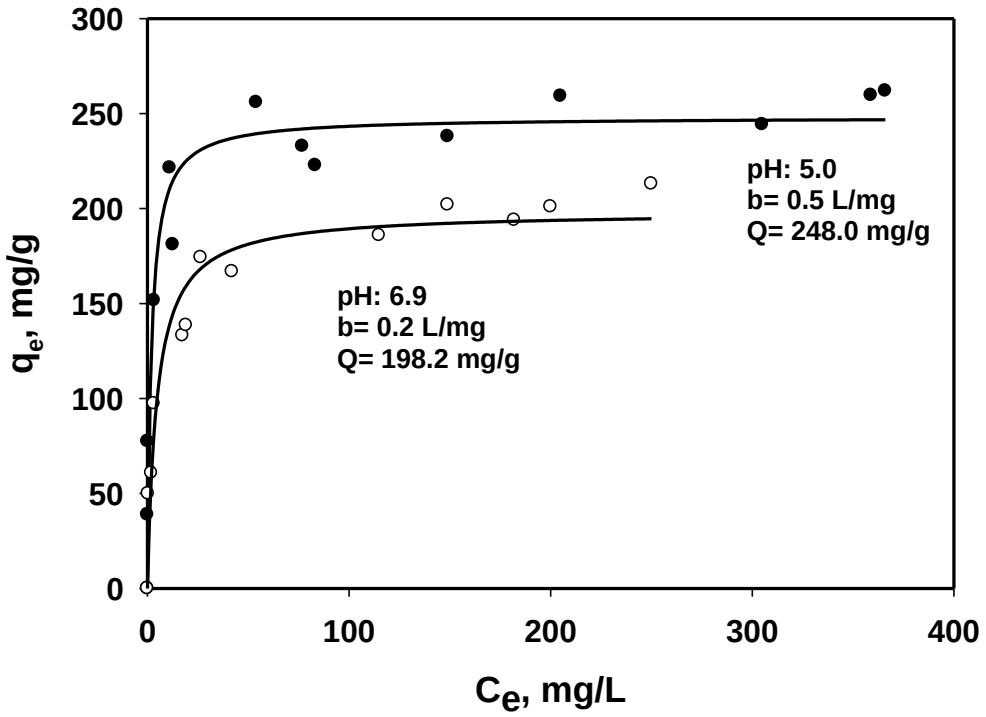

Fig. 3-5 Arsenate sorption isotherms for starch-bridged magnetite particles at pH 5.0 and pH 6.9 (final pH) from a spent brine solution (symbols: observed data; lines: Langmuir model fits). Brine compositions: initial As(V) = 38 - 617 mg/L, SO_4^{2-} = 600 mg/L, HCO_3^- = 305 mg/L, NaCl = 6 wt.% (w/w).

experimental data. The best data fitting gave both maximum adsorption capacity (*Q*) and the Langmuir affinity constant (b).

$$q_e = \frac{bQC_e}{1+bC_e} \tag{3-5}$$

The resulting *Q* is 248 mg/g at pH 5.0±0.1, and 198 mg/g at pH 6.9±0.1. To our knowledge, these values are much greater than those reported for other iron oxides including magnetite particles reported to date. Earlier, Yean et al. (2005) reported a *Q* value of 152 µmol/g (11.4 mg/g as As) at pH 4.8 and 101 µmol/g (7.6 mg/g as As(V)) at pH 6.1 for commercial aggregated magnetite nanoparticles of a mean size of 20 nm, and obtained a much higher *Q* value of 172.5 mg/g as As(V) using magnetite of 11 nm mean size synthesized using oleic acid as a stabilizer. A magnetic separator was needed to separate the fully stabilized particles. Later, Yavuz et al. (2006) synthesized magnetite nanoparticles (mean size = 12 nm) stabilized with a surfactant (Igepal CO 630) and reported a *Q* value of 200 mg/g as As(V). Ohe et al. (2005) prepared magnetite by precipitation of ferric and ferrous at pH 12 without any stabilizer and reported a *Q* value of 171 mg/g as As(V). Granular ferric hydroxide (GFH) (mean size = 0.32 – 2 mm) (Banerjee et al., 2008) and maghemite (γ-Fe_2O_3) (mean size = 3.8 nm) (Tuutijärvi et al., 2009) showed a *Q* value of 1.1 and 50 mg/g, respectively.

FTIR spectroscopy was used to identify the nature of the chemical bonding between magnetite, starch, and arsenate. Fig. 3-6 shows the FTIR spectra for bare magnetite particles and starch-bridged samples before and after sorption of arsenate. The absorption band at 571 cm^{-1} was obtained for all three types of magnetite samples tested, and it can be assigned to the Fe–O stretching vibration for the Fe_3O_4 particles (Cornell

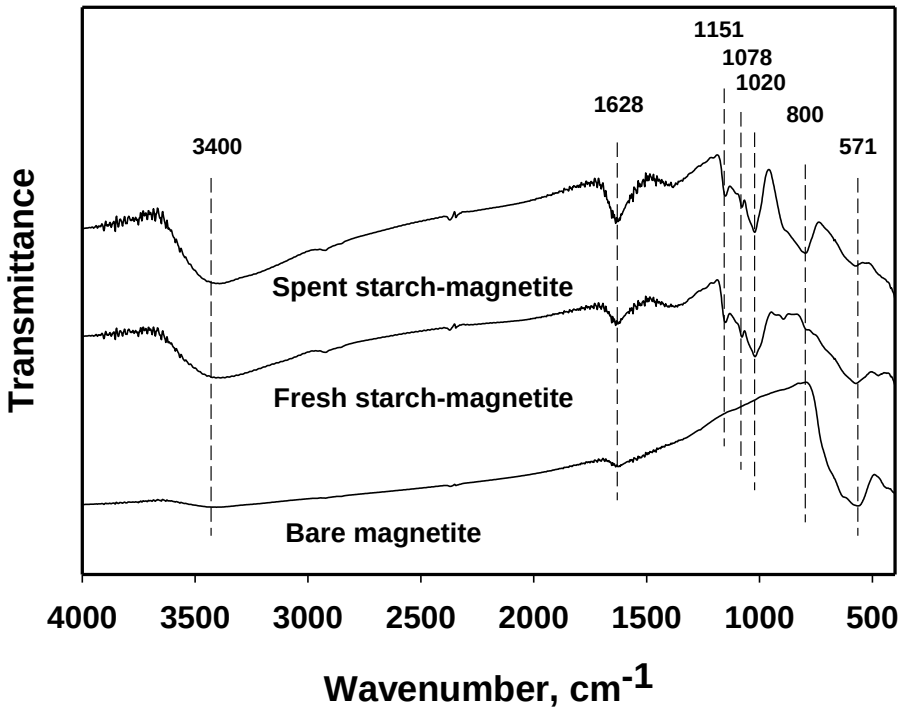

Fig. 3-6 FTIR spectra of arsenate on bare, fresh starch-bridged, and arsenate-loaded starch-bridged magnetite particles. Magnetite particles were prepared at 0.57 g/L as Fe with 0.049 wt.% of starch. Arsenate was loaded at pH 5. Arsenic loaded on nanoparticles = 250 mg/g as As.

and Schwertmann, 2003). The presence of starch coating reduced the absorption of the radiation by the core magnetite, and thus, weakened the peak intensity for the two starch-coated samples. As starch mainly consists of amylose and amylopectin, three new peaks appeared at 1020, 1151, and 1078 cm^{-1}, respectively, for starched magnetite particles. The peaks at 1151 and 1078 cm^{-1} represent the C-O stretching vibrations in the C-O-H groups, whereas the 1151 cm^{-1} peak corresponds to the C-O stretching vibration in the C-O-C groups, which is in agreement with previous amylose studies (Huang et al., 2006). A peak at 1628 cm^{-1} and another at 3400 cm^{-1} were observed for all three samples though the intensities varied. The weakest peaks were observed for the bare magnetite, corresponding to the O-H bond from H_2O (Maity and Agrawal, 2007). The peaks were greatly intensified for the starch-bearing magnetite due to the H-bonded OH groups of amylose and amylopectin of starch, which agrees with the results by Maity and Agrawal, 2007 (Huang et al., 2006).

Comparing the spectra of the starch-bridged magnetite before and after arsenate sorption, a new broad band was evident between 750 and 850 cm^{-1} for the arsenate-laden magnetite. According to Goldberg and Johnston (2001) who conducted FTIR study of As(V) sorption to amorphous iron oxide, the band could be assigned to the Fe-O-As groups. This is consistent with the results by Pena et al. (2006) who observed an FTIR band at 808 cm^{-1} at pH 5 for As(V) sorbed on TiO_2 and ascribed the band to the Ti-O-As groups. Pena et al. (2006) also compared FTIR bands for sorbed and dissolved arsenate species, noted a marked shift in the band positions of arsenate upon sorption. For dissolved $H_2AsO_4^-$, two peaks were observed at 878 and 909 cm^{-1} corresponding to the symmetric and asymmetric stretching vibrations of As-O bonds. Upon adsorption, the peaks were shifted to 808 and 830 cm^{-1}, respectively. According to Goldberg and Johnston (2001) and Pena et al. (2006), the shift on band positions was attributed to symmetry

reduction resulting from inner-sphere complex formation (i.e. formation Fe-O-As complexes). Goldberg and Johnston (2001) also reported that for arsenate sorbed on amorphous iron oxide, there existed two distinct bands corresponding to surface complexed and non-surface-complexed As-O groups, respectively. In our case, however, only one single band was observed and the wave number was shifted to ~800 cm^{-1}, indicating that surface complexation was the predominant mechanism for arsenate sorption to the starch-bridged nanoparticles. In addition, Zhang et al. (2005) reported that the rise in M-As-O (M: metal) peak was coupled with weakening of M-OH peak when As(V) was adsorbed to Fe-Ce oxide, and the researchers ascribed this phenomenon to ion exchange reaction between –OH and arsenate anions. However, no M-OH bond was evident in this work, suggesting that the sorption of As(V) to the magnetite nanoparticles did not necessarily conform to the standard ion exchange stoichiometry.

3.3.4. Effect of salt concentration on arsenic removal

Fig. 3-7 shows equilibrium arsenic uptake in the presence of various concentrations of NaCl ranging from 0% to 10% but under otherwise identical conditions. Evidently, the presence of brine at concentrations as high as 10% did not show any appreciable decrease in arsenic uptake. This observation violates the principle of selectivity reversal commonly cited in standard ion exchange regeneration (Clifford, 1999). However, this supports that FTIR results that specific interactions such as strong inner sphere complexation other than ion pairing was involved between arsenic and the nanoparticles. To quantify the relative affinity, the arsenate and chloride binary separation factor $\alpha_{As/Cl}$ is calculated based on the equilibrium sorption data (Clifford, 1999):

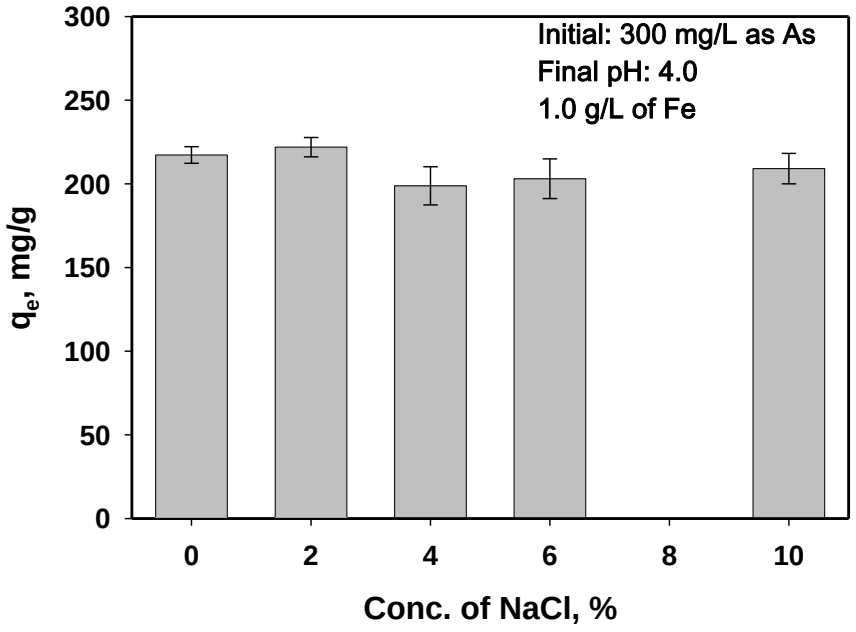

Fig. 3-7 Arsenate uptake by starch-bridged magnetite nanoparticles in the presence of various concentrations of NaCl ranging from 0 to 10%. The magnetite particles were initially prepared at 0.57 g/L as Fe with 0.049 wt.% of starch.

$$\alpha_{As/Cl} = \frac{q_{As} C_{Cl}}{C_{As} q_{Cl}} \tag{3-6}$$

where q_{As} and q_{Cl} are the concentrations of arsenate and chloride, respectively, in the solid phase; whereas C_{As} and C_{Cl} are the concentration of arsenate and sulfate in the solution, respectively. As a rule, a separation factor value of greater than one indicates greater selectivity for arsenate than chloride. The calculated $\alpha_{As/Cl}$ values were 102, 139, 147, and 290 at 2%, 4%, 6%, and 10% of NaCl, respectively, indicating the nanoparticles' affinity for arsenate far exceeds that for chloride.

The observed minimal salt effect on arsenic removal contrasts with the results reported by Shipley et al. (2009), who found that increasing ionic strength to 0.1 M with KNO_3 decreased arsenate adsorption by 10% with a commercial bare magnetite of 20 nm size. The authors explained the phenomenon with the classical double layer compression theory. In the presence of high concentrations of cation (K^+), the electrostatic double layer thickness on the particle surface is reduced, increasing the likelihood of nanoparticle aggregation and thus decreasing the available surface area during arsenate adsorption. Aggregation of bare magnetite particles was observed immediately after the particles were prepared, and the bare magnetite precipitated faster with 6% NaCl than without the salt addition (Fig. 3-3B). However, for starch-bridged magnetite particles, the particles were bridged yet held apart due to the interparticle steric repulsion arising from the osmotic force of the starch on the particle surface. In the presence of salt, the starched particle surface potential was almost zero throughout the pH range (see Section 3.5) and increasing ionic strength did not affect the surface charge as the ionic strength exerts little impact on the steric repulsion. Consequently, the high sorption capacity was maintained even in the presence of the extremely high concentrations of NaCl.

3.3.5. Effect of pH and chemical stability of starch-bridged nanoparticles

Solution pH can affect both arsenate speciation (pKa values for H_3AsO_4 are 2.2, 7.0 and 11.5) and surface charge of the starch-bridged nanoparticles. In addition, the nanoparticles may be partially dissolved under low pH. Therefore, it is expected that pH will affect the arsenate sorption capacity. Fig. 3-8 shows equilibrium arsenate uptake as a function of final solution pH for bare and starch-bridged magnetite, under otherwise identical conditions. In terms of sorption capacity, the starch-bridged nanoparticles displayed an overall much greater arsenic uptake capacity than the bare particles throughout the pH range tested. In addition, the pH sensitivity also differed markedly for the two classes of sorbents. While lower pH favored arsenate sorption for both cases, the bare particles were much more sensitive to pH. For instance, at pH <7.0, arsenic uptake for the bare particles increased sharply and nearly linearly with decreasing pH. In contrast, a maximum sorption plateau was evident in the pH range of 4 to 6 for the starch-bridged magnetite, indicating that the starch coating not only resulted in greater sorption capacity, but altered the surface potential of the particles. When the 2-day and 50-day sorption data are compared, greater capacity was observed at pH below ~5 for starch-bridged particles, suggesting that the starch-coating somewhat hindered the sorption kinetics. Ma and Bruckard (Ma and Bruckard, 2010) reported that adsorption of a cornstarch to kaolinite can be strongly affected by solution pH with lower pH favoring the starch uptake. The same adsorption trend for potato and cornstarch was obtained by Husband (1998). A microscopic study by Hirashima et al. (2005) revealed that more glucose chains were leached out from starch macromolecules as pH was decreased from 6.0 to 3.6, resulting in elevated solution viscosity. Based on these findings, the observed slower arsenic removal kinetics at pH <5 can be attributed to: 1) increased sorption of starch at lower pH, 2) elevated viscosity, and 3) sorption of the leached glucose chains and the

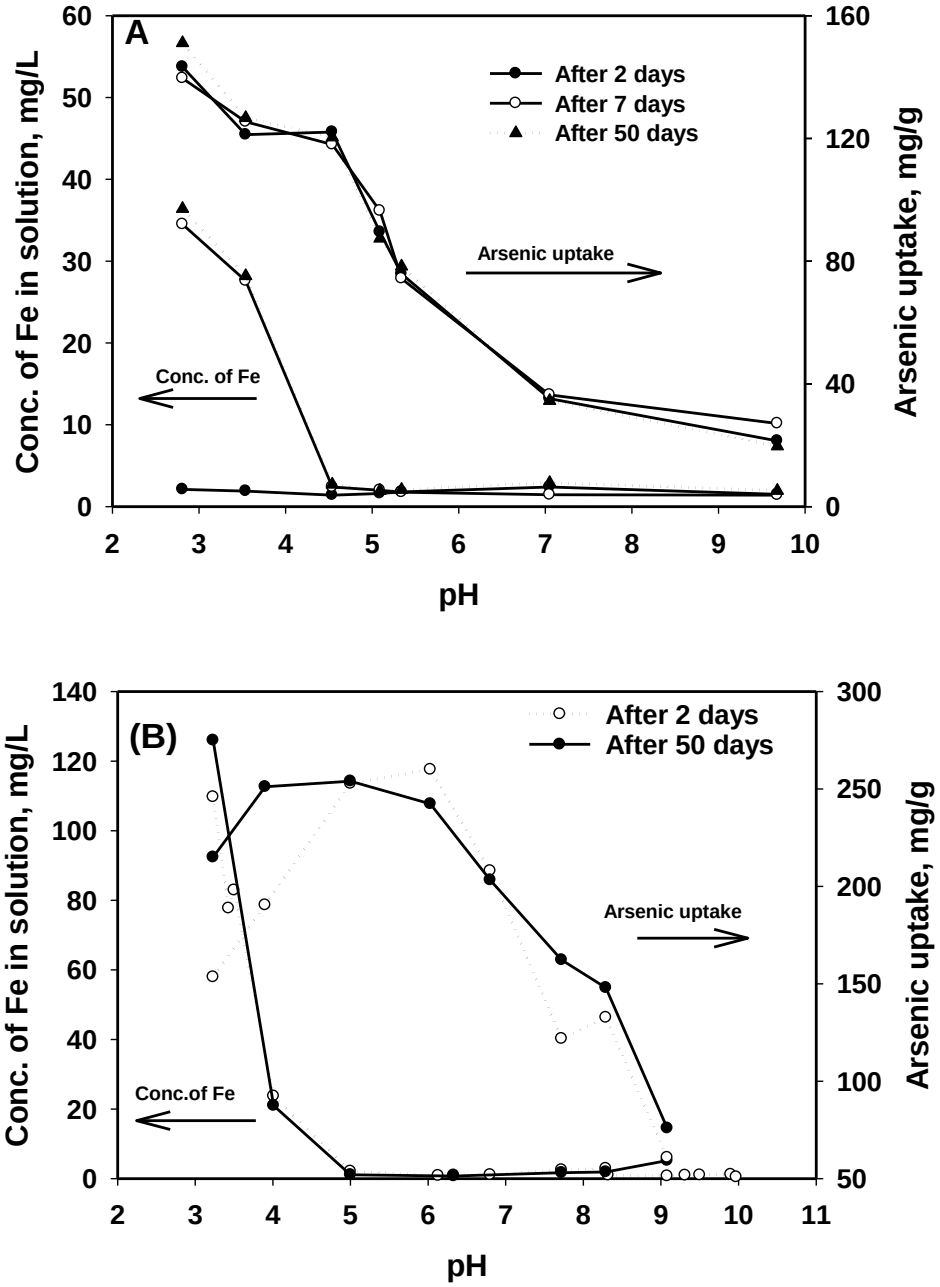

Fig. 3-8 Arsenate uptake and dissolved Fe concentration as a function of pH: (A) bare magnetite particles after 2, 7 and 50 days, and (B) starch-bridged magnetite (prepared at 0.57 g/L and with 0.049 wt.% starch) after 2 and 50 days. Initial As concentration = 300 mg/L, Magnetite = 1.0 g/L as Fe.

break-down smaller segments of starch, all of which are in favor of a greater mass transfer resistance, and thus, slower sorption rate.

However, it should be noted that the diminished arsenic uptake at pH below 5 can be in part attributed to dissolution of the nanoparticles. Figs. 3-8A and -8B indicate that while both bare and starch-bridged particles became partially dissolved at pH <4, the starch-bridged particles were more prone to acid dissolution than the bare particles. For example, 13% of starch-bridged nanoparticles at pH 3.2 was dissolved compared to 3.2% for the bare particles at pH 2.8. At pH $\geq$5.0, the particles are chemically robust.

Fig. 3-9 shows the measured zeta potential for the particles as a function of solution pH and under various conditions. Fig. 3-9A plots ζ for bare magnetite particles and those prepared with, respectively, 0.025, 0.049, and 0.081 wt.% of starch over a wide range of pH. Based on the results, the pH at the point of zero charge (pH_{PZC}) was estimated to be ~6.1 for the bare particles whereas pH_{PZC} for the starched particles varied from 3.7 to 4.4. The value for the bare magnetite particle is slightly lower than those reported. Prakash et al. (1999), Anastassakis (1999), and Yean et al. (2005) have reported a pH_{PZC} of, respectively, 6.8, 7.0, and 6.8, for various bare colloidal magnetite particles. It is noteworthy that the presence of starch greatly shielded the sensitivity of ζ to the potential-determining ions (H^+/OH^-). For example, between pH 5 and 8, the ζ value varied from +20 to -40 mV for the bare particles, but only -2 to -12 mV with 0.081 and 0.049% starch. When the starched particles are compared, Fig. 3-9A reveals that the presence of higher starch concentrations (0.081 and 0.049%) resulted in a much less negative surface potential than the case of 0.025% of starch. Evidently, the sorbed starch, a neutral polymer with dense H-bonding (Biggs, 2006; Ravishankara et al., 1995), on the surface of magnetite serves as a strong surface buffer that diminishes the effect of H^+/OH^- on the surface charge.

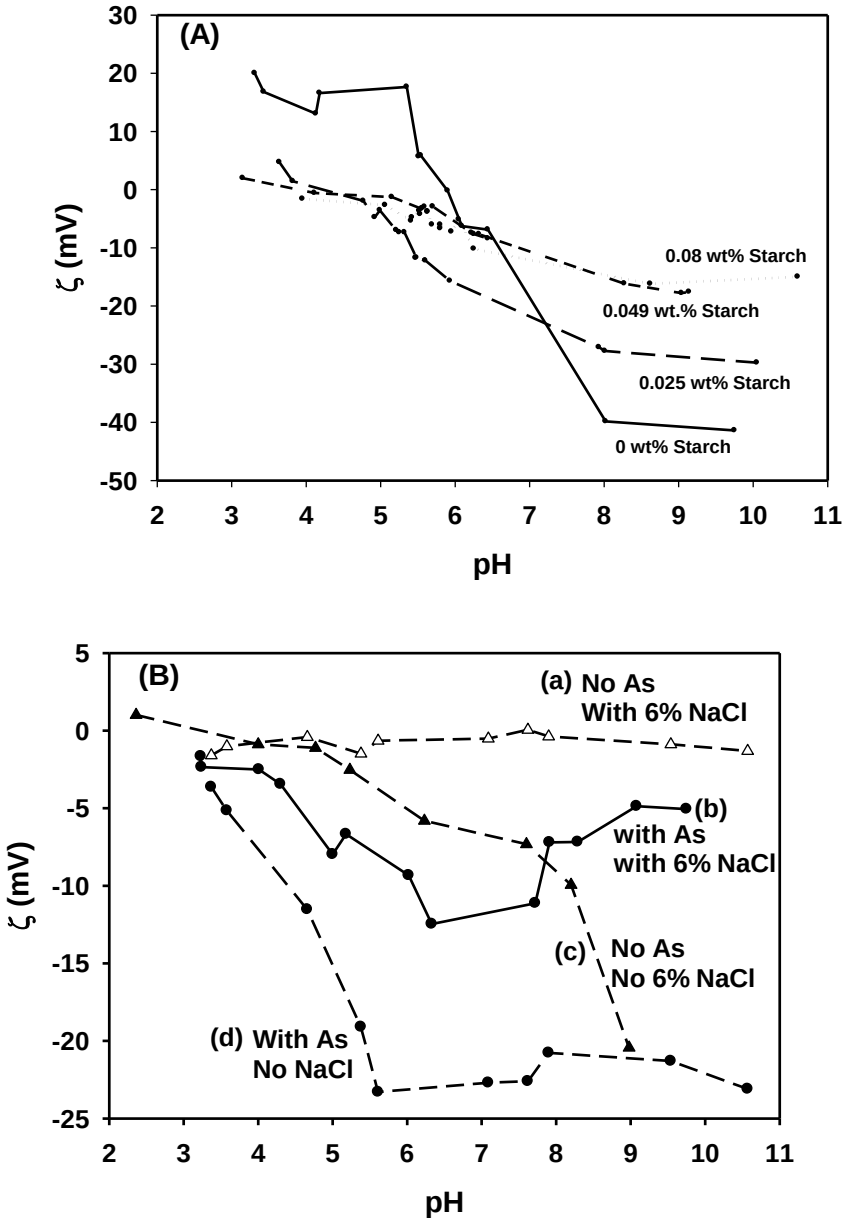

Fig. 3-9 (A) Zeta potential (ζ) as a function of pH for magnetite nanoparticles synthesized with different concentrations of starch at a fixed magnetite concentration of 1.0 g/L as Fe; (B) Effects of salt and sorbed arsenate on ζ of starched bridged magnetite nanoparticels (Magnetite prepared at 0.57 g/L as Fe with 0.049 wt% starch, As in solid phase = 242 mg/g).

Fig. 3-9B shows the effects of 6% NaCl and sorbed arsenate anions on the surface potential of starched magnetite particles. It is evident by comparing curves (a) and (c) that the presence of 6% NaCl nearly zeroed the negative ζ of the starched magnetite particles over the wide pH range. This is consistent with the classical double-layer compression theory and is attributed to the associated suppression effect of the surface potential due to elevated surface density of Na^+ ions. An examination of curves (a) vs. (b) and (c) vs. (d) indicates that sorption of arsenate anions induced a marked negative potential especially in the pH range of 5 to 8. This observation again suggests that sorption of arsenate ions, which are present as monodentate (pH<7) or bidentate (pH>7) anionic ligands, is not a simple ion pairing or ion exchange process, but rather, involves more specific interactions such as Lewis acid-base interaction in accord with the inner sphere complexation between arsenate's donor atoms (oxygen) and the acceptors (Fe) of the magnetite. Note that at pH > 8, although arsenate is present as bidentate ligands, the competition of hydroxyl anions becomes fiercer. As a result, arsenate uptake was actually reduced and the surface negative potential was suppressed as well (curve b).

3.3.6 Leachability of arsenic from magnetite waste

TCLP has been widely employed in the U.S. to determine if a process waste may be disposed of in landfills (Phenrat et al., 2008). To probe the arsenic leachability, the arsenic-laden magnetite precipitate was air-dried and subjected to the TCLP procedure. Fig. 3-10 shows that the TCLP leachability varied with iron dosage during the As removal treatment. Increasing the Fe/As molar ratio from 5 to 15 resulted in a 90% decrease in the leached arsenic concentration, and at an Fe/As molar ratio of 15, the precipitate satisfied the current TCLP limit of 5 mg/L As. Nonetheless, the long-term arsenic stability under real landfill conditions needs to be further investigated due to the intrinsic limitation of the TCLP method (Ghosh et al., 2004).

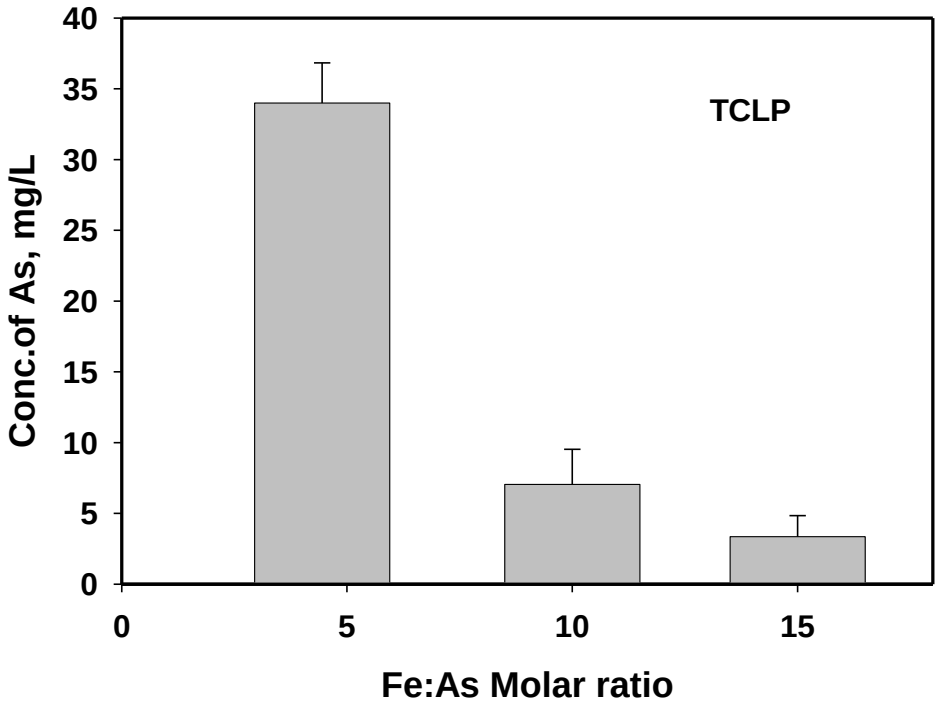

Fig. 3-10 Leachability of arsenate from spent starch-bridged magnetite precipitates when subjected to TCLP. The Fe:As molar ratio indicates the amount of magnetite applied in relation to the As concentration during the As removal treatment. Data plotted as mean of duplicates, errors indicate deviation from the mean

3.4. Conclusions

The major findings from this study are summarized as follows:

- A water-soluble potato starch was successfully used as a bridging agent to prepare a class of bridged magnetite nanoparticles. Based on TEM images, the starch-bridged nanoparticles displayed a mean particle size of 26.6 ± 4.8 nm.
- Batch kinetic tests revealed that the concentration of starch can substantially affect the arsenic sorption capacity. The optimum starch concentration for 0.57 g/L as Fe nanoparticles was found to be 0.049 wt.%. Based on the kinetic data, the starched nanoparticles removed 5 times more arsenic than bare magnetite particles under otherwise identical conditions, yet the bridged nanoparticles can be easily separated from water by gravity.
- The maximum Langmuir capacity for As(V) sorption was determined to be 248 mg/g at pH 5.0 in the presence of 6% of NaCl. Because of the starch coating, the high arsenate sorption capacity was not diminished as NaCl concentration was increased to 10%.
- The starch coating rendered the sorbent less sensitive to pH change and the sorbent high arsenic capacity was observed over a broader pH range, compared to bare magnetite particles. The maximum arsenate uptake was obtained in the pH range of 4 to 6 for the starched nanoparticles.
- FTIR and surface potential analyses suggested that arsenate was sorbed to the starch nanoparticels through inner-sphere surface complexation (Lewis acid-base interaction) between the electron-pair acceptor (Fe) of magnetite and the donor (O) of arsenate.
- Sorption of starch to the nanoparticles greatly altered the surface potential, resulting in an unusual near-zero surface potential in the presence of 6% NaCl over a wide pH range.

- The nanoparticles were chemically stable and did not dissolve at pH >5. At pH 3.2, 13% of the starched magnetite was dissolved over a 50 day period.
- At an Fe-to-As molar ratio of 5, the arsenic laden precipitate was able to pass the 5 mg/L TCLP standard set by US EPA.

Chapter 4. Immobilization of As(III) in a Soil Using Polysaccharide-Modified Fe-Mn Nanoparticles

This chapter studies the oxidation of As(III) using stabilized Fe-Mn nanoparticles in water treatment. Batch arsenic adsorption tests as a function of pH and isotherm tests varying pH are used to investigate the adsorption capacity. Stabilized Fe-Mn nanoparticles using CMC as a stabilizer are successfully prepared and are applied to increase arsenic immobilization from As(III) loaded sandy soil. It is shown that the stabilized Fe-Mn nanoparticles are highly mobile in sandy soil and are very effective for arsenic immobilization.

4.1. Introduction

Because of our growing knowledge on arsenic toxicity, regulations on arsenic (As) in drinking water have been tightened worldwide. In 2006, the U.S. EPA has enforced a revised maximum contaminant level of 10 μg/L As in drinking water, which is 5-fold tightening from its previous standard. Accordingly, cost-effective treatment technologies have been consistently sought for decades.

Arsenic naturally exists in both inorganic and organic forms. Of the two, naturally occurring organic arsenic if of less a concern because of its lower toxicity and its susceptibility of transforming inorganic arsenic species (Jackson et al., 2003). The most common inorganic species of arsenic take the oxidation state of either As(III) or As(V), depending on the environmental conditions. In general, As(V) exists in aerobic condition whereas As(III) is

dominant in anaerobic conditions such as those typically found in ground water or soil (Smedley and Kinniburgh, 2002). For examples, in a groundwater of Aquia, MD, USA, arsenic was detected at 18.2 μg/L as As(III) and 2.1 μg/L as As(V) (Haque et al., 2008). Comparing As(III) and As(V), As(III) has been known to be 25-60 times more toxic and is also more mobile than As(V) (Jain and Ali, 2000).

Among the most cited As removal technologies are adsorption, enhanced coagulation, membrane filtration, and electrolysis (Chen et al., 1999). While quite promising, most of the technologies are more effective for removing As(V) than for As(III). For example, standard anion exchanger resins can only remove As(V) oxyanions under normal groundwater conditions (Clifford and Lin, 1991). Hering et al. (1996), Kang et al. (2000), and Jang et al. (2005) studied the removal of As(V) and As(III) from water through enhanced precipitation/coprecipitation, reverse osmosis (RO), and adsorption by hydro ferric oxide (HFO), respectively. Their results revealed that the removal efficiency of As(III) is generally less than that of As(V), and competitive As(III) and As(V) removal was only observed at alkaline pH when arsenite is dissociated.

Under typical groundwater water conditions (e.g. pH 6-8), As(III) exists mainly as the nonionic form H_3AsO_3, whereas the dominant As(V) can exist as anionic $H_2AsO_4^-$ and/or $HAsO_4^{2-}$. The pK_a values are 2.2, 7.0, and 11.5 for arsenate, and 9.2, 12.1, 13.4 for arsenite. Typically, the As(V) oxyanions are more favorably adsorbed by various metallic adsorbents such as cupric oxide and magnetite than the neutral As(III) species (Martinson and Reddy, 2009; Su and Puls, 2008). As a result, conventional water treatment technologies are often less effective for removing As(III) species, and often times, an additional oxidation unit is required to concert As(III) to As(V).

However, the oxidation kinetics of As(III) by air has been found very slow. For example, Clifford et al. (1983) reported that 25% of As(III) in a solution was oxidized in 5 days by purging with air. To speed up the reaction rate, the following enhanced oxidation techniques have been employed to oxidize As(III) to As(V): use of pure O_2 (Frank and Clifford, 1986; Cullen and Reimer, 1989), H_2O_2 (Pettine, 1999), O_3 (Kim and Nriagu, 2000), chlorine (Dodd et al., 2000), UV/H_2O_2 (Yang et al., 1999), UV/TiO_2 (Yoon and Lee, 2005; Bissen et al., 2001), Fe(II)/H_2O_2 (Krishna et al., 2001; Hug and Leupin, 2003), and bio-catalyzed oxidation (Lytle et al., 2007). Unfortunately, this additional oxidation step often proves unpractical either for its prohibitively high cost or the associated adverse impacts on the water quality. For examples, biological processes are less suitable for drinking water treatment, and oxidation with pure oxygen is slow and rather costly. The oxidation of As(III) with H_2O_2 was found to be limited by solution pH: H_3AsO_3 (pK_{a1} = 9.22) cannot be oxidized by H_2O_2 below pH 9 (Pettine et al., 1999). Oxidation of As(III) by ozone was found effective more expensive (Jiang, 2001). Consequently, there remains a dire need for a simple, easy-to-operate and low-cost method to oxidize and remove As(III).

Scott and Morgan (Scott and Morgan, 1995) studied As(III) oxidation rate using synthetic birnessite (δ-MnO_2). In spite of the low arsenic removal capacity of manganese dioxide itself (Edwards, 1994), manganese in natural systems is known to play an important role in oxidation of As(III) (Manning et al., 2002). The arsenic (III) adsorption capacity was reported to be 7.5 mg/g for synthesized birnessite (Manning et al., 2002) and 13.5 mg/g for manganese dioxide (Bissen and Frimmel, 2003). By virtue of the oxidation effect of manganese and the high sorption capacity of iron oxides toward arsenate, Zhang et al. (2007) reported enhanced arsenite removal of As(III) by applying a binary Fe-Mn oxide adsorbent.

In recent years, iron based nanoscale particles have enticed growing interest for water treatment and environmental remediation (Huber , 2005; Jolivet, 2000; Kanel et al., 2006; Liu and Zhao, 2007; Ponder et al., 2000; Xu and Zhao, 2007). To overcome agglomeration of the particles and to control the particle size, organic polymers are often employed as a stabilizer, such as starch (He and Zhao, 2005; Kim et al., 2003), carboxymethyl cellulose (CMC) (He and Zhao, 2007), oleic acid (Kvalenko et al., 2006; Yean et al., 2005), polyvinyl alcohol (PVA) (Chasellain et al., 2004), and poly acrylic acid (PAA) (Iijima et al., 2006). The stabilizers can be coated on the nanoparticles, and prevent the particles from aggregation through steric and/or electrostatic stabilization mechanisms, leading to improved physical stability, better mobility in soil, and greater specific surface area. Yean et al. (2005) observed that the arsenic sorption capacity of magnetite nanoparticles stabilized with oleic acid was 4.6 times greater than a commercial powder magnetite. Furthermore, particle stabilization allows for the nanoparticles to be delivered in situ to the contaminated subsurface. For example, stabilized ZVI nanoparticles have been tested at contaminated sites and shown to be deliverable into the contaminated source zones (Pennett et al., 2010; He et al., 2010). Our previous work also revealed that stabilized nanoparticles such as ZVI (Xu and Zhao) and FeS (Xiong et al., 2009) may be used for *in situ* immobilization of chromate and mercury in contaminated soils, respectively. The *in situ* remediation technology through injection of nanoparticles not only holds the potential to cut down the remediation cost substantially, but represents an innovative approach to tackle contaminants located in otherwise hardly reachable aquifer zones such as in deep aquifer or aquifers underneath a city or other developed areas.

Remediation of arsenic contaminated soils has been a challenge for decades. In practice, excavation of contaminated soil has been a rather common practice, though this approach is

known to be both expensive and environmentally disruptive (Miretzk and Cirelli, 2010). Researchers have also intensively studied a variety of alternative technologies, including phytoremediation (Aldrich et al., 2007; Meharg and Hartley-Whitaker, 2002), solidification/stabilization using inorganic binders such as cement (He and Zhao, 2005), soil washing (Jang et al., 2005), electrokinetic remediation (Amrate and Akretche, 2005; Kim et al., 2005), and *in situ* immobilization using granular or powdered ZVI (Su and Puls,2001) and magnetite (Fe_3O_4) (Zhang et al., 2010). However, effective *in situ* remediation of As-contaminated soils remains confronted with some key technical challenges, such as soil deliverability and sorption capacity of the particles.

The overall goal of this research was to investigate the feasibility of using a new class of stabilized Fe-Mn oxide nanoparticles (denoted as Fe-Mn) for in situ remediation immobilization or removal of both As(III) and As(V) in contaminated soils. The specific objectives of this work were to: 1) prepare and characterize a new class of stabilized Fe-Mn nanoparticles, 2) determine the effectiveness of the stabilized nanoparticles for As(III) and As(V) removal from water, 3) examine mobility of the stabilized Fe-Mn nanoparticles in a model soil, and 4) test effectiveness of the stabilized Fe-Mn nanoparticles for immobilizing As(III) in a contaminated soil.

4.2. Materials and methods

4.2.1 Chemicals

Chemicals used in this research were in the analytical grade or higher and were used as received. $FeSO_4 \cdot 7H_2O$, $KMnO_4$, and sodium carboxymethyl cellulose (CMC, M.W: 90000) were purchased from Acros Organics (Morris Plains, NJ, USA). A potato hydrolyzed starch and $Na_2HAsO_4 \cdot 7H_2O$ were obtained from Sigma-Aldrich (Milwaukee, WI, USA). $NaAsO_3$ and

$MnCl_2$ were purchased from Fisher Scientific (Pittsburgh, PA, USA). All solutions were prepared with ultrapure deionized (DI) water ($18.2\Omega cm^{-1}$).

4.2.2. Preparation of stabilized Fe-Mn nanoparticles

The binary Fe-Mn oxide nanoparticles were prepared by modifying the method used by Zhang et al. (2007). The key modification was to apply a low-cost and "green" polysaccharide stabilizer (starch or CMC) during the particle formation. In principle, the Fe-Mn binary oxide was obtained according to the following redox reaction stoichiometry (Snoeyink and Jenkins, 1980):

$$MnO_4^- + 3e + 2H_2O \rightarrow MnO_{2(s)} + 4OH^- \qquad E° = +0.59 \qquad (4\text{-}1)$$

$$3Fe^{2+} \rightarrow 3Fe^{3+} + 3e \qquad E° = -0.77 \qquad (4\text{-}2)$$

Thus, the overall reaction can be expressed as:

$$3Fe^{2+} + MnO_4^- + 4H+ \rightarrow MnO_{2(s)} + 3Fe^{3+} + 2H_2O \qquad (4\text{-}3)$$

where 1 mole of permanganate oxidizes 3 moles of Fe^{2+} to Fe^{3+}, and results in 1 mole of $MnO_{2\,(s)}$ First, prepare a 1 wt.% stock solution of starch or CMC (proper heating was needed to dissolve the stabilizers in water). Then, take a desired volume (from 0 to 28 mL) of the starch or CMC solution and dilute by adding DI water to 120 mL, and mix for 10 min. Prepare an $FeSO_4 \cdot 7H_2O$ solution of 13.9 g/L and another solution of 2.65 g/L of $KMnO_4$ in DI water, and then add 10 mL of the $FeSO_4 \cdot 7H_2O$ solution into the 120 mL stabilizer solution and mix for 15 min. The redox reaction was then initiated by adding 10 mL of the $KMnO_4$ solution into the mixture of iron sulfate and one of the stabilizers under vigorous magnetic stirring. Immediately increase the pH of the mixture to ~7.5 using 4M NaOH, and shake the mixture on a platform shaker (New Brunswick Scientific, NJ, USA) at 200 rpm for one hour. Fe-Mn nanoparticles were then obtained as either precipitates or fully stabilized suspension depending on the concentration and

type of the stabilizers present. The Fe-Mn particles were tested or used within 1 hour of preparation.

4.2.3. Physical characterization of Fe-Mn nanoparticles

XRD patterns of the samples, namely bare, starch-, and CMC-stabilized Fe-Mn nanoparticles were obtained using a diffractometer (MiniFlex X-ray diffractomer, Rigaku, Japan) equipped with Cu K-alpha radiation. The nanoparticles were first prepared at 0.27 g/L as total Fe-Mn, and then separated from water and vacuum-dried. The dried samples were ground to a homogenous mixture using a mortar and pestle and then affixed to glass microscope slides after cleaning slides using acetone. The samples were diffracted over a 2θ range from 10° to 90°. Zeta potentials (ξ) of the particles was measured with a Zetasizer nano ZS (Malvern Instruments, UK) at 25℃. Typically, 0.75 mL of a nanoparticle suspension of 0.27 g/L of Fe-Mn was filled in a folded-capillary cell and then measured. For bare Fe-Mn nanoparticles, that precipitated rapidly, the samples were first sonicated with a sonicator (550 Dismembrator, Fisher Scientific, Pittsburg, PA, USA) right before the measurements.

4.2.4. Kinetic tests

Batch kinetic tests were conducted to test arsenic sorption rate of the nanoparticles. First, Fe-Mn particles or suspensions were prepared at 0.27 g/L as Fe-Mn (Fe=0.2 and Mn=0.07 g/L) in the presence of 0, 0.16 wt.% CMC, and 0.19 wt.% starch. Then, the sorption tests were initiated by adding an arsenic stock solution to the nanoparticle suspension, which resulted in the following conditions: suspension volume = 140 mL, initial As concentration = 100 mg/L, initial pH = 5.0. The solution pH was kept at 5.0±0.1 during the tests through intermittent adjustment using 0.1 M NaOH or HCl. The vials were then placed on a platform shaker operated at 200 rpm. At

predetermined times, samples were taken at 4 mL each and passed through a 25 nm membrane filter (0.025 µm VSWP, Millipore, USA). The filtrate was then acidified with one drop of 1 M nitric acid, and then analyzed for arsenic remaining in the aqueous phase.

4.2.5. Batch As(III)/As(V) adsorption equilibrium tests

A series of equilibrium tests were performed to determine the arsenic removal effectiveness with bare and stabilized Fe-Mn nanoparticles. To test the effect of stabilizers on the sorption capacity, Fe-Mn nanoparticles of 0.27 g/L as Fe-Mn were synthesized with various concentrations (0 to 0.26 wt.%) of CMC or starch. Then, the adsorption was initiated by adding a known mass of As(III) or As(V) from a stock solution to the Fe-Mn suspensions to yield an initial concentration of arsenic of 100 mg/L as As. The pH of the suspension was initially maintained at 5.5 during the tests through intermittent adjusting. The samples were equilibrated for 2 days under shaking at 200 rpm. Then, samples were taken, filtered and analyzed for arsenic remaining following the same method as described above.

Batch isotherm tests were performed for As(III) and As(V) adsorption following the similar procedure. The following conditions were applied: initial arsenic concentration ranged from 0 to 140 mg/L as As, suspension volume = 140 mL, CMC (sodium form) = 0.16 wt.%, Fe-Mn = 0.27 g/L. The isotherms were constructed at two pH levels of 5.5 and 3.0, which were maintained through intermittent adjustment.

To further investigate the pH effect on arsenic sorption, batch arsenic adsorption tests were carried out over a broad pH range from 2 to 10 for bare and stabilized (with either 0.16 wt.% CMC or 0.19 wt.% starch) Fe-Mn but under otherwise identical conditions, i.e. initial concentration of As = 100 mg/L and Fe-Mn = 0.27 g/L. For comparison, As(V) was also examined in parallel.

4.2.6. FTIR analysis

Fourier transform infrared spectroscopy (FTIR) was performed to determine arsenic adsorption mechanisms and interactions between the stabilizers (CMC and starch) and Fe-Mn oxide nanoparticles. FTIR spectra were obtained for neat CMC and starch samples as well as bare, CMC- and starch-stabilized Fe-Mn nanoparticles before and after adsorption of arsenate or arsenite. The samples were first vacuum-dried, and then ground in a mortar to fine powders, which were then mixed with KBr at a sample-to-KBr ratio of 5:95 by weight. The mixtures were pressed into thin films under a hydraulic press at 9 metric tons for 2 min. The specimen were then scanned and characterized using an IR Prestige-21 spectrometer (Shimadzu) over the wave number ranging from 400 to 4000 cm^{-1}.

4.2.7. Preparation of As(III)-spiked soil

A sandy soil was obtained near the Auburn University's E.V. Smith Research Center in Tallassee, AL, USA. Prior to use, the sandy soil was washed with tap water several times to remove all soluble components such as dissolved organic matter and other soluble impurities until the supernatant was clear. The sandy soil was air-dried at room temperature for several days and then sieved through a 2-mm screen (#10) before being used in the soil treatment experiments. The prepared soil was digested following U.S. EPA method 3050B and analyzed for mineral metals, which gave the following background metal concentrations: Fe = 758 mg/kg, Ca = 240 mg/kg, and Mg = 179 mg/kg. To prepare the As(III) spiked samples, 800 g of the air-dried sandy soil was placed into 1 L of As(III) solution containing 150 mg/L as As. The mixture was continuously shaken for 2 weeks to reach equilibrium. During loading, the pH of the mixture was

maintained at ~6 through intermittent adjusting using 1 M NaCl and 1 M HCl. The final As(III) loading on the sandy soil sample was 103.5 mg of As(III)/kg of dry soil (w/w).

4.2.8. As(III) immobilization in soil: batch tests

To investigate the nanoparticles' effectiveness for immobilization of As(III) in the soil, a series of batch tests were carried out by treating the As(III)-spiked soil with stabilized Fe-Mn nanoparticles. In each test, 2g of the air-dried As(III) loaded sandy soil was mixed with 30 mL of a suspension of the Fe-Mn nanoparticles stabilized with either 0.16 wt.% CMC or 0.19 wt.% starch in a 30 mL Corning plastic centrifuge tube. The nanoparticle dosage was varied from an Fe-to-As molar ratio of 0 to 6.5, 13, 26, and 39. Each sample was rotated using an end-to-end rotator at 30 rpm at room temperature (21±0.1 ℃) for 4 days to reach equilibrium. The pH of the aqueous phase was kept at 5.5 through intermittent adjustment with 0.1 NaCl or HCl. After 4 days of equilibration, the samples were centrifuged at 6500 rpm (5857g of RCF) for 15 min, and then the supernatant was filtered through a 25 nm membrane filter to remove the nanoparticles. Finally, the filtrate was analyzed for As(III), which gave the total leachable As(III) in the system. To compare the effect of the stabilized Fe-Mn nanoparticles on the leachability of the soil-sorbed As(III), As(III) leaching tests were also carried out in parallel by mixing the soil sample with a simulated ground water (SGW) prepared following the method by Lien and Wilkin (Lien and Wilkin, 2005).

4.2.9. Fixed-bed column tests

Fixed-bed column tests were conducted to evaluate soil mobility and breakthrough behaviors of the stabilized Fe-Mn nanoparticles and the potential for the attempted *in situ* immobilization of As(III) in contaminated soils. Approximate 9 g of the dried sandy soil (without As(III) loaded)

was packed in a Plexiglas column (inner diameter = 1.0 cm and length = 10 cm; Omnifit, Cambridge, UK), resulting in a soil bed porosity of 0.40 and a bulk bed volume of 6.4 mL. The CMC-stabilized Fe-Mn nanoparticle suspension was then passed through the soil-packed column at a flow rate of 0.18 mL/min in the down-flow mode, which translated into an empty bed contact time (EBCT) of 35.6 min and a superficial liquid velocity (SLV) of 3.8×10^{-5} m/s. The effluent samples were collected with a fraction collector (Eldex Laboraries, Napa, CA, USA). The samples were then completely acidified using 0.1M HCl and analyzed for total Fe, whci represents the concentration of the nanoparticles in the effluent. For comparison, a tracer test was performed using a KBr solution (50 mg/L as Br^-) under otherwise identical operating conditions.

To evaluate the effectiveness of the nanoparticles for *in situ* As(III) immobilization, column elution tests were carried out under the same hydrodynamic conditions. To this end, ~9 g of As(III)-loaded soil was packed in the column, and then the contaminated soil bed was treated by passing 22 pore volumes (PV) of a suspension containing CMC-stabilized Fe-Mn nanoparticles (Fe-Mn = 0.27 g/L, CMC=0.16 wt%). The effluent samples were then analyzed in two ways. First, the samples were acidified by HNO_3 to completely dissolve the nanoparticles, and then analyzed for total As (adsorbed and free As) in the effluent; Second, the samples were first filtered using a 25 nm membrane filter to remove all the nanoparticles and then the filtrate analyzed for the free or soluble As. For comparison, As(III) elution using the simulated groundwater was also performed in parallel.

4.2.10. Leachability of As(III) in soil

The toxicity characteristic leaching procedure (TCLP) specified in EPA Method 1311 was employed to determine the leachability of arsenite from untreated and nanoparticle amended soil. Soil samples treated by Fe-Mn nanoparticles or subjected to SGW after the batch or column tests

were first air-dried at room temperature and then mixed with the #1 TCLP fluid (pH = 4.93) at a solid–to-solution ratio of 1:20 (i.e. 2 g dried soil and 40 mL of #1 TCLP fluid). The mixtures were rotated for 18 hr at 30 rpm and then centrifuged at 6500 rpm (5857 g of RCF) for 20 min. Arsenic leached in the supernatants was then analyzed. All tests were conducted in duplicate.

4.2.11. Chemical analyses

Solution or suspension pH was measured using an Oakton pH meter (pH 510 Benchtop Meter, Oakton, CA, USA). Arsenic was analyzed with a Perkin Elmer Atomic Adsorption Spectrophotometer, which has a detection limit of 3 µg/L as As. Concentration of iron and manganese were measured using an ICP-AES (Liberty-SERIES II, Varian). Bromide was analyzed using a Dionex Ion Chromatograph (Model DX-20) equipped with an AS14 column.

4.3. Results and discussion

4.3.1. Characterization of Fe-Mn nanoparticles by XRD and FTIR

XRD patterns (not shown) for bare, and CMC- or starch-stabilized Fe-Mn nanoparticles revealed no significant peaks (intensity), indicating that all the binary Fe-Mn oxide particles are not characterized with a crystalline structure (Chen, 2007). These results are in accordance with the study by Zhang et al. (Zhang et al., 2007) and suggest that the prepared Fe-Mn oxide particles are in the more stable amorphous form. Based on the XPS spectra for Fe-Mn binary oxide, Zhang et al. (2007) identified peaks at 724.8 and 711.1 eV for Fe 2p1/2 and Fe 2p3/2, respectively, and at 653.0 and 642.0 eV for Mn 2p1/2 and 2p3/2, respectively. These binding energy values indicate that the iron exists in the form of $Fe(OH)_3$ (Piche and Larachi, 2005) and that Mn is present in the form of MnO_2 (Allen et al., 1989; Ivanov-Emin et al., 1982).

Fig. 4-1 shows the FTIR spectra of neat CMC and starch, and bare and stabilized Fe-Mn nanoparticles. Fig. 4-1a compares the characteristics of the stretching frequencies for neat stabilizers and the corresponding stabilized Fe-Mn nanoparticles. The peak at 3444 and 3430 cm^{-1} was found for neat starch and CMC stabilizer, respectively, and the peaks at 3400 cm^{-1} were detected for both types of stabilized Fe-Mn nanoparticles. These peaks correspond to O-H stretching bond from H_2O, CMC or starch, which is accordance with Maity and Agrawal (Maity and Agrawal, 2007) reporting ~3400 cm^{-1} bond of iron oxide and oleic acid. Upon sorption of the stabilizers to the Fe-Mn particles, a shift was observed from 3444 to 3400 cm^{-1} for CMC-stabilized Fe-Mn and from 3430 to 3400 cm^{-1} for starch-stabilized Fe-Mn. Such a shift can be attributed to the increased strength of intermolecular hydrogen bonds between the stabilizers and surface of the Fe-Mn particles (Sylvestre et al., 2004). Given the abundance of -OH groups in both CMC and starch, this type of hydrogen bonding can be important in binding the stabilizers to the Fe-Mn particles. He et al. (2007) reported a shift from 3447 cm^{-1} for neat CMC to 3419 cm^{-1} for CMC-stabilized ZVI nanoparticles. The peaks observed at around 2875 cm^{-1} for all four cases indicate C-H stretching vibrations from the CH_2 groups of the stabilizers. Fig. 4-1a revealed a shift from 1607 cm^{-1} for neat CMC to 1562 cm^{-1} for CMC-stabilized Fe-Mn. Si et al. (Si et al., 2004) reported the same shift and ascribed it to the decrease in force constant resulting from the inhibition of conjugation of COO^- when attached to a particle surface. A shift from 1647 cm^{-1}, which is due to O-H bond from water, for neat starch to 1572 cm^{-1} for starch-stabilized Fe-Mn was observed, indicating that more water molecules were bound on the surface of Fe-Mn particles. The same shift was reported by Pushpadass et al. (Pushpadass et al., 2008) for cornstarch film and Zhang and Han (Zhang and Han, 2006) for pea starch film. Jones et al. (Jones et al., 1998) showed that monodentate and bidentate chelating was operative between the

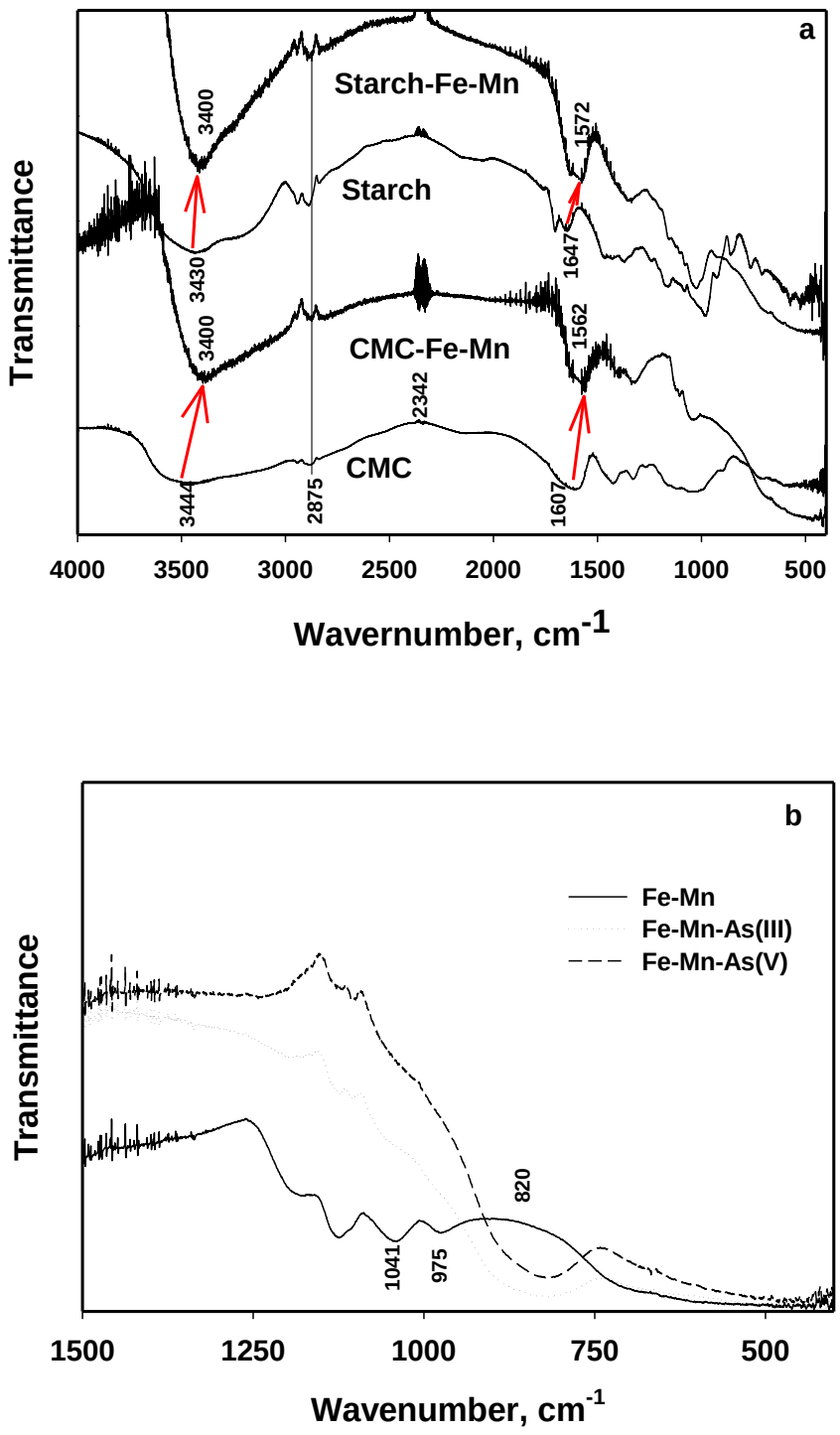

Fig. 4-1. FTIR spectra of (a) neat CMC and starch, and CMC- or starch-stabilized Fe-Mn nanoparticles (arrows indicate shifts of the peaks), (b) non-stabilized Fe-Mn particles with or without arsenic.

carboxylate groups of CMC and surface Fe. However, in the present work, such interaction was not clearly evident based on the FTIR spectra.

Fig.4-1b shows FTIR spectra for bare Fe-Mn particles before and after arsenic uptake. FTIR studies of various iron oxides have been widely reported, and the following characteristic wave numbers have been reported: 580 cm^{-1} for magnetite (Zhang et al., 2005), 560 cm^{-1} for ferrihydrite film (Voegelin and Hug, 2003), and 441 and 580 cm^{-1} for low crystalline ferrihydrite or amorphous iron(III)-hydroxide (Ristic et al., 2007). However, the FTIR spectra in Fig. 4-1 did not show any of these peaks. Instead, two new peaks in Fig 4-1b were evident at 1041 and 975 cm^{-1}, respectively. Apparently, the presence of Mn in iron oxide reduced the band strength of Fe-O groups. The two new peaks could be ascribed to Fe-OH. Similar observations were reported by Zhang et al. (2005) who studied Fe-Ce binary metal oxides for arsenate adsorption. They observed that the intensity of Fe-O peak at 580 cm^{-1} was progressively weakened as the Ce concentration was raised, and the peak became undetectable at an Fe:Ce molar ratio of 3:1, where two new peaks at 1126 and 1067 cm^{-1} appeared representing the Fe-OH groups (Keiser et al., 1982). Fig. 4-1b shows that the Fe-OH peaks disappeared upon uptake of As(III) or As(V) to the bare Fe-Mn particles. Furthermore, the sorption of arsenic gave rise to a new broad band at 820 cm^{-1} corresponding to As-O stretching vibration, which is characteristic of As(V) sorption (Zhang et al., 2005; Voegeli and Hug, 2003; Goldberg and Johnston, 2001). For As(III) sorption to bare Fe-Mn, Zhang et al. (Zhang et al., 2007) observed a peak at 577 cm^{-1}, which was attributed to the As-O vibration. However, in this work, the peak was not detected for bare or stabilized Fe-Mn particles. Based on this observation and the presence of the strong broad peaks at 820 cm^{-1} for both As(III)- and As(V)-laden Fe-Mn, it is evident that As(III) was first oxidized to As(V) and then adsorbed onto the surface of the Fe-Mn oxides. Earlier, Voegelin and Hug

(2003) reported a weak peak for As(III) at 774 cm^{-1} on the surface of ferrihydrite. However, in our case, this weak peak was likely further weakened upon oxidation of As(III), and was overwhelmed by the strong peak at 820 cm^{-1}. Pena et al. (2006) compared FTIR bands for sorbed and dissolved arsenate species and observed that two peaks at 878 and 909 cm^{-1} for dissolved $H_2AsO_4^-$ corresponding, respectively, to the symmetric and asymmetric stretching vibrations of As-O bonds. Upon adsorption, the peaks were shifted to 808 and 830 cm^{-1}, respectively. According to Goldberg and Johnston (2001) and Pena et al. (2006), the shift on band positions was attributed to symmetry reduction resulting from inner-sphere complex formation (i.e. formation Fe-O-As complexes). In our study, the presence of the one broad band at 820 cm^{-1} suggested that similar surface complexation was the predominant mechanism for arsenate sorption to the Fe-Mn particles.

4.3.2. Effect of stabilizers on zeta potential of Fe-Mn nanoparticles

Fig. 4-2 shows the measured zeta potential (ζ) as a function of pH for bare and stabilized Fe-Mn particles. Evidently, coating of the neutral starch and negatively charged CMC molecules (pKa=4.3) greatly altered the ζ value over a broad pH range. For the bare Fe-Mn binary oxides, the ζ value underwent a sharp change from +2 to -45 mV over the pH range of 5.7 to 8.9, which revealed a point of zero charge (PZC) of pH ~6. Kosmulski et al. (2003) reported PZC values of 8.32 and 7.99, respectively, for goethite and Fe(III) hydroxides. Su and Suarez (2000) reported a PZC of 8.5 for synthetic amorphous $Fe(OH)_3$. For synthetic birnessite (δ-MnO_2), the PZC was reported to fall in a typical range from 1.5 to 2.5 (Sposite, 1989; Tan et al., 2008). Comparing the ζ-pH profile of bare Fe-Mn and those of typical iron oxide minerals, it appears that $Fe(OH)_3$ dominates the characteristics of the Fe-Mn binary oxides. In the presence of 0.19 wt.% of starch, however, the surface potential was largely shielded. Over the pH range of 3.3 to 7.2, ζ was nearly

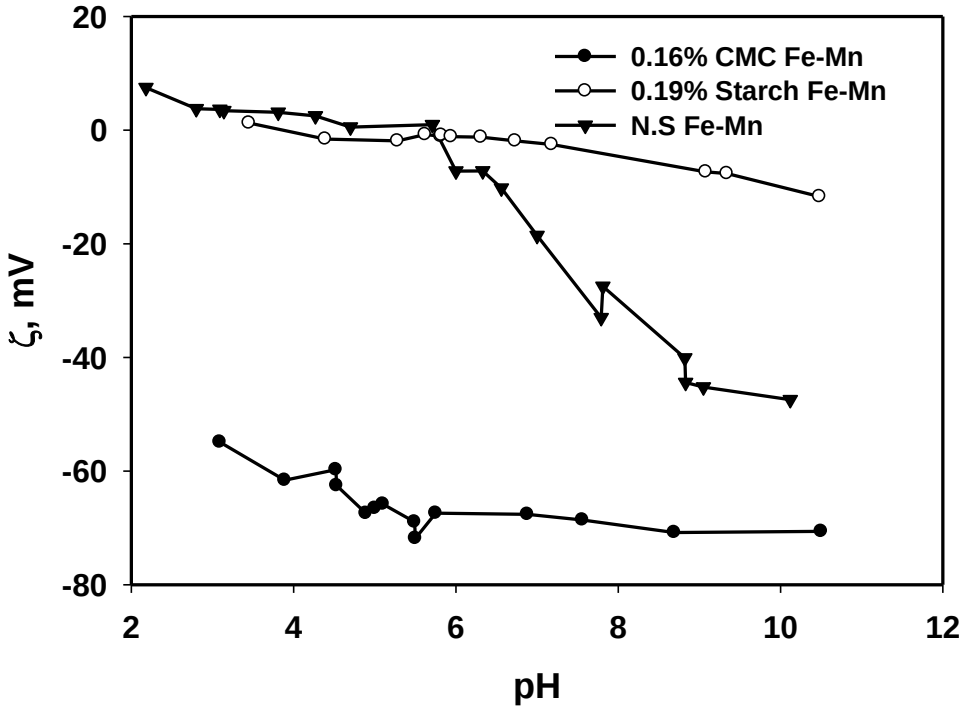

Fig. 4-2. Zeta potential as a function of pH for bare and stabilized Fe-Mn nanoparticles.

zero, and it was only changed to -10 mV when pH was extended to 10.5. Evidently, the presence of starch, which is a neutral polymer with dense H-bonding (Biggs, 2006; Ravishankara et al., 1995) results in a strong surface "buffer" that diminishes the effect of H^+/OH^- on the surface charge. This is plausible given that the starch macromolecules have pre-occupied the functional sites of the core Fe-Mn particles, which impedes protonation or deprotonation of these functional groups. In contrast, in the presence of 0.16 wt.% of CMC, ζ was substantially lowered to below -50 mV throughout the pH range (<-65 mV at pH >5). From the particle stabilization viewpoint, the surface potential values indicate that steric stabilization is the predominant mechanism for starch, while electrosteric stabilization is operative for CMC, i.e. CMC is likely to be a more effective stabilizer than starch. With respect to arsenic sorption, however, the highly negative surface charge induced by CMC would tend to exclude the arsenate anions, which is expected to offset, at least in part, the benefit of greater specific surface area of the nanoparticles.

4.3.3. Kinetic tests

Fig. 4-3 shows As(III) adsorption rates of bare and CMC- or starch-stabilized Fe-Mn particles at a fixed dosage of 0.27 g/L as Fe-Mn. For the stabilized Fe-Mn particles, equilibrium was reached within 1 h, whereas for the bare Fe-Mn particles, the sorption was characterized with a rapid initial (<4h) followed by a rather slow uptake. The equilibrium As(III) removal was 69%, 75%, and 77% for CMC-stabilized, bare, and starch-stabilized Fe-Mn, respectively. In terms of sorption capacity, the results appear to be counter-intuitive. While stabilized particles are expected to offer much greater surface area, the particle stabilization did not offer the expected capacity hike. In fact, the capacity for CMC-stabilized particles was 6% lower than for the bare particles. Apparently, while these stabilized nanoparticles may offer comparably greater specific area, the particle-laden stabilizers on the particle surface may inhibit arsenic uptake both

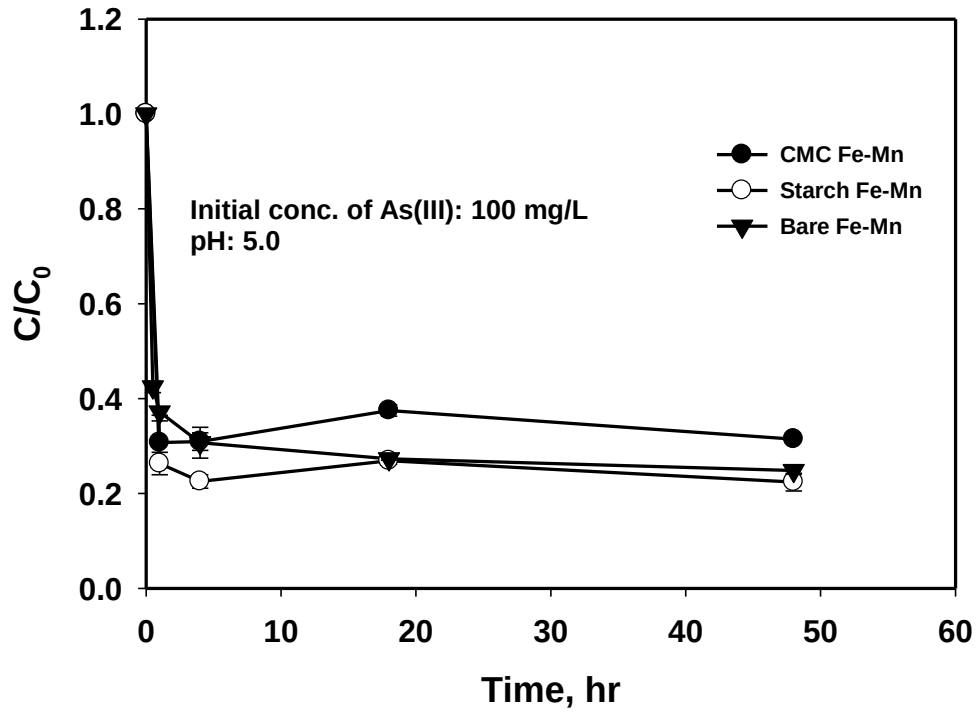

Fig. 4-3. Arsenite removal as a function of time using bare or stabilized Fe-Mn nanoparticles under otherwise identical conditions. Experimental conditions: CMC = 0.16 wt.% for CMC-stabilized particles; Fe =0.20 g/L; Mn = 0.07 g/L; Starch=0.19 wt.% for starch-stabilized particles. Solution pH was kept at 5.0 in all cases. Data are plotted as mean of duplicate, errors indicate deviation from the mean.

thermodynamically (due to reduced sorption sites and site accessibility) and kinetically (due to increased mass transfer resistance). In addition, coating the nanoparticles with the stabilizers also greatly alters the surface potential, which can also affects sorption of the arsenic species. For CMC-coated Fe-Mn nanoparticles, it was the highly negative surface potential (Fig. 4-2) that caused the observed capacity drop. From a soil remediation standpoint, however, the particle stabilization is of great significance. As to be shown later, the stabilizers prevent the nanoparticles from aggregation and enable the particles to be deliverable into contaminated soil.

4.3.4. Batch arsenic uptake tests

Batch equilibrium adsorption experiments were carried out at a fixed Fe-Mn of 0.27 g/L, a constant pH of 5.5, and in a range of stabilizer concentrations to determine the effect of stabilizers on arsenic uptake. Fig. 4-4 shows the percentage arsenic removal as a function of type and concentration of stabilizers. The average removal of As(III) was 81, 80, and 75% for bare, starch-, and CMC-stabilized Fe-Mn particles, respectively. Increasing CMC from 0.03% to 0.13% progressively reduced the As(III) removal. For As(V), the removal rate was about the same at ~68% for bare and stabilized particles. Again, the presence of the stabilizers did not appear to offer any advantage in terms of sorption capacity for As(III) and As(V). Instead, use of CMC for As(III) rather decreased to 6% of removal efficiency which is consistent with the kinetic tests. It is noteworthy that the nanoparticles displayed ~10% greater removal for As(III) than for As(V) under the experimental conditions. The same phenomenon was also reported by Zhang et al. (2007) and Deschamps et al. (2005), who ascribed it to the creation of more fresh sites upon reduction of MnO_2 by As(III) as proposed by Manning et al. (2002).

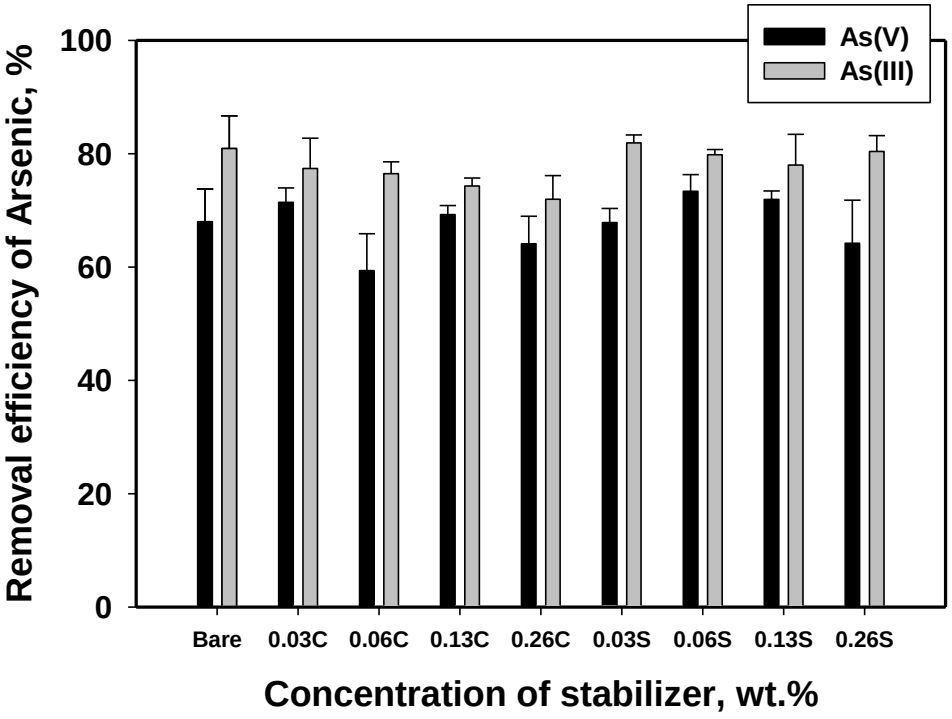

Fig. 4-4. Arsenic removal as a function of type and concentrations of a stabilizer. Experimental conditions: Fe = 0.2 g/L; Mn = 0.7 g/L; pH=5.5; Initial As(V) = 100 mg/L; and Initial As(III) = 108 mg/L of As(III). (Notations: Bare: non-stabilized Fe-Mn particles, C: CMC, S: Starch; numbers refer to wt% of a stabilizer added).

Fig. 4-5 shows sorption isotherms for As(III) and As(V) at two different pH levels of 5.5 and 3 using 0.16 wt.% CMC-stabilized Fe-Mn. The classical Langmuir isotherm model, Eq. (4-4), was employed to interpret the experimental data. The best data fitting gave both maximum adsorption capacity (Q) and the Langmuir affinity constant (b).

$$q_e = \frac{bQC_e}{1+bC_e} \tag{4-4}$$

where q_e is the equilibrium As uptake (mg/g), C_e is the equilibrium concentration of As in water (mg/L), and b and Q are the Langmuir affinity and capacity coefficients, respectively. Table 4-1 lists the model-fitted b and Q values. The results revealed that sorption of the two arsenic species by Fe-Mn is highly pH dependent, i.e. the sorption capacity for As(III) and As(V) varies with pH. At pH 5.5, the sorbent prefers As(V) over As (III) (Q = 338 mg/g for As(III) and Q = 272 mg/g for As(V)), as has been commonly noted. Despite the inhibitive effect of CMC on the sorption capacity, the fitted b and Q values for the CMC-stabilized Fe-Mn are much greater than those reported for other adsorbents, for examples, 135 mg-As(III)/g for magnetite (Yean et al., 2005) and 55 mg-As(III)/g for Ce-Ti powder (Li et al., 2010). Moreover, the maximum adsorption capacity is higher than other Fe-Mn products reported in the literature, for example, 138 mg-As(III)/g (Chang et al., 2009) and 113 mg-As(V)/g (Zhang et al., 2007). However, at pH 3.0, As(V) becomes much more preferred species over As(III). The Q value was determined to be 372 mg/g for As(V), surpassing the value of 182 mg/g for As(III) by a factor of 2.4. In contrast, Deschamps et al. (2005) showed that the Q value for As(III) at pH 3 and pH 5.5 was 14.7 and 12.0 mg/g, respectively, when a natural Fe-Mn sorbent was used.

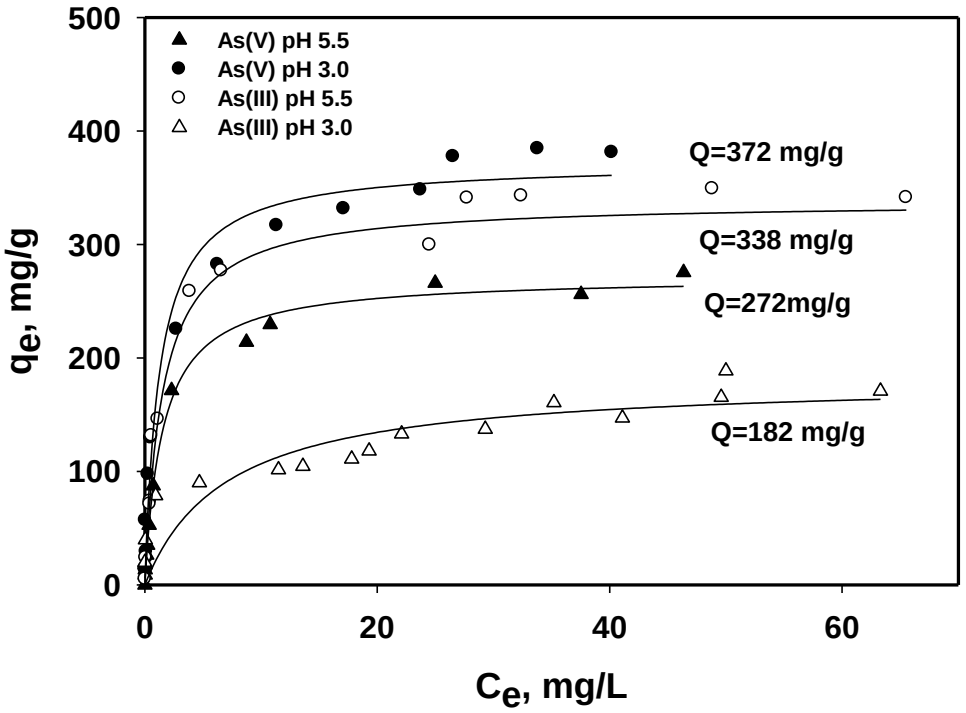

Fig. 4-5. As(III) and As(V) sorption isotherms for CMC-stabilized Fe-Mn nanoparticles at pH 3.0 and 5.5. (Symbols: Observed data; lines: Langmuir model fits). Initial arsenic = 5 – 140 mg/L, Fe-Mn = 0.27 g/L as Fe-Mn, CMC in Na form = 0.16 wt.%.

Table 4-1. Model-fitted Langmuir parameters (*Q*, *b*).

pH	Arsenic	*Q* (mg/g)	*b* (L/mg)
3.0	As(III)	182(19.9)	0.14(0.067)
3.0	As(V)	372(13.0)	0.80 (0.18)
5.5	As(III)	338 (9.5)	0.66 (0.096)
5.5	As(V)	272 (5.1)	0.65 (0.062)

4.3.5. Effect of pH

The effect of pH on sorption of As(III) and AS(V) onto the Fe-Mn particles was investigated further. Solution pH can affect both the ζ potential of iron oxide and arsenic speciation. Equilibrium arsenic adsorption tests were conducted as a function of pH for As(III) and As(V) with bare, CMC-, or starch-stabilized Fe-Mn particles. Fig. 4-6 provides the arsenic adsorption profiles over a broad solution pH range. As stated earlier, the dominant mechanism for As(V) adsorption is believed to be surface complexation between Fe and the ligands ($H_2AsO_4^-$ and/or $HAsO_4^{2-}$), forming Fe-O-As groups. As shown in Fig. 4-6, As(V) adsorption was strongly dependent on the solution pH, and As(V) uptake increased with decreasing pH. In the pH range of 2.2-10, As(V) existed predominately in the form of $H_2AsO_4^-$or $HAsO_4^2$. At lower pH, more of the surface hydroxyl groups are protonated to OH_2^+, resulting on more adsorption sites for arsenate. At elevated pH, deprotonation of surface hydroxyl groups would result in a negatively charged surface. This unfavorable adsorption condition for As(V) is exacerbated at very alkaline pH (e.g. pH > 9) due to direct competition of OH^- with arsenate (Zhao and SenGupta, 2000). In As(III) adsorption, pH did not show obvious effect for bare Fe-Mn particle. In fact, based on pK_{a1} value of As(III), 9.2, As(III) existed as H_3AsO_3 under the designed pH range. Therefore, solution pH was not significantly affected on As(III) adsorption. However, the removal efficiency for both stabilized Fe-Mn nanoparticles at below pH 6 is lower than for bare Fe-Mn particles, and at pH 3, 15% of As(III) reduction was obtained. The reduction can be explained by As(III) oxidation by MnO_2. After As(III) adsorption on Fe-Mn particles with 100 mg/L as As(III) at pH 3.4 and 3.8, the concentration of Mn^{2+} in solution which was produced after As(III) oxidation by MnO_2 is 34.4 and 32.2 mg/L for bare Fe-Mn particles and 27.8 and 24.5 mg/L for

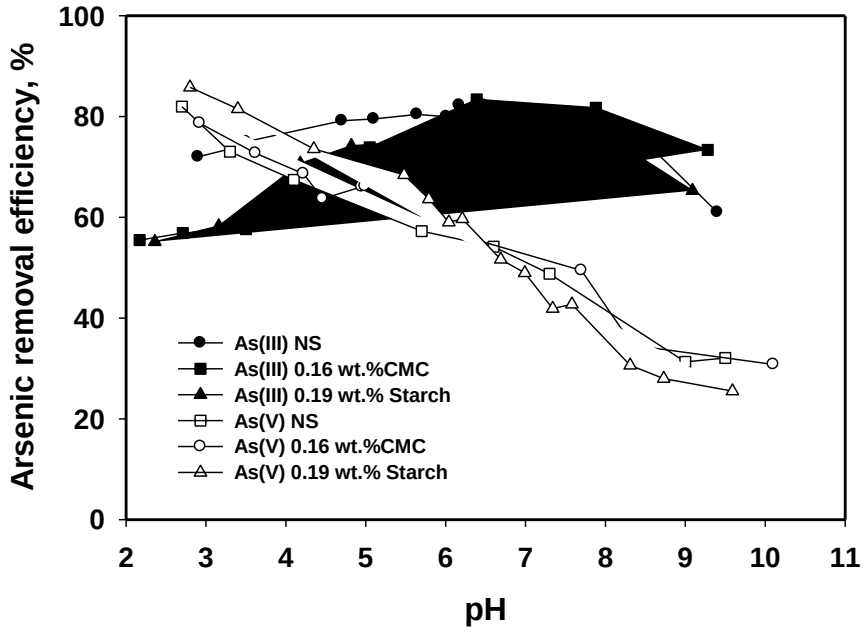

Fig. 4-6. As(III) and As(V) uptake as a function of solution pH for bare, 0.16 wt.% CMC-, 0.19 wt.% starch-stabilized Fe-Mn nanoparticles. Initial arsenic = 100 mg/L; Fe = 0.2 g/L; Mn = 0.7 g/L.

0.16 wt.% CMC Fe-Mn nanoparticles. Therefore, more oxidized As(V) from As(III) was adsorbed on bare Fe-Mn particles.

In general, As(V) adsorption on amorphous iron oxide decreases with increasing solution pH and As(III) adsorption on amorphous oxides increases with increasing solution pH, reaching a maximum at around pH 7 (Goldberg and Johnston, 2001; Grafe et al., 2001; Guo and Chen, 2005; Masue et al., 2007; Raven et al., 1998) resulting from arsenic speciation and surface charge of adsorbent. The profiles of As(III) and As(V) adsorption by Fe-Mn nanoparticles as a function of pH closely follow the results reported by these previous arsenic adsorption studies using iron oxides. The adsorption results in Fig. 4-6 also indicate that sorption of As(III) is not all in its oxidized form, i.e. the presence of MnO_2 (Mn/As molar ratio of 1.2:1.3) may not completely oxidize all As(III) to As(V). Scott and Morgan (1995) reported that during sorption of As(III) on to synthesized birnesite (δ-MnO_2), only 70% of As(III) was oxidized even at a Mn:As molar ratio of 6.4.

4.3.6. Oxidation of As(III) to As(V) by manganese dioxide

The FTIR results in Fig. 4-1b suggested that As(III) is adsorption, at least in part, through first oxidation by MnO_2 and then adsorption in the form of As(V). This oxidative adsorption process can be described by the following stoichiometry (Zhang et al., 2007):

$$MnO_{2(s)} + 4H^+(aq) + 2e^- \rightarrow Mn^{2+}(aq) + 2H_2O \qquad E°(V) = +1.23 \qquad (4\text{-}5)$$

$$H_3AsO_3(aq) + H_2O \rightarrow H_3AsO_4(aq) + 2H^+(aq) + 2e^- \qquad E°(V) = -0.56 \qquad (4\text{-}6)$$

$$MnO_{2(s)} + H_3AsO_3 + 2H^+ = Mn^{2+} + H_3AsO_4 + H_2O \qquad E°(V) = +0.67 \qquad (4\text{-}7)$$

According to Eq (4-7), 1 M of As(III) can be oxidized by 1 M of $MnO_{2(s)}$ and subsequently 1 M of Mn^{2+} is released into the aqueous phase. Therefore, the concentration of Mn^{2+} in the solution following the adsorption of As(III) can serve as a measure of the extent to which As(III) is

oxidized to As(V). Thermodynamically, this overall reaction is favorable under the experimental conditions. Table 4-2 shows the concentration of soluble iron and manganese following the adsorption of 100 mg/L of As(III) and As(V). The concentration of dissolved iron was always below 0.47 mg/L in all cases. However, the concentration of manganese ranged from 9 to 13 mg/L for the case of As(III) adsorption, compared to only 0.046 to 0.72 mg/L for the case of As(V) adsorption. The measured soluble manganese accounted for 14.5-21.0 wt.% of the total Mn in the particles. The presence of either stabilizer showed no effect on the As(III) oxidation at pH 5.5. Manning et al. (2002) and Scott and Morgan (1995) reported that about 70, 90, 95, and ~100% As(III) was oxidized to As(V) by synthesized birnessite (δ-MnO_2) at a Mn/As molar ratio of 6.2, 44.5, 15, and 29, respectively, within 10 h.

While the presence of soluble Mn^{2+} and As(V) clearly supports the notion that As(III) is at least partially oxidized by MnO_2, quantifying the extent of As(III) oxidation should consider adsorption of Mn^{2+} to the sorbent (primarily ferric hydroxide in this case). Scott and Morgan (1995) reported that upon oxidation of As(III) by birnessite, the molar ratio of Mn^{2+}/As(V) was approximately 0.93, suggesting that ~7% Mn^{2+} was adsorbed. Based on Mn^{2+} batch adsorption tests with the Fe-Mn particles (Fe=0.2 g/L, Mn=0.07 g/L, initial concentration of Mn^{2+}=90 mg/L), Mn^{2+} uptake by the binary oxide was strongly dependent on pH. At a final pH 4.5, 5.6, 5.9, 6.5, and 7.5 the removal of Mn^{2+} was 7, 15, 27, 83, and 99% of Mn^{2+} was removed, respectively. Based on these removal rates and the measured aqueous phase Mn^{2+} concentrations, the amount of As(III) oxidized was estimated to be ~25 mg/L under the experiment conditions: pH=5.5, initial As(III)=100 mg/L, and Fe-Mn=0.27 g/L.

Table 4-2. Concentration of Fe and Mn in solution following As(III) or As(V) adsorption onto various types of Fe-Mn nanoparticles.

	As(III)			As(V)		
	Fe mg/L	Mn mg/L	Released Mn,Wt.%	Fe (mg/L)	Mn (mg/L)	Released Mn, Wt.%
Non-stabilized Fe-Mn	0.011	9.0	15	0.056	0.046	0.075
Fe-Mn with 0.048 wt.% CMC	0.38	12	20	0.16	0.19	0.31
Fe-Mn with 0.048 wt.% Starch	0.036	9.3	15	0.11	0.11	0.18
Fe-Mn with 0.14 wt.% CMC	0.47	11	18	0.37	0.72	1.2
Fe-Mn with 0.14 wt.% Starch	0.018	13	21	0.025	0.14	0.23

4.3.7. Mobility of stabilized Fe-Mn nanoparticles in a sandy soil

For *in situ* immobilization uses, the Fe-Mn nanoparticles must be mobile enough to allow for effective delivery into arsenic contaminated soils. To this end, effective particle stabilization is of paramount importance (He and Zhao, 2007; He et al., 2010). To preliminarily demonstrate the mobility of the stabilized nanoparticles, column breakthrough tests of the CMC-stabilized Fe-Mn nanoparticles were carried out using a sand soil. Fig. 4-7 shows the breakthrough curves and elution profiles of the nanoparticles. For comparison, the breakthrough curve for a tracer, Br^-, is also superimposed. The breakthrough of the CMC-stabilized Fe-Mn nanoparticles started almost simultaneously with the tracer at ~1 PV (pore volumes) and reached a plateau (complete breakthrough) at ~4 PVs. At full breakthrough, the effluent concentration of iron accounted for ~90% (C_e/C_0), indicating that ~10% of the nanoparticles was consistently retained in the soil bed. Similar breakthrough profiles were observed by He et al. (2009) who tested transport of CMC-stabilized ZVI nanoparticles through various porous media, including a sand, glass beads and a sandy soil (He et al., 2009). Fig. 4-7 shows that the nanoparticles are quite mobile, and thus, are likely to be deliverable in soil. The particle removal has been generally attributed to the filtration effect in accordance with classical filtration theory, where particles are transported to the media matrix surfaces by Brownian diffusing, interception, and/or gravitational sedimentation, resulting in deposition of particles to the matrix surface (Kretzschmar et al., 1999). From a practical view point, such soil-associated nanoparticles serve as a permanent sink for immobilization of arsenic. Two sets of factors may govern the particle deposition: physical parameters, such as particle size and density, pore fluid velocity, pore structure, and the accessible surface area of the matrix; and the solution and surface chemistry. The hydrodynamic conditions especially pore water velocity can greatly affect particle deposition (He et al., 2009), and thus, manipulating the pore velocity

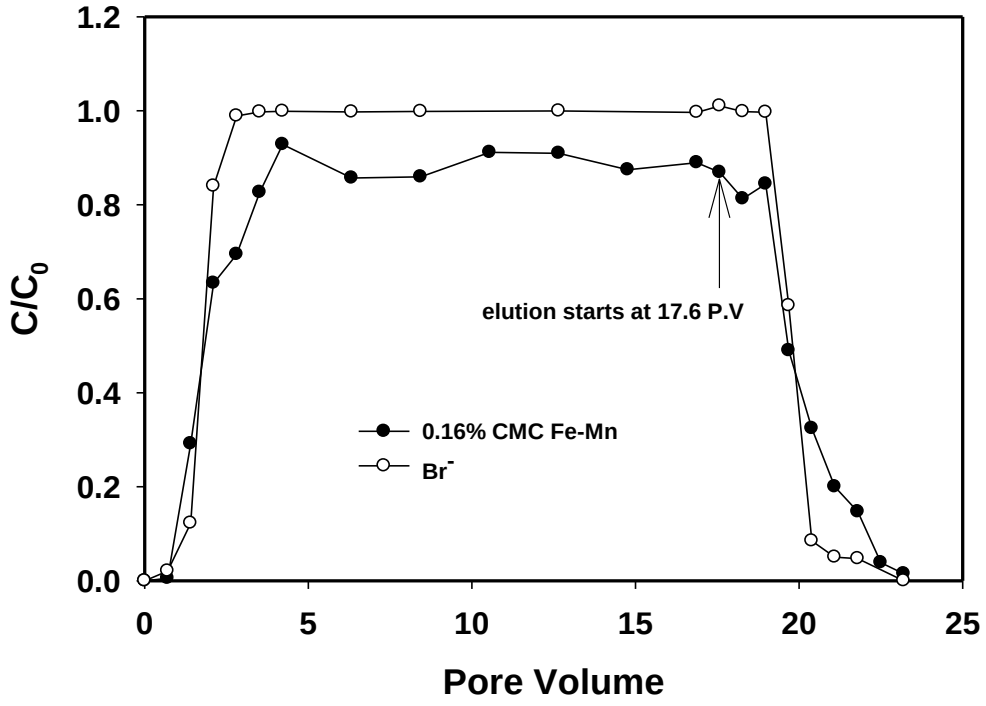

Fig. 4-7. Breakthrough curves of a tracer (Br^-) and 0.16% CMC-stabilized Fe-Mn nanoparticles through a sandy soil. Experimental conditions: EBCT: 35.6 min, SLV: 3.8×10^{-5} m/s, influent pH = 7±0.1. (Arrow indicates the point where elution was started)

may facilitate particle delivery and control the soil retention of the nanoparticles. The elution curve in Fig. 4-7 shows that ~36% of the retained nanoparticles was eluted at the same pore velocity, indicating that most of the retained nanoparticles were irreversibly deposited even at the fairly high elution flow rate. Based on our earlier work (He et al., 2009), the nanoparticles, whether retained or not, will most likely remain immobile under typical natural groundwater conditions. The starch-stabilized Fe-Mn nanoparticles were less mobile (data not shown). Nearly all particles were removed at ~10 PVs due to soil clogging. Non-stabilized Fe-Mn particles were not mobile and were all removed on the top of the soil bed.

4.3.8. Immobilization of As(III): batch tests

The effectiveness of stabilized Fe-Mn nanoparticles for As(III) immobilization in a sandy soil was investigated in batch tests at various dosages of stabilized Fe-Mn nanoparticles. Fig. 4-8a compares the concentrations of arsenic leached into the solution phase from the As-laden sandy soil in the absence and the presence of various dosages of the nanoparticles. In the absence of the nanoparticles (i.e. when the As-laden soil was mixed with the simulated ground water), the released As concentration reached 3800 µg/L. In contrast, when the soil was amended with the nanoparticle suspensions, the leachable As concentration was greatly reduced. At an Fe-to-As molar ration of 6.5, the leached arsenic concentration was reduced by 91% to 336 µg/L with CMC-stabilized Fe-Mn and by 84% to 603 µg/L with starch-stabilized Fe-Mn. When the dosage was increased to 39 (Fe:As), the leachable As was further reduced by 5% for CMC-stabilized Fe-Mn and 14% for the starched nanoparticles. The results clearly demonstrated that both types of the nanoparticles were highly effective to transfer soluble As(III) into the nanoparticle phase. Thus, As(III) can be effectively immobilized as the nanoparticles are deposited in the soil matrix.

To further investigate the effect of the nanoparticles on the leachability of arsenite remaining in the sandy soil, TCLP leaching tests were performed on the sandy soil following the batch treatments represented in Fig. 4-8a. Fig. 4-8b shows that the TCLP leachable As concentration amounted to 3000 µg/L for the water amended sandy soil. In contrast, the TCLP leachability was reduced by 94%-98% for samples treated with CMC-stabilized Fe-Mn at Fe-As of 6.5-39, and by 90%-99% with starch-stabilized Fe-Mn. The findings are consistent with the FTIR results. The formation of strong surface complexes between arsenic and the added iron greatly enhanced binding of the arsenic species to the solid phase. In all cases, the nanoparticle amendment rendered the As concentration in the TCLP fluid far below the current threshold concentration of 5 mg/L, which was based on the prior MCL of 0.05 mg/L as As. As a rule, the TCLP threshold is coupled with the corresponding MCL by a factor of 100, and it is believed that the TCLP threshold value is likely to be tightened significantly in the future. To this end, the nanoparticle amendment is of great practical significance for handling of As-laden wastes, as it may offer a powerful tool to convert a potentially hazardous waste into a less or non-hazardous material.

4.3.9. Immobilization of As(III) in soil: Column tests

CMC-stabilized Fe-Mn nanoparticles were tested for treating the arsenite-laden sandy soil through fixed-bed column experiments. Fig. 4-9a compares the arsenic elution histories during two column runs: one with SGW and the other with CMC-stabilized Fe-Mn nanoparticle suspension under otherwise identical conditions. In both cases, the elution curves displayed an immediate peaking followed by a gradual tailing. Based on mass balance, SGW eluted ~17% of arsenic loaded in the sandy soil while the Fe-Mn suspension leached ~15%. However, when the effluent samples of the nanoparticle suspension were further examined, ~94% of the eluted As

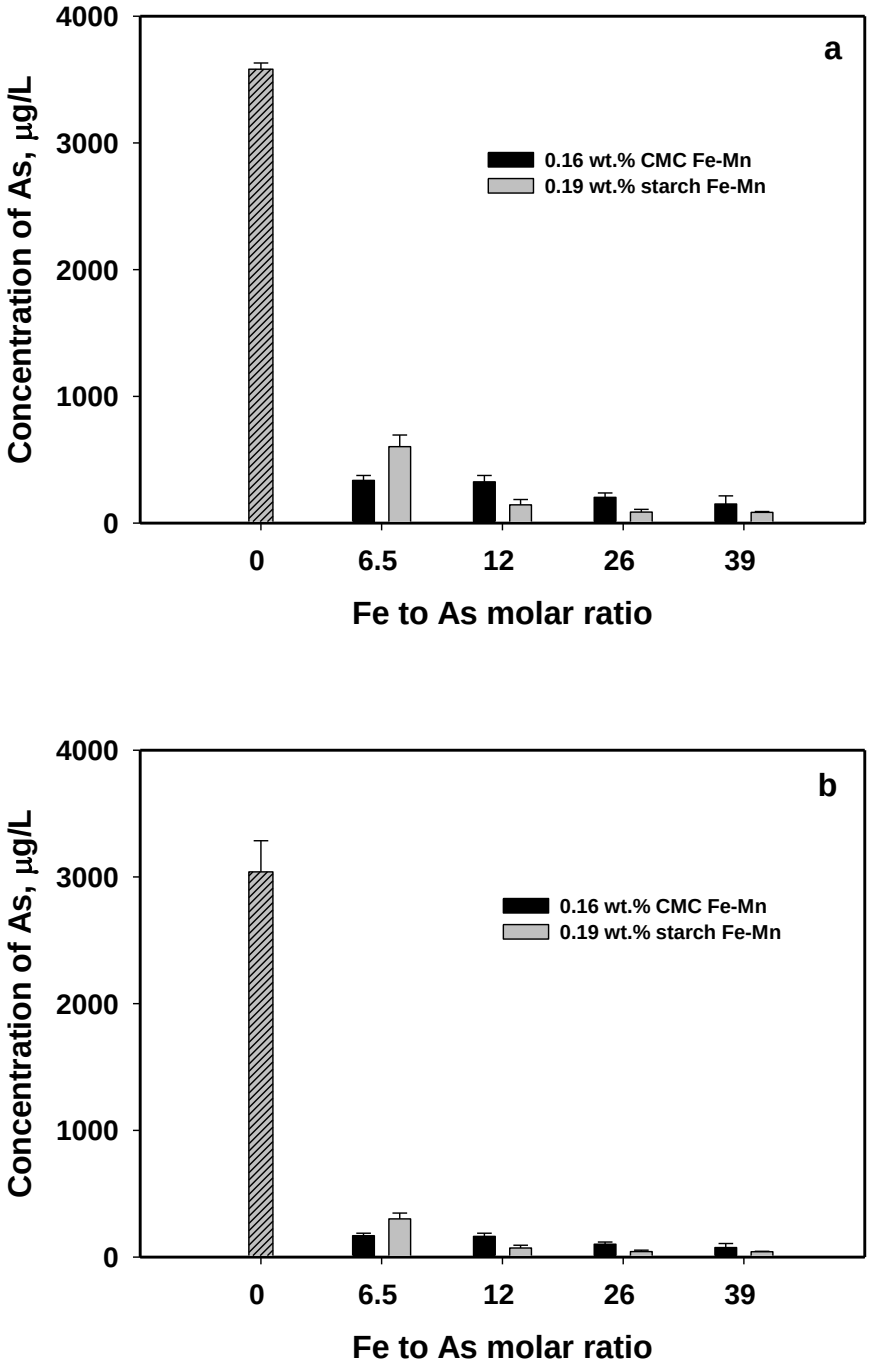

Fig. 4-8. (a) Arsenic concentration in the aqueous phase when an As(III)-laden soil was amended with water or various doses of stabilized Fe-Mn nanoparticles for 4 days; (b) Arsenic concentration in the TCLP fluid when the soil samples in (a) were subjected to TCLP tests.

was associated with the nanoparticles, while all As eluted by SGW was soluble. Evidently, the nanoparticles coverted nearly all water-soluble As into nanoparticle-associated As. Because the nanoparticles are virtually immobile under natural groundwater conditions, i.e. even the nanoparticles eluted at the high experimental pore velocity will eventually deposited in the soil matrix down the stream once the injection pore velocity is removed. This is of great practical significance in reducing As mobility and bioavailability. He et al. (2009) showed that under natural groundwater conditions, CMC-stabilized ZVI nanoparticles, which have an iron oxide shell, are mobile under high pore velocity, but immobile when the pressure was removed. Based on the nanoparticle breakthrough shown in Fig. 4-7 and following the modeling approach by He et al. (2009) the maximum travel distance of the CMC-stabilized Fe-Mn nanoparticles was estimated to be 2.8 m under a typical pore groundwater velocity of 0.18 m/s. Consequently, the delivered nanoparticels are more likely to serve as a sink for immobilization of water-leachable arsenite, rather than facilitate mobilization of the contaminant.

Following the elution tests, the TCLP leachability for As remaining in the SGW or nanoparticle amended soil was determined. Noting that the As mass remaining in the soil bed was about the same after the two elution tests, Fig. 4-9b shows that the nanoparticle amendment reduced the TCLP leachability by more than 76%, which can be attributed to the added sorption capacity and affinity due to the soil-retained Fe-Mn nanoparticles to the sandy soil. The presence of iron in soil has been known to retain more arsenic in the soil phase. For examples, Kim et al. (2003) demonstrated that amorphous iron treatment in highly contaminated mine tailings reduced extractable As, and Hartley et al. (2004) reported that various iron species could facilitate arsenic immobilization at a former landfill site and the effectiveness followed the sequence Fe^{3+} > Fe^{2+} > iron grit > goethite > Lime. The results from Figs. 4-9a and 9b indicate that the nanoparticle

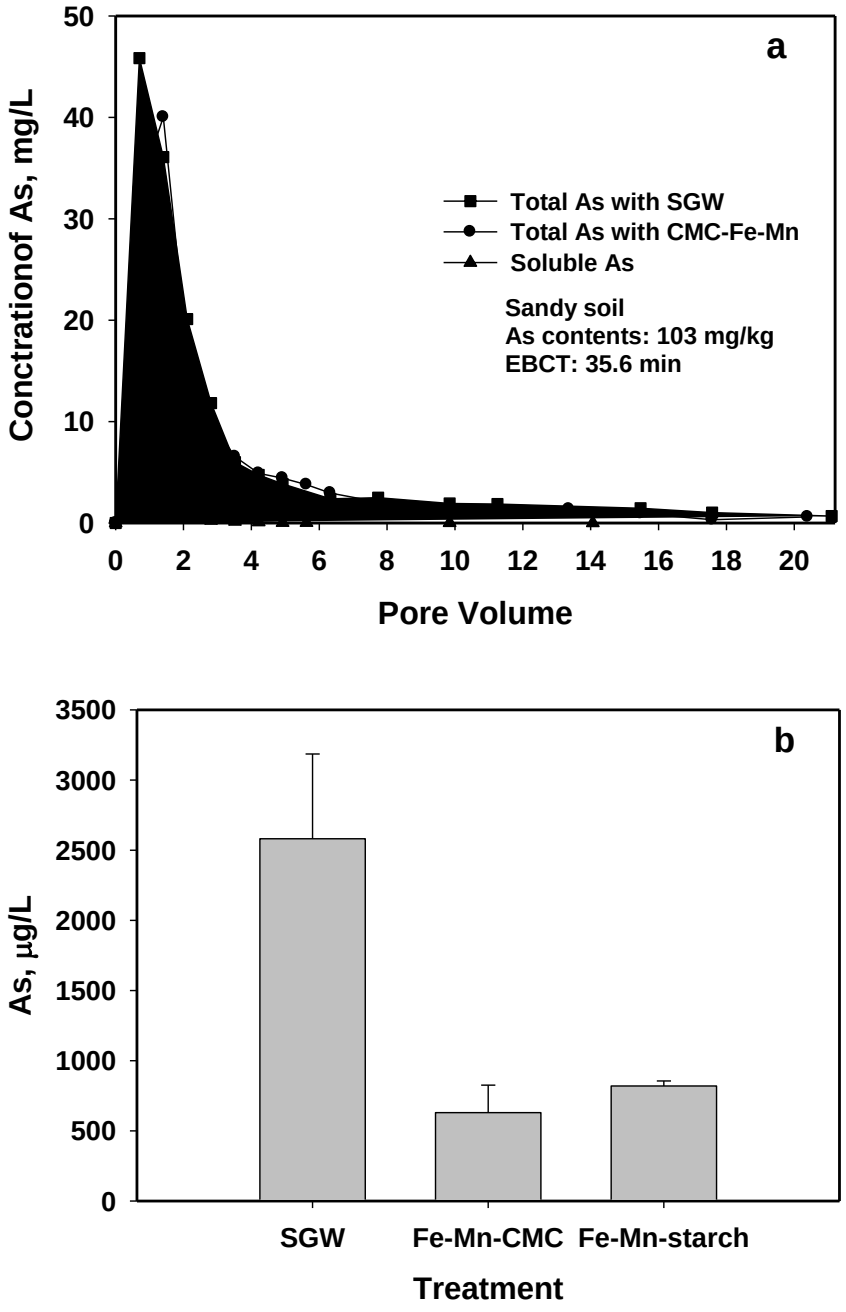

Fig. 4-9. (a) Arsenic elution profiles using simulated groundwater or CMC-stabilized Fe-Mn nanoparticle suspension (soluble As refers to As concentration after nanoparticels are removed), and (b) arsenic concentration in the TCLP fluid when the soil samples from (a) were subjected to TCLP tests.

amendment can not only immobilize the groundwater soluble As(III), but reduce the leachability of the remaining As(III) in the soil phase.

4.4. Conclusions

The main findings and conclusions can be summarized as follows:

- Based on XRD patterns, the starch- and CMC-stabilized Fe-Mn particles are characterized with amorphous structure.
- FTIR analyses showed that both As(V) and at least part of As(III) were adsorbed to the Fe-Mn particles through inner-sphere surface complexation via Fe-O-As bonding.
- Batch equilibrium adsorption experiments revealed that the stabilized nanoparticles offered comparable arsenic adsorption capacity to bare Fe-Mn particles. The sorbents preferred arsenite over arsenate at pH>5, but the opposite is true at pH<4. The maximum Langmuir capacity was determined to be 338 and 272 mg/g for As(III) and As(V) at pH 5.5, respectively, compared to 372 mg/g and 182 mg/g at pH 3.0.
- The adsorption of As(III) is less sensitive than that of As(V) and the maximum arsenic uptakes for As(III) and As(V) can be achieved at pH 6 and 3, respectively.
- Column breakthrough tests and elution profiles demonstrated the mobility of the CMC-stabilized nanoparticles, and 10% of the nanoparticles were consistently retained in the soil bed. Based on the breakthrough curve and filtration modeling, the maximum travel distance of the CMC-stabilized Fe-Mn nanoparticles was estimated to be 2.8 m under a typical pore groundwater velocity of 0.18 m/s. Consequently, the delivered nanoparticles can be considered immobile once the external pressure is released.

- Batch immobilization tests showed that the stabilized Fe-Mn nanoparticles were highly effective for immobilizing arsenic in a sandy soil. When treated with CMC-stabilized Fe-Mn at an Fe-to-As molar ratio of 6.5-39, the water leachable arsenic concentration was reduced by 91%-96%, and the TCLP leachability of arsenic was reduced by 94%-98%.
- Column elution of an As(III)-laden soil indicated that application of CMC-stabilized Fe-Mn suspension transferred virtually all water-soluble As(III) to the nanoparticle phase. Consequently, As(III) is immobilized as the nanoparticles are immobilized. In addition, the simple nanoparticle amendment was able to reduce the TCLP leachability of As(III) remaining in the soil by 78%.

Chapter 5. Conclusions and Suggestions for Future Research

5.1. Summary and Conclusions

Six new chelating resins were prepared by functionalizing three commercially available XAD resins of various matrix properties, including XAD1180, XAD16 and XAD7HP. Two types of functional groups were loaded on these sorbents, one with two nitrogen donor atoms (2N) per functional group and the other with three N-donor (3N) atoms per functional group. Consequently, six polymeric ligand exchangers (PLE's) were prepared by immobilizing Cu(II) ions onto these chelating resins, where Cu(II) serves as the surface central metal. The highest Cu(II) loading was determined to be 41 mg/g for XAD16-2N-Cu. Unlike standard strong base anion exchangers, the PLE's displayed greater affinity toward arsenate than for sulfate. The binary arsenate-sulfate separation factor ($\alpha_{As/S}$) ranged from 5.1 to 10. Bench-scale column breakthrough tests confirmed the greater selectivity for arsenate over other common anions (sulfate, bicarbonate and chloride). The breakthrough of arsenate occurred last at ~920 BV for XAD1180-3N-Cu. From batch kinetic tests, the intraparticle diffusivity *(D)* was determined to be 2.0×10^{-6} cm^2/sec for XAD1180-3N-Cu. The PLE's can be effectively regenerated using 6-8% NaCl at pH10. 100% of arsenate capacity can be recovered using 8% of NaCl at pH 10.

Ion exchange (IX) is considered by US EPA as one of the best available technologies for removing arsenic from drinking water. However, typical IX processes will generate large volumes of arsenic-laden regenerant brine that requires costly further

handling and disposal. This study aimed to develop an engineered strategy to minimize the production and arsenic leachability of the process waste residual. We prepared and tested a new class of starch-bridged magnetite nanoparticles for removal of arsenate from spent IX brine. A low-cost, "green" starch at 0.049% (w/w) was used as a stabilizer to prevent the nanoparticles from agglomerating and as a bridging agent allowing the nanoparticles to flocculate and precipitate while maintaining their high arsenic sorption capacity. When applied to a simulated spent IX brine containing 300 mg/L As and 6% (w/w) NaCl, nearly 100% removal of arsenic was achieved within 1 hour using the starch-bridged nanoparticles at an Fe-to-As molar ratio of 7.6, compared to only 20% removal when bare magnetite particles were used. Increasing NaCl in the brine from 0 to 10% w/w had little effect on the arsenic sorption capacity. Maximum uptake was observed within a pH range of 4 to 6. The Langmuir capacity coefficient was determined to be 248 mg/g at pH 5.0. The final treatment sludge was able to pass the TCLP (Toxicity Characteristic Leaching Procedure) based leachability of 5 mg/L as As.

Arsenite, As(III), generally found in the subsurface under anoxic conditions, is known to be more toxic and more difficult to remove from water using conventional water treatment techniques. Fe-Mn nanoparticles, which combine a strong adsorption capacity (iron oxide) with an effective oxidizing agent (manganese dioxide), were prepared at an Fe:Mn molar ratio of 3:1 with carboxymethyl cellulose as a stabilizer and were tested to remove both As(III) and As(V) from contaminated water and soil. Batch adsorption tests showed that 81, 80, and 75% of As(III) was removed from bare, starch, CMC Fe-Mn particles, whereas ~68% of As(III) was removed for all Fe-Mn particles from water treatment at pH 5.5 and Fe-Mn to As molar ratio of 3.6. As(III) and As(V) adsorption as a function of pH revealed a maximum adsorption capacity obtained at pH 6 and 3, respectively. The Langmuir capacity coefficient was determined to be 338 and 272

mg/g for As(III) and As(V) at pH 5.5, respectively. Transport column tests of 0.16 wt.% CMC Fe-Mn nanoparticles showed it can be effectively dispersed in soil. From amended soil with nanoparticle suspensions, the leached arsenic concentration was reduced by 91% at an Fe-to-As molar ratio of 6.5. The TCLP leachability of arsenic was reduced to 94% after batch treatment and 76% after column test with 20 pore volumn at an Fe-Mn to As molar ratio of 6.5.

5.2. Suggestions for future work

The specific recommendations for future work were made as follows:

1. Even though PLEs show great affinity for arsenate over strong competing anions such as sulfate and bicarbonate, the selectivity of arsenite which exists in the natural environment pH as H3AsO3 is less than other competing anions. As a result of low affinity, arsenite sorption capacity can be significantly reduced compared to that of arsenate. Further effort is suggested to search for pre-oxidation of arsenite to arsenate, before utilizing PLEs for arsenite treatment.
2. X-ray diffraction (XRD), x-ray photoelectron spectroscopy (XPS), extended x-ray absorption fine structure (EXAFS), and scanning electron microscopy (SEM), and transmission electron micrograph (TEM) image tests on stabilized nanoparticles synthesized with CMC and starch before and after arsenic adsorption can provide more confident evidence to elucidate the structure and the size of stabilized nanoparticles, and the mechanism of arsenic adsorption.
3. Fourier transform infrared spectroscopy (FTIR) which determines arsenate sorption mechanisms and interactions between starch and the nanoparticles shows the effect of the stabilizer on the metallic adsorbent. More elaborated analysis of FTIR before and after arsenic adsorption in the presence or absence of other ions can clearly prove the adsorption mechanism on the nanoparticles.

4. Environmental fate and impacts of stabilized Fe-Mn and arsenite in the arsenic contaminated soil is a necessary research field to apply nanoparticles to practical soil treatments. The impact of nanoparticles in the soil can be determined by the various factors such as pH, ORP, DO, and microbial community. Therefore, it is required to determine and evaluate the effect of each parameter in the soil for the application of nanoparticles.

References

Aldrich, M.V., Peralta-Videa, J.R., Parsons, J.G., Gardea-Torresdey, J.L., 2007. Examination of arsenic (III) and (V) uptake by the desert plant species mesquite (Prosopis spp.) using x-ray absorption spectroscopy. Sci. Total Environ. 379, 249-255.

Alibeigi, S., Vaezi, M.R., 2008. Phase transformation of iron oxide nanoparticles by varying the molar ratio of F^{2+}: Fe^{3+}, Chem. Eng. Technol. 31 (11), 1591-1596.

Allen, G.C., Harris, S.J., Jutson, J.A., Dyke, J.M., 1989. A study of a number of mixed transition metal oxide spinels using X-ray photoelectron spectroscopy. Appl. Surf. Sci. 37, 111-134.

Amrate, S., Akretche, D.E., 2005. Modeling EDTA enhanced electrokinetic remediation of lead contaminated soils. Chemosphere 60, 1376-1383.

An, B., Steinwinder, T.R., Zhao, D., 2005. Selective removal of arsenate from drinking water using a polymeric ligand exchanger, Water Res. 39, 4993-5004.

Anastassakis, G.N., 1999. A study on the separation of magnetite fines by magnetic carrier methods. Colloids Surf. A Physicochem. Eng. Aspects 149. 585–593.

Anderson, L.D.C., Bruland, K.W., 1991. Biogeochemistry of arsenic in natural waters: The importance of methylated species. Environ. Sci. Technol. 25, 420-427.

Anderson, P.J., 1957. On the ion adsorption properties of synthetic magnetite. Proc. 2nd International Congress on Surface Activity (3), 67-80.

Aria, Y., Sparks, D.L., Davis, J.A., 2004. Effects of dissolved carbonate on arsenate adsorption and surface speciation at the hematite water interface. Environ. Sci. Technol. 38, 817-824.

Ataie, A., Heshmati-Manesh, S., 2001. Synthesis of ultra-fine particles of strontium hexaferrite by a modified co-precipitation method. J. Eur. Ceram. Soc. 21, 1951–1955.

Badruzzaman, M., Westerhoff, P., Knappe, D.R.U., 2004. Intraparticle diffusion and adsorption of arsenate onto granular ferric hydroxide (GFH). Water Res. 38, 4002–4012.

Ballinas, M.L., Rodriguez de San Miguel, E., De Jesus Rodriguez, M.T., Silva, O., Munoz, M., De Gyves, J., 2004. Arsenic(V) removal with polymer inclusion membranes from sulfuric acid media using DBBP as carrier. Environ. Sci. Technol. 38 (3), 886-891.

Banerjee, K., Amy, G.L., Prevost, M., Nour, S., Jekel, M., Gallagher, P.M., Blumernschein, C.D., 2008. Kenetic and thermodynamic aspects of adsorption of arsenic onto granular ferric hydroxide (GFH). Water Res. 42, 3371-3378.

Benjamin, M.M., Sletten, R.S., Bailey R.P., Bennett, T., 1996. Sorption and filtration of metals using iron-oxide-coated sand. Water Res. 30, 2609–2620.

Bennett, P., He, F., Zhao, D., Aiken, B., Feldman, L., 2010. In situ testing of metallic iron nanoparticle mobility and reactivity in a shallow granular aquifer. J. Contam. Hydrol. 116, 35-46.

Berg, M.H.C., Nguyen, T.C., Pham, H.V., Schertenleib, R., Giger, W., 2001. Arsenic contamination of groundwater and drinking water in Vietnam: A human health threat. Environ. Sci. Technol. 35, 2621-2626.

Biggs, S., 2006. Polymeric Flocculants, in: Encyclopedia of surface and colloid science: 2nd Ed, Somasundaran, P. Vol. 7. Taylor and Francis, New York.

Bissen, M., Frimmel, F.H., 2003. Arsenic- a Review. Part II: Oxidation of arsenic and its removal in water treatment. Acta Hydrochim. Hydrobiol. 31, 97-107.

Bissen, M., Vieillard-Baron, M.M., Schindelin, A.J., Frimmel, F.H., 2001. TiO_2-catalyzed photooxidation of arsenite to arsenate in aqueous samples. Chemosphere 44, 751–757.

Bowell, R., Parshley, J., 2001. Arsenic cycling in the mining environment. http://www.epa.gov/ttbnrmrl/ArsenicPress/89.pdf . Accessed May 2006.

British Geological Survey (BGS), 2000. Executive summary of the main report of phase I, Groundwater Studies of As contamination in Bangladesh, UK.

Camps, M., Charzopoulos, M., Montheard, J-P., 1982. Chloromethylstyrene: Synthesis, polymerization, transformations, applications. Polym. Rev. 22, 343-407.

Chang, F.F., Qu, J.H., Liu, H., Liu, R., Zhao, X., Fe-Mn binary oxide incorporated into diatomite as an adsorbent for arsenite removal: Preparation and evaluation, J. Colloid Inter. Sci. 338 (2009) 353-358.

Chanda, M., O'Driscoll, K.F., Rempel, G.L., 1988. Ligand exchange sorption of arsenate and arsenite anions by chelationg resins in ferric ion form. React. Polym. 8, 85-95.

Chastellain, M., Petri, A., Hofmann, H., 2004. Particle size investigations of a multistep synthesis of PVA coated superparamagnetic nanoparticles. J. Colloid Interf. Sci. 278, 353-60.

Chatterjee, A., Das, D., Mandal, B.K., Chowdhury, T.R., Samanta, G., Chakraborti, D., 1995. Arsenic in ground water in six districts of West Bengal, India: The biggest arsenic calamity in the world. Part I. Arsenic species in drinking water and urine of the affected people. Analyst 120, 643-650.

Chen, H.W., Frey, M.M., Clifford, D., McNeil, L.S., Edwards, M., 1999. Arsenic treatment considerations. J. Am. Water Works Assoc. 91, 74-85.

Chen, X., Quan, C., Wang, W., Chen, Z., Wu, Z., Wu, Z., 2007. X-ray diffraction and X-ray absorption spectroscopy studies on the chemical transformation and formation of nanoscale $LaMnO_{3.12}$. J. Phys. Chem. 111, 4512-4518.

Chwirka, J.D., Colvin, C., Gomez, J.D., 2004. Arsenic removal from drinking water using the coagulation/cicrofiltration process. J. Am. Water Works Assoc. 96(3), 106-114.

Clifford, D., Ceber, L., Chow, S., 1983. Arsneic(III)/arsenic(V) separation by chloride-from ion exchange resins. XI. AWWA Water Qual. Tech. Conf., Norfolk, VA.

Clifford, D., Lin, C.C., 1991. Arsenic III and arsenic V removal from drinking water in San Ysidro, New Mexico. EPA/600/2-91/011. U.S. EPA, Cincinnati, OH.

Clifford, D., 1999. Ion exchange and inorganic adsorption, in: Water Quality and Treatment, A Handbook of Community Water Supplies. American Water Works Association, 9.1-9.91. McGraw Hill, New York.

Clifford, D.A., Ghurye, G.L., Tripp, A.R., 2003. As removal using ion exchange with spent brine recycling. J. Am. Water Works Assoc. 95 (6), 119-130.

Coker, V.S., Gault, A.G., Pearce, C.I., Van der Laan, G., Telling, N.D., Charnock, J.M., Polya, D.A., Lloyd, J.R., 2006. XAS and XMCD evidence for species-dependent partitioning of arsenic during microbial reduction of ferrihydrite to magnetite. Environ. Sci. Technol. 40, 7745-7750.

Compean-Jasso, M.E., Ruiz, F., Martinez, J.R., Herrera-Gomez, A., 2008. Magnetic properties of magnetite nanoparticles synthesized by forced hydrolysis. Mater. Lett. 62, 4248-4250.

Cornell, R.M., Schwertmann, U., 2003. The iron oxides: Structure, properties, reactions, occurrences, and uses, 2nd Ed. Wiley-VCH, Weinheim, Germany.

Crank, J., 1975. The mathematics of diffusion. 2nd Ed, Clarendon Press, Oxford, U.K.

Cullen, W.R., Reimer, K.J., 1989. Arsenic speciation in the environment. Chem. Rev. 89, 713–764.

Cumbal, L., SenGupta, A.K., 2005. Arsenic removal using polymer-supported hydrated iron (III) oxide nanoparticles: Role of donnan membrane effect. Environ. Sci. Technol. 39, 6508-6515.

Deschamps, E., Ciminelli, V.S.T., Holl, W.H., 2005. Removal of As(III) and As(V) from water using a natural and Mn enriched sample. Water Res. 39, 5212-5220.

Dixit, S., Hering, J.G., 2003. Comparison of arsenic(V) and arsenic(III) sorption onto iron oxide minerals: Implications for arsenic mobility. Environ. Sci. Technol. 37, 4182-4189.

Dodd, M.C., Vu, N.D., Ammann, A., Le, V.C., Kissner, R., Pham, H.V., Cao, T.H., Berg, M., Gunten, U.V., 2006. Kinetics and mechanistic aspects of As(III) oxidation by aqueous chlorine, chloramines, and ozone: Relevance to drinking water treatment. Environ. Sci. Technol. 40, 3285–3292.

Edwards, M., 1994. Chemistry of arsenic removal during coagulation and Fe-Mn oxidation. J. Am. Water Works Assoc. 86, 64-78.

EPA. 1992 Test methods for evaluating waste, physical/chemical methods, 3rd Edition, SW-846 Method 1311, U.S. Government Printing Office, Washington, D.C.

EPA, 2000a. Arsenic removal from drinking water by ion exchange and activated alumina plants. EPA/600/R-00/088. Cincinnati. OH. 2000.

EPA, 2000b. Technologies and costs for removal of arsenic from drinking water. EPA/815/R-00/028. Office of Water.www.epa.gov.

EPA, 2001. Treatment of arsenic residuals from drinking water removal processes. EPA/600/R-01/033. Office of Research and Development, Washington, DC.

Fendorf, S.E., Eick, M.J., Grossl, P., Sparks, D.L., 1997. Arsenate and chromate retention mechanisms on goethite. 1. Surface structure. Environ. Sci. Technol. 31 (2), 315-320.

Frechetand, J. M. J., Farrall, M. J., 1977. Functionalization of crosslinked polystyrene resins by chemical modification: A Review, In: Labana, S.S. (Ed.) Chemistry and properties of crosslinked polymers, Academic Press Inc. New York.

Ferguson, J.F., Gavis, J.A., 1972. Review of the arsenic cycle in natural waters. Water Res. 6, 1259-1274.

Ferguson, J.F., Anderson, M.A., 1974. Chemical form of arsenic in water supplies and their removal. In: Rubin, A.J. (Eds.) Chemistry of water supply, treatment, and distribution. Ann Arbor Science. Ann Arbor, MI.

Frank, P., Clifford, D., 1986. Arsenic(III) oxidation and removal from drinking water. US Environ Prot Agency Report. EPA-600-52-86/021.

Frey, M., Chwirka, J.D., Kommineni, S., Chowdhury, Z., Marasimhan, R., 2000. Cost implications of a lower arsenic MCL. AWWA Research Foundation, Denver, CO.

German, J., 2001. Arsenic trappers could allay national sticker shock of new EPA standard. Sandia Lab. News 53 (5).

Ghimire, N. K., Inoue, K., Yamaguchi, H., Makino, K., Miyajima, T., 2003. Adsorptive separation of arsenate and arsenite anions from aqueous medium by using orange waste. Water Res. 37, 4945-4953.

Ghosh, A., Mukiibi, M., Ela, W., 2004. TCLP underestimates leaching of arsenic from solid residuals under landfill conditions. Environ. Sci. Technol. 38 (17) 4677-4682.

Ghurye, G., Clifford, D., Tripp, A., 2004. Iron coagulation and direct microfiltration to remove arsenic from groundwater. J. Am. Water Works Assoc. 96(4) 143-152.

Gilles, G., Mathis, J., 2002. Using advanced adsorptive media for arsenic treatment. Water Eng. Mangr. 149, 33-37.

Gimenez, J., Martinez, M., Pablo, J., Rovira, M., Duroc, L., 2007. Arsenic sorption onto natural hematite, magnetite, and goethite. J. Hazard. Mater. 141, 575-580.

Goldberg, S., Johnston, C.T., 2001. Mechanisms of arsenic adsorption on amorphous oxides evaluated using macroscopic measurements, vibrational spectroscopy, and surface complexation modeling. J. Colloid Int. Sci. 234, 204–216.

Grafe, M., Eick, M.J., Grossl, P.R., 2001. Adsorption of arsenate (V) and arsenite (III) on goethite in the presence and absence of dissolved organic carbon. Soil Sci. Soc. Am. J. 65, 1680-1687.

Greig, J.A., Sherrington, D.C., 1979. Electrophilic substitution of highly crosslinked polystyrene resins Eur. Polym. J. 15, 867-871.

Grinstead, R.R., Nasutavicus, W.A., 1977. Water insoluble chelate exchange resins having a crosslinked polymer matrix and pendant thereto a plurality of methyleneaminopyridine groups. US Patent #4031038.

Gu, Z.M., Fang, J., Deng, B.L., 2005. Preparation and evaluation of GAC-based iron-containing adsorbents for arsenic removal. Environ. Sci. Technol. 39, 3833–3843.

Guo, X., Chen, F., 2005. Removal of arsenic by bead cellulose loaded with iron oxyhydroxide from groundwater. Environ. Sci. Technol. 39, 6808-6818

Haque, S., Ji, J., Johannesson, K.H., 2008. Evaluating mobilization and transprot of arsenic in sediments and groundwaters of Aquia aquifer, Maryland, USA. J. Contam. Hydrol. 99, 68-84.

Hartley, W., Edwards, R., Lepp, N.W., 2004. Arsenic and heavy metal mobility in iron oxide-amended contaminated soils as evaluated by short- and long- term leaching test. Environ. Pollut. 131, 495-504.

He, F., Zhao, D., 2005. Preparation and characterization of a new class of starch-stabilized bimetallic nanoparticles for degradation of chlorinated hydrocarbons in water. Environ. Sci. Technol. 39, 3314-3320.

He, F., Zhao, D., 2007, Manipulating the size and dispersibility of zerovalent iron nanoparticles by use of carboxymethyl cellulose stabilizers. Environ. Sci. Technol. 41, 6216-6221.

He, F., Zhao, D., Liu, J., Roberts, C.B., 2007. Stabilization of Fe/pd bimetallic nanopaticles with sodium carboxymethyl cellulose to facilitate dechlorination of trichloroethene and soil transportablility. Ind. Eng. Chem. Res. 46, 29-34.

He, F., Zhang, M., Qian, T., Zhao, D., 2009. Transpsort of carboxymethyl cellulose stabilized iron nanoparticles in porous media: Column experiments and modeling. J. Colloid Interf. Sci. 334, 96-102.

He, F., Zhao, D., Paul, C., 2010. Field assessment of carboxymethyl cellulose stabilized iron nanoparticles for in situ destruction of chlorinated solvents in source zones. Water Res. 44, 2360-2370.

Helfferich, F., 1962. Ion exchange, McGraw-Hill book company, Inc; New York.

Hering, J.G., Chen, P-Y., Wilkie, J.A., Elimelech, M., Liang, S., 1996. Arsenic removal by ferric chloride. J. Am. Water Works Assoc. 88 (4), 155-167.

Hering J.G., Chen, P-Y., Wilkie, J.A., Elimelech, M., 1997. Arsenic removal from drinking water during coagulation. J.Environ. Eng. ASCE. 123, 800-807.

Hirashima, M., Takahashi, R., Nishinari, K., 2005. Effects of adding acids before and after gelatinization on the viscoelasticity of cornstarch pastes. Food Hydrocolloid. 19, 909-914

Holm, T. R. 2002. Effects of CO_3^{2-}/bicarbonate, Si, PO_4^{3-} on Arsenic sorption to HFO. J. Am. Water Works Assoc. 94 (4) 1740179.

Huang, M., Wang, H., Yu, J., 2006. Studies of biodegradable thermoplastic amylose/kaolin composites: Fabrication, characterization, and properties. Polym. Composite. 27, 309-314.

Hubbard, K. L., Finch, J. A., Darling, G. G., 1998. The preparation and characteristics of poly(divinylbenzene-co-ethylvinylbenzene), including ambeflite XAD-4. styrenic resins with pendant vinylbenzene groups. React. Funct. Polym. 36, 17-30.

Huber, D.L., 2005. Synthesis, properties, and applications of iron nanoparticles. Small 1 (5), 482-501.

Hug, S.J., Leupin, O., 2003. Iron-catalyzed oxidation of arsenic(III) by oxygen and by hydrogen peroxide: pH-dependent formation of oxidants in the Fenton reaction. Environ. Sci. Technol. **37**, 2734–2742.

Husband, J.C., 1998. The adsorption of starch derivatives onto kaolin. Colloids and surfaces A: Physicochemical and engineering Aspects 131, 145-159.

Iijima, M., Yonemochi, Y., Tsukada, M., Kamiya, H., 2006. Microstructure control of iron hydroxide nanopaticles using surfactants with different molecular structures. J. Colloid. Interf. Sci. 298, 202-208.

Ivanov-Emin, B.N., Nevskaya, N.A., Zaitsev, B.E., Ivanova, T.M., 1982. Zh. Neorg. Khim. 27, 3101.

Jackson, B.P., Bertsch, P.M., Cabrera, M.L., Camberato, J.J., Seaman, J.C., Wood, C.W., 2003. Trace element speciation in poultry litter. J. Environ. Qual. 32, 535-540.

Jain, C.K., Ali, I., 2000. Arsenic: Occurrence, toxicity and speciation. Water Res. **34**, 4304–4312.

Jang, M., Hwang, J.S., Choi, S.I., Park, J.K., 2005. Remediation of arsenic-contaminated soils and washing effluents. Chemosphere 60, 344-354.

Jiang, J.Q., 2001. Removing arsenic from groundwater for the developing world-a review. Water Sci. Technol. 44, 89-98.

Jolivet, J-P., 2000. Metal oxide chemistry and synthesis: From solution to solid state, Wiley, Chichester. Germany.

Jones, F., Farrow, J.B., Bronswijk, W.V., 1998. An infrared study of a polyacrylate flocculant adsorbed on hematite. Langmuir 14 (22), 6512-6517.

Kanel, S.R., Greneche, J.M., Choi, H., 2006. Arsenic(V) removal from groundwater using nano scale zero-valent iron as a colloidal reactive barrier material. Environ. Sci. Technol. 40, 2045-2050.

Kanel, S.R., Nepal, D., Manning, M., Choi, H., 2007. Transport of surface-modified iron nanoparticles in porous media and application to arsenic(III) remediation J. Nanopart. Res. 9, 725-735.

Kang, M., Kawasaki, M. Tamada, S., Kamei, T., Magara, Y., 2000. Effect of pH on the removal of arsenic and antimony using reverse osmosis membranes. Desalination 131,293-298.

Keiser, J.T., Brown, C.W., Heidersbach, R.H., 1982. The electrochemical reduction of rest films on weathering surface. J. Electrochem. Soc. 129, 2686-2689.

Kim, J., Benjamin, M.M., Kwan, P., 2003a. A novel ion exchange process for As removal. J. Am. Water Works Assoc. 95 (3), 77-85.

Kim, J., Davis, A.P., Kim, K-W., 2003b. Stabilization of available arsenic in highly contaminated mine tailings using iron. Environ. Sci. Technol. 37, 189-195.

Kim, M.J., Nriagu, J., 2000. Oxidation of arsenite in groundwater using ozone and oxygen. Sci. Total Environ. 247, 71–79.

Kim, S-O., Kim, W-S., Kim K-W., 2005. Evaluation of electrokinetic remediation of arsenic-contaminated soils. Environ. Geochem. Health 27, 443-453.

Kosmulskia, M., Maczkaa, E., Jartychc, E., Rosenholmb, J.B., 2003. Synthesis and characterization of goethite and goethite–hematite composite: Experimental study and literature survey. Adv. Colloid Interfac. 103, 57-76.

Kovalenko, M.V., Bodnarchuk, M.I., Lechner, R.T., Hesser, G., Schaffler, F., Heiss, W., 2006. Fatty acid salts as stabilizers in size- and shape-controlled nanocrystal synthesis: The case of inverse spinel iron oxide. J. Am. Chem. Soc. 129, 6352-6353.

Kretzschmar, R., Borkovec, M., Grolimund, D., Elimelech, M., 1999. Mobile subsurface colloids and their role in contaminant transport. Adv. Agron. 66, 121-193.

Krishna, B., Chadrasekaran, K., Karunasagar, D., Arunachalam, J., 2001. A combined treatment approach using Fenton's reagent and zero-valent iron for the removal of arsenic from drinking water. J. Hazard. Mater. B 84, 229–240.

Lee, K.M., Kim, S-G., Kim, W-S., Kim, S.S., 2002. Properties of iron oxide particles prepared in the presence of dextran. Korean J. Chem. Eng. 19 (3), 480-485.

Li, Z., Deng, S., Yu, G., Huang, J., Lim, V.C., 2010. As(V) and As(III) removal from water by a Ce-Ti oxide adsorbent: Behavior and mechanism. Chem. Eng. J. 161, 106-113.

Lien, H-L., Wilkin, R.T., 2005. High-level arsenite removal from groundwater by zero-valent iron. Chemosphere 59, 377-386.

Liu, R., Zhao, D., 2007. Reducing leachability and bioaccessibility of lead from soils using a new class of stabilized iron phosphate nanoparticles. Water Res. 41, 2491-2502.

Lufor, M.R., Silong, S., Zin, W.M., Ab Rahman, M.Z., Ahmad, M., Haron, J., 2000. Preparation and characterization of poly(amidoxime) chelating resin from polyacrylonitrile grafted sago starch. Eur. Polym. J. 36, 2105-2113.

Lytle, D.A., Chen, A.S., Sorg, T.J., Phillips, S., French, K., 2007. Microbial As(III) oxidation in water treatment plant filters. J. Am. Water Works Assoc. 99 (12), 72-86.

Ma, X., Bruckard, W.J., 2010. The effect of pH and ionic strength on starch-kaolinite interactins. Int. J. Miner. Process. 94, 111-114.

Maity, D., Agrawal, D.C., 2007. Synthesis of iron oxide nanoparticles under oxidizing environment and their stabilization in aqueous and non-aqueous media. J. Magn. Magn. Mater. 308, 46–55.

Manning, B.A., Fendorf, S.E., Bostick, B., Suarez, D.L., 2002. Aarsenic(III) oxidation and arsenic(V) adsorption reactions on synthetic birnessite. Envrion. Sci. Technol. 36, 976-981.

Marquez, E. B., Gurian, P. L., Barud-Zubillaga, A., Goodell, P., 2005. Geochemistry of groundwater arsenic in the El Paso Region. Proc. National Ground Water Association Naturally Occurring Contaminants Conference, Charleston. SC.

Martinson, C.A., Reddy, K.J., 2009. Adsorption of arsenic(III) and arsenic(V) by cupric oxide nanoparticles. J. Colloid Int. Sci. 336 (2), 406-411.

Masue, Y., Loeppert, R.H., Kramer, T.A., 2007. Arsenate and arsenite adsorption and desorption behavior on coprecipitated aluminum: Iron hydroxides. Environ. Sci. Technol. 41, 837-842.

Meharg, A.A., Hartley-Whitaker, J., 2002. Arsenic uptake and metabolism in arsenic resistant and non resistant plant species. New Phytol. 154, 29-43.

Melby, L.R., 1975. Polymers for selective chelation of transition metal ions. J. Am. Chem. Soc. 97, 4044-4051.

Miretzk, P., Cirelli, A.R., 2010. Remediation of arsenic-contaminated soils by iron amendments: A review. Crit. Rev. Eng. Sci. Tec. 40, 93-115.

National Academy of Sciences. 1977. Arsenic: Medical and biologic effects of environmental pollutants. Natl. Acad. Press, Washington, D.C.

Nishio, Y., Yamada, A., Ezaki, K., Miyashita, Y., Furukawa, H., Horie, K., 2004. Preparation and magnetometric characterization of iron oxide-containing alginate/poly(vinyl alcohol) networks. Polymer, 45 (21), 7129-7136.

NRC, 2001. Arsenic in drinking water: 2001 update. National Research Council, National Academy Press, Washington DC.

Nriagu, J.O., 1994. (Ed), Arsenic in the Environment: Part 1: Cycling and Characterizations. Wiley, New York.

Ohe, K., Tagai, Y., Nakamura, S., Oshima, T., Baba, Y., 2005. Adsorption behavior of arsenic(III) and arsenic(V) using magnetite. J. Chem. Eng. Jpn. 38, 671-676.

O'Neill, P., 1990. Arsenic. In: Alloway, B.J. (Eds) Heavy Metals in Soils. 2nd Ed. Blackie, London.

Pena, M., Meng, X., Korfiatis, P.G., Jing, C., 2006. Adsorption mechanism of arsenic on nanocrystalline titanium dioxide. Environ. Sci. Technol. 40, 1257-1262.

Pettine, M., Campanella, L., Millero, F.J., 1999. Arsenite oxidation by H_2O_2 in aqueous solutions. Goechim. Cosmochim. Acta 63, 2727–2735.

Phenrat, T., Marhaba, T.F., Rachakornkij, M., 2008. Leaching behaviors of arsenic from arsenic-Iron hydroxide sludge during TCLP. J. Envir. Engrg. 134 (8), 671-682.

Piche´, M., Al Larachi, F. 2005. Degradability of iron(III)-aminopolycarboxylate complexes in alkaline media: Statistical design and X-ray photoelectron spectroscopy studies. Ind. Eng. Chem. Res. 44, 5053-5062.

Pierce, M.L., Moore, C.B., 1982. Adsorption of arsenic and arsenate on amorphous iron hydroxide. Water Res. 16, 1247-1253.

Ponder, S.M., Darab, J.G., Mallouk, T. E., 2000. Remediation of Cr(VI)and Pb(II) aqueous solutions using supported, nanoscale zerovalent iron. Environ. Sci. Technol. 34, 2564-2569.

Prakash, S., Das, B., Mohanty, J.K., Venugopal, R., 1999. The recovery of fine iron minerals from quartz and corundum mixtures using selective magnetic coating. Int. J. Miner. Process. 57, 87–103.

Prepper, K.W., H.M., Paisley, H.W., Young, M.A., 1953. Properties of ion-exchange resins in relation to their structure. Part VI. Anion-exchange resins derived from styrene-divinyl-benzene copolymers**.** J. Chem. Soc. 4097-4105.

Pushpadass, H.A., Ma, D.B., Hanna, M.A., 2008. Effects of extrusion temperature and plasticizers on the physical and functional properties of starch films. 60, 527-538.

Qian, Y., Xie,Y., He, C., Li, J., Chen, Z., 1994. Hydrothermal preparation and characterization of ultrafine magnetite powders. Mater. Res. Bull. 29 (9), 953-957.

Ramana, A., SenGupta, A.K., 1992. Removing selenium(IV) and arsenic(V) oxyanions with tailored chelating polymers. J. Env. Eng. 118, 755–775.

Raven, K.P., Jain, Amita., Loeppert, R.H., 1998. Arsenite and arsenate adsorption on ferrihydrite: Kinetics, equilibrium, and adsorption envelopes. Environ. Sci. Technol. 32, 344-349.

Raveendran, P., Fu, J., Wallen, S.L., 2003. Complete "green" synthesis and stabilization of metal nanoparticles. J. Am. Chem. Soc. 125, 13940-13941.

Ravishankara, S.A., Pradip, Khosla, N.K., 1995. Selective flocculation of iron oxide from its synthetic mixtures with clays: A comparison of polyacrylic acid and starch polymers. Int. J. Miner. Process. 43, 235-247.

Ristic, M., De Grave, E., Music, S., Popovic, S., Orehovec, Z., 2007. Transformation of low crystalline ferrihydrite to α-Fe_2O_3 in the solid state. J. Mol. Struct. 834-836, 454-460.

Schwertmann, U., Cornell, R.M., 2000. Iron oxide in the laboratory Wiley-vch, Weinheim, Germany.

Scott, M.J., Morgan, J.J., 1995. Reactions at oxide surfaces. 1. Oxidation of As(III) by synthetic birnessite. Environ. Sci. Technol., 29, 1898-1905.

Shipley, H.J., Yean, S., Kan, A.T., Tomson, M.B., 2009. Adsorption of arsenic to magnetite nanoparticles: Effect of particle concentration, pH, ionic strength, and temperature. Environ. Toxicol. Chem. 28, 509-515.

Si, S., Kotal, A., Mandal, T.K., Giri, S., Nakamura, H., Kohara, T., 2004. Size-controlled synthesis of magnetite nanoparticles in the presence of polyelectrolytes. Chem. Mater. 16, 3489-3496.

Smedley, P.L., Kinniburgh, D.G., 2002. A review of the source, behavior and distribution of arsenic in natural waters. Appl. Geochem. 17, 517-568.

Snoeyink, V., Jenkins, D., 1980. Water chemistry. John Wiley and Sons, Inc. New York.

Sposite, G., 1989. The chemistry of soils. Oxford Univ. Press, New York.

Su, C.M., Puls, R.W., 2001. Arsenate and arsnite removal by zerovalent iron kinetics, redox transformation, and implications for in situ groundwater remediation. Envirion. Sci. Technol, 35, 1478-1492.

Su, C., Puls, R.W., 2008. Arsenate and arsenite sorption on magnetite: Relations to groundwater arsenic treatment using zerovalent iron and natural attenuation. Water Air Soil Pollut. 193, 65–78.

Su, C., Suarez, D.L., 2000. Selenate and selenite sorption on iron oxides: An infrared and electrophoretic study. Soil Sci. Soc. Am. J. 64, 101–111.

Sun, X., Doner, H.E., 1996. An investigation of arsenate and arsenite bonding structure on goethite by FTIR. Soil Sci. 161, 865-872.

Sylvester, P., Westerhoff, P., Möller, T., Badruzzaman, M., Boyd, O., 2007. A hybrid sorbent utilizing nanoparticles of hydrous iron oxide for arsenic removal from drinking water. Environ. Eng. Sci. 24, 104–112.

Tamaura, Y., Takahasi, K., Kodera, Y., Saito, Y., Inada, Y., 1986. Chemical modification of lipase with ferromagnetic modifier — A ferromagnetic-modified lipase Biotechnol. Lett. 8, 877-880.

Tan W. F., Lu, S. J., Fan, L., Feng, X. H., He, J. Z., Coopal, L. K., 2008. Determination of the point-of-zero charge of manganese oxides with different methods including an improved salt titration method. Soil Sci. 173, 277–286.

Tang, J., Mayers, M., Bosnick, K.A., Brus, L.E., 2003. Magnetite Fe_3O_4 nanocrystals: Spectroscopic observation of aqueous oxidation kinetics. J. Phys. Chem. B 107, 7501-7506.

Tang, N.J., Zhong, W., Jiang, H.Y., Wu, X.L., Liu, W., Du, Y.W., 2004. Nanostructured magnetite (Fe_3O_4) thin films prepared by sol-gel method, J. Magn. Magn. Mater. 282, 92-95.

Tuutijärvi, T., Lu, J., Sillanpää, M., Chen, G., 2009. As(V) adsorption on maghemite nanoparticles. J. Hazard. Mater. 166, 1415-1420.

Voegelin, A., Hug, S., 2003. Catalyzed oxidation of arsenic(III) by hydrogen peroxide on the surface of ferrihydrite: An in situ ATR-FTIR study. Environ. Sci. Technol. 37, 972-978.

Wang, S., Xin, H., Qian, Y., 1997. Preparation of nanocrystalline Fe_3O_4 by γ-ray radiation. Mater. Lett. 33, 113-116.

Warshawsky, A., 1986. Modern research in ion exchange, in: A.E. Rodriguez(Ed) Ion Exchange: Science and Technology, NATO ASI Series, Martinus Nijhoff Publishers, Boston, MA, pp. 67-116.

Waychunas, G.A., Rea, B.A., Fuller, C.C., Davis, J.A., 1993. Surface chemistry of ferrihydrite: part1. EXAFS studies of the geometry of coprecipitated and adsorbed arsenate. Geochim. Cosmochim. Acta. 57 (10), 2251-2269.

Wilkie, J.A., Hering, J.G., 1996. Adsorption of arsenic onto hydrous ferric oxide: effects of adsorbate/adsorbent ratios and co-occurring solutes, Colloid Surf. A: Physicochem. Eng. Aspects 107, 97–110.

World Health Organization (WHO), 2006. Arsenic in the drinking water Fact Sheet 210. World Health Organization, Geneva, Switzerland.

Xiong, Z., He, F., Zhao, D., Barnett, M.O., 2009. Immobilization of mercury in sediment using stabilized iron sulfide nanopartilces. Water Res. 43, 5171-5179.

Xu, Y., Zhao, D., 2007. Reductive immobilization of chromate in water and soil using stabilized iron nanopartilces. Water Res. 41, 2101-2108.

Yang, H., Lin, W.Y., Rajeshwar, K., 1999. Homogeneous and heterogeneous photocatalytic reactions involving As(III) and As(V) species in aqueous media. J. Photochem. Photobiol. A: Chemistry 123, 137–143.

Yavuz, C.T., Mayo, J.T., Yu, W.W., Prakash, A., Falkner, J.C., Yean, S., Cong, L., Shipley, H.J., Kan., A., Tomson, M., Natelson, D., Colvin, V.L., 2006. Low-field magnetic separatin of monodisperse Fe_3O_4 nanocrystals. Science, 314, 964-967.

Yean, S., Cong,L., Yavuz, C.T., Mayo, J.T., Yu, W.W., Kan, A.T., Colvin, V.L., Tomson, M.B., 2005. Effect of magnetite particles on adsorption and desorption of arsenite and arsenate. J. Mater. Res. 20 (12), 3255-3264.

Yokoi, H., Kantoh, T., 1993. Thermal decomposition of the iron(III) hydroxide and magnetite composites of poly(vinyl alcohol). Preparation of magnetite and metallic iron particles. B. Chem. Soc. Jpn. 66, 1536-1541.

Yoon, S-H., Lee, J.H., 2005. Oxidation mechanism of As(III) in the UV/TiO_2 system: Evidence for a direct hole oxidation mechanism. Environ. Sci. Technol. 39, 9695-9701.

Yuan, C., Lien, H., 2006. Removal of arsenate from aqueous solution using nanoscale iron particles. Water Qual. Res. J. Can. 41, 210-215.

Zhang, M., Wang, Y., Zhao, D., Pan, G., 2010. Immobilization of arsenic in soils by stabilized nanoscale zero-valent iron, iron sulfide (FeS), and magnetite (Fe_3O_4) particles. Chinese science bulletin. 55, 365-372.

Zhang, G., Qu, J., Liu, H., Liu,R., Wu, R., 2007a. Preparation and evaluation of a novel Fe-Mn binary oxide adsorbent for effective arsenite removal. Water res. 41, 1921-1928.

Zhang, G-S., Qu, J-H., Liu, H-J., Liu, R-P., Li, G-T., 2007b. Removal mechanism of As(III) by a novel Fe-Mn binary oxide adsorbent: Oxidation and sorption. Environ. Sci. Technol. 41 (2007) 4613-4619.

Zhang, G., Liu, H., Liu, R., Qu, J., 2009. Adsorption behavior and mechanism of arsenate at Fe–Mn binary oxide/water interface. J. Hazard. Mater. 168, 820-825.

Zhang, Y., Yang, M., Dou, X-M., He, H., Wang, D-S., 2005. Arsenate adsorption on an Fe-Ce bimetal oxide adsorbent: Role of surface properties. Envirion. Sci. Technol. 39 (18), 7246-7253.

Zhang, Y., Han, J.H., 2006. Plasticization of pea starch films with monosaccharides and polyols. J. Food Sci. 71, E253-E261.

Zhao, D. Polymeric ligand exchange: A new approach for enhanced separation of environmental contaminants. Department of Civil and Environmental Engineering, Lehigh University, Bethlehem, PA, Ph.D Thesis. 1997.

Zhao, D., SenGupta, A.K., 1998. Ultimate removal of phosphate from wastewater using a new class of polymeric ion exchanger, Water Res. 32, 1613–1625.

Zhao, D., SenGupta, A.K., 2000. Ligand separation with a Cu(II)-loaded polymeric ligand exchanger. Ind. Eng. Chem. Res. 39, 455-462.

Appendix Additional Experiment

Intorduction

In both groundwater and surface water sources, arsenic (As) contamination is rapidly becoming a global environmental issue because the presence of arsenic in drinking water can cause serious health problems for human beings, for example, bladder, lung and skin cancer as well as kidney and liver cancer (NRC, 2001). Therefore, the United States and US EPA adopted a new maximum contaminant level for As in drinking water of 10 μg/L in 2001 that went into effect in January 2006. This lowering of the maximum allowable level has been impetus for the development of many improved As-removal technologies designed to satisfy the new Maximum Contaminant Level (MCL).

Several new techniques, including granular ferric sorptive media (Driehaus, 1998), metal-loaded ion exchange (IX) resin (An et al., 2005), and nano-scale magnetite (Yavuz et al., 2006), have been introduced to increase the removal efficiency of arsenic from the aquatic phase and it is now possible to reduce As concentration below the allowable limits over a range of conditions. Of these new technologies, Dambies (2004) reported that metal-loaded polymers exhibited selective removal of As(V) species in drinking water and improved upon many conventional techniques. A novel metal-loaded polymer resin using Cu^{2+} as the metal loaded to a chelating resin, DOW 3N, for As(V) removal was developed by An et al. (2005). This new class of ion exchangers, termed polymeric ligand exchanger (PLE), has been proven to be highly selective for As(V) due to both the Lewis acid-base interaction and electrostatic interaction between

the loaded Cu^{2+} and arsenate even in the presence of strong competing anions such as sulfate, which is more selectable onto conventional ion exchanger than arsenate, bicarbonate or chloride. Despite its obvious advantages for arsenate removal from drinking water, however, simply using PLE like other commercial ion exchanger results in a huge volume of spent brine solution with high concentrations of As and other co-contaminants after multiple regenerations. The brine solutions used for regeneration release high concentrations of As(V), sulfate, bicarbonate, and chloride from the saturated PLEs, and the reused brine solution becomes useless for regeneration after 8 times reuse (An et al., 2005). As yet, there has been no thorough investigation to determine the optimal conditions for treatment of the spent brine.

Fe^{3+} and Al^{3+} are well known coagulants for water treatment to remove colloidal particles and the use of ferric chloride ($FeCl_3$) and aluminum chloride ($AlCl_3$) are well documented techniques for the removal of As from solution via co-precipitation/adsorption. Both ferric chloride and aluminum chloride have been studied in depth for drinking water treatment (Pierce and Moore, 1982; Cheng et al., 1994; Hering et al., 1996; McNeill and Edwards, 1997; Ghurye et al., 2004), but there have been few studies with extremely high As concentrations and ionic strength in brine solutions. Co-anions such as sulfate, bicarbonate, and chloride that act as competing anions during As removal treatment by PLE may also be concentrated in spent regeneration brine. Therefore, it can be hypothesized that optimal conditions determined for drinking water treatment via Fe^{3+} and Al^{3+} may differ from those identified for brine treatment due to the high ionic strength of the brine solution. Another consideration is the amount of process residuals produced by the brine treatment and the leachability of As from these residuals toward soil or water after the Al or Fe oxide treatment.

The recent literature indicates that there is a need for further study of the interactions/reactions that occur with treatment residuals in their disposed environments such as landfills and lagoons. Toxicity Characteristic Leaching Procedure (TCLP) established by the US EPA is commonly used to test the leachability of solid waste residuals. However, TCLP extraction method is in question because it does not simulate true landfill conditions including alkaline pH and low redox potential. As a result, simply applying TCLP may underestimate the leachable concentration of As (Ghosh et al., 2004). In California, the Waste Extraction Test (WET) method has been adopted to estimate the level of hazard posed by waste. The primary difference between these two methods is that citrate and acetate are added as the leachant for extraction fluid of WET and TCLP, respectively. Citrate, which is a trident ligand forming chelates with free metal ions in solution, is more stable than acetate existing with mono-dentated ligands. Therefore, the application of WET method is a more aggressive way to evaluate leachability (Mohamed et al., 1991; Lackovic, et al., 1997). Both TCLP and WET leaching tests are currently set to have a maximum concentration of 5 mg/L for As in the extraction fluid, which is 500 times higher than the current MCL, 10μg/L. A subsequent tightening of the TCLP and WET limits in response to the new MCL will force facilities to consider treatment technology that results in a low treated brine volume and stable waste residual.

To enhance the immobility of As in solid residuals highly concentrated with As, the presence of calcium has been shown to further immobilize As at high pH (Parks et al., 2003; Bothe and Brown, 1999). Another condition that enhances the immobility of As is pH; at pH 5-7, the leachability of As for treatment adsorbents such as granular ferric hydroxide (GFH) and granular ferric oxide (GFO) is at its lowest (Jing et al., 2005a).

The waste streams associated with different As-removal techniques are often very expensive to handle, transport, and dispose of safely. Frey et al. (1998) reported that the handling and disposal of process wastes on average makes up 12 – 34% of the total process costs. The toxicity of the waste will also affect the disposal costs. Treatment residuals failing the TCLP or WET will be deemed hazardous waste, thus increasing the disposal cost considerably (Meng et al., 2001). $FeCl_3$ in the proper concentration can form As-laden precipitates that will pass the leaching tests but these additives can also be expensive. Many utilities add cheap stabilizers to the residuals such as lime or cement to decrease As leaching (Jing et al., 2003; Jing et al., 2005b), but this greatly increases the amount of sludge produced, thus again increasing disposal costs. Palfy et al. (1999) had to add 7 g of cement to every 1 g of As-laden sludge in order to meet leachability standards.

Disposal costs are determined on a 'per ton' basis so reducing the mass produced is desirable. It is evident that optimizing the conditions involves balancing the costs of chemical additives, As leachability in residuals and mass of sludge produced, and that this is imperative for the development of an efficient brine treatment process.

Our objectives were therefore to: (1) determine the optimal conditions for the treatment of spent regeneration brine using ferric chloride or aluminum chloride; and (2) develop a brine treatment process that will maximize the stability of the solid, As-laden waste product.

Experimental Methods

Chemicals

The following chemicals (ACS grade or higher) were purchased from Fisher Scientific (Pittsburgh, PA, USA): sodium sulfate (Na_2SO_4), sodium bicarbonate ($NaHCO_3$), sodium chloride (NaCl), $AlCl_3$, $FeCl_3$, $Ca(OH)_2$ HCl and NaOH. Reagent grade sodium hydrogen arsenate ($Na_2HAsO_4 \cdot 7H_2O$) was purchased from Sigma-Aldrich (Milwaukee, WI, USA). All solutions were prepared with ultrapure deionized (DI)(18.2 $M\Omega cm^{-1}$) water.

Simulation of spent regeneration brine

Spent regeneration brine (SRB) was simulated based on an analysis of the spent brine collected from column tests performed on a PLE resin (DOW 3N-Cu) used to conduct brine treatment experiments (An et al., 2005), where the brine had been reused to regenerate the resin multiple times until finally reaching its capacity. The spent brine solution was prepared using the following concentrations: As = 300 mg/L, SO_4^{2-} = 600 mg/L, HCO_3^- = 305 mg/L, and NaCl = 4% (w/w) (or 24 g/L as Cl^-). The average pH and ionic strength (I) of the simulated spent brine were 9.3 and 1.8 M, respectively.

Brine treatment

A series of batch experiments were carried out to determine the optimal conditions and process for brine treatment, including solution pH and the concentration of Al or Fe. First, different dosages of $FeCl_3$/$AlCl_3$ were added to SRB solution and the efficiency of arsenic removal was determined. Several 100 mL sample solutions of SRB were separated into 125 mL Nalgene HDPE bottles. $FeCl_3$/$AlCl_3$ was then added to the bottles at an Al/Fe:As molar ratio of 0 (i.e.

without $FeCl_3$/$AlCl_3$), 1, 2, 5, 10, 15, 20, 25, 30, and 40. After addition of $FeCl_3$/$AlCl_3$, the solution pH was measured and adjusted to a desired pH value ranging from 4 to 11 using 1 M sodium hydroxide (NaOH) or 1 M hydrochloric acid (HCl). The sample bottles were then placed on a gang mixer for ~2 hours at 200 rpm. During mixing, the solution pH was monitored and adjusted. Finally, the mixtures were stored at a temperature of 22 ℃ and allowed to settle for ~24 hours. Once the settling time was completed, samples were taken from the clear supernatant to measure the concentration of As and centrifuged. Finally, the arsenic content was analyzed using a Perkin-Elmer Graphite Furnace AA after filtration with 0.45µm syringe filter. All experiment was duplicates.

Effect on addition of Ca for leachability of residuals

To estimate the leachability of As from waste residuals, 500 mL batch tests were carried out. Compared to brine treatment, larger batch tests were needed to produce ample precipitates for multiple leaching tests. Al and Fe were added, as $FeCl_3$ and $AlCl_3$, to SRB in the Al/Fe:As molar ratio of 5, 10, 15, and 20. The supernatant was decanted and the ample precipitates were completely dried. Each leaching test was performed to determine how much As can be released back from precipitates dried under each condition. Calcium hydroxide was added simultaneously with $FeCl_3$ to the treatment process using a fixed molar ratio for Fe/As of 15 in the amounts of 0, 30, 90, 150, and 210 mM Ca. Note that the optimal conditions of the treatment (As removal) process do not necessarily correspond to the conditions minimizing As leaching from the ferric hydroxide precipitate. Using a Fe:As molar ratio of 10, 500 mL batch experiments were performed where the pH of the treatment process was 3.6, 6.3, 9.4, and 12.1. The effect of pH on leachable As was determined by the WET test.

Leaching tests

Both TCLP and WET methods were used to estimate As leachability and thus evaluate the relative stability of the As-laden solid residual. TCLP was performed following EPA method 1311. In brief, TCLP fluid #1 was prepared by adding 5.7 mL glacial CH_3COOH and 64.3 mL of 1 N NaOH to 500 mL DI water and diluting to 1 L with DI water. After mixing completely, the final pH of the solution is required to be 4.93±0.05 (EPA, 1992). Prepared TCLP fluid #1 and 1 g of solid sample dried at air were placed into scintillation vials. The vials were placed on an end-over-end mixer and mixed for 18±2 hours until they reached the extraction equilibrium. The TCLP-ext (extended) followed the same procedure as the TCLP, but the extraction mixing period was extended to 30 hours.

WET was performed following the procedure prescribed by the California Department of Health Services (SOP No. 910). In brief, a citrate buffer extraction solution was prepared and purged with nitrogen gas for at least 30 minutes. The 0.2 M citrate solution was prepared by dissolving 42.0 g monohydrate citric acid in 950 mL of DI water. The solution was titrated to pH 5 with 50% NaOH and diluted to 1 L with DI water (California Code of Regulations, 1985). Prepared WET solution was also purged with nitrogen gas for 30 minutes to simulate an anoxic environment. Dry As-laden sludge samples pulverized were placed by weight in 25 mL scintillation vials (The sample to extraction solutions ratio was 1:10 (1 g sample to 10 mL solution). The ratio of dry As-laden sludge sample to extraction solution was 1:10 (1 g sample to 10 mL solution). All samples were prepared under the identical procedure with duplicates and an extraction period was allowed for 48 hours. Some headspace was left in the scintillation vials. The WET is reported to be a more stringent test with ferric hydroxide residuals than TCLP because the citric acid solution is a stronger complexing agent than the TCLP acetic acid solution

and because WET extraction is carried out in an anoxic environment as well as because 48 hours are needed to extract the target contaminant from the treated sludge.

Leaching tests with landfill leachate were performed using both WET and TCLP procedures as guidelines. A landfill leachate was obtained from a confidential source. The leachate was purged with nitrogen gas for 30 minutes to deoxygenate. Dry As-laden treatment residuals were placed in 40 mL glass vials. The leachate to solid ratio was 20:1 (g/g) or the same as the TCLP. The headspace in the vials was purged with nitrogen gas. The vials were placed on a shaker table for the 18 hour extraction period.

The EPA method 3050B was used to determine the total Fe and As content of the treatment residuals. The method consists of acid digestion with repeated additions of nitric acid (HNO_3) and hydrogen peroxide (H_2O_2).

Chemical Analysis

Digestates were diluted and analyzed using a Perkin Elmer Atomic Adsorption Spectrophotometer, which has a detection limit of 3 µg/L as As. Dissolved iron was measured using a Flame Atomic Absorption Spectrometer (Varian Spectra 220 FS). pH was measured using an Orion p H meter (model 520A).

Results and Discussion

Arsenic removal from spent brine

Two series of batch experiments exploring the effects of the concentration of both ferric and aluminum carried out on removal of arsenic from simulated brine treatment solution are shown in Fig. A-1. Over 99% of As can be removed from the brine for both aluminum and ferric at molar ratios of 5 or over, whereas at a molar ratio of 1 for Al/Fe:As the efficiency obtained dropped to 69% and 80%, respectively, indicating an increase in removal of As with increasing Fe or Al at pH 6. Cheng et al. (1994) reported the same trend in jar tests where $FeCl_3$ as coagulant was added to raw water containing an 17-20 µg/L as the initial concentration, which is four orders of magnitude lower than the concentration used here of ~300,000 µg/L. This result can be attributed to the increased availability of Al or Fe for co-precipitation and increased number of surface sites on aluminum or ferric precipitates facilitating the adsorption of As(V). In addition, it was observed that using $FeCl_3$ as a coagulant is slightly more effective than using alum for removal of As, which was confirmed at a molar ratio of 1, showing 69% and 80% removal efficiency using $AlCl_3$ and $FeCl_3$, respectively. However, at higher molar ratios there was no observable difference. An optimal range in $AlCl_3$ and $FeCl_3$ addition (Al/Fe:As 5-20) can thus be determined from Fig. A-1. At Fe/As > 20 no increased benefit is observed, but the increased cost of $FeCl_3$ addition becomes inefficient.

Fig. A-2 compares the pH effect on arsenate removal in the range 4-11. Both $AlCl_3$ and $FeCl_3$ obtain greater than 95% As removal within the pH range of 5-7.0 at an Al/Fe:As molar ratio of 5, whereas above pH 7, the removal efficiency dramatically decreases with increased pH. At pH 4, 20 and 100 % were obtained for $AlCl_3$ and $FeCl_3$ at an Al/Fe:As molar ratio of 5, respectively. In contrast, using a Fe:As ratio of 20, >95% As removal was achieved across the entire pH range.

These results suggest that there is an optimal pH range (5-7) for As removal from the spent brine, but an increase in $AlCl_3$ and $FeCl_3$ addition will allow for effective As removal outside of this optimal range.

As pH increased, removal for all anions was observed to decrease (data not shown). The decrease in removal efficiency at higher pH indicates that removal is a function of both the available sorbent and pH. The pristine point of zero charge for fresh ferric hydroxide is 7.9-8.2 (Dzombak and Morel, 1990). We can therefore expect the isoelectric point in these batch tests to be lower due to aging of the ferric hydroxide and the extremely high ionic strength (~2 M) (Dzombak and Morel, 1990). Solution pH will also affect the removal efficiency by changing the electrostatic state of competing anions such as sulfate and bicarbonate.

The observed optimal pH range in these experiments agrees with those determined by Hering et al. (1996) for As(V) removal from drinking using $FeCl_3$ addition. Hering et al. (1996) observed 100% As(V) removal between pH 4-7.5, after which the removal efficiency decreased sharply. This sharp decrease, also observed in Fig. A-2, can be attributed to a surface charge reversal on the ferric hydroxide precipitate. As pH increases above the isoelectric point, the surface becomes more negative (Dzombak and Morel, 1990) and electrostatic repulsion of As anions begins to occur. Although the initial conditions differ (As(V)=20 µg/L and 4.9 mg/L of $FeCl_3$), the concurring observations between Hering (1996) and this study indicate that the mechanisms that control removal at low As concentrations and low ionic strength also prevail in more extreme conditions. Anderson et al (1976) reported the adsorption of arsenate on amorphous aluminum hydroxide as a function of pH in different initial Arsenate concentrations. This is consistent with our result for the pH effect. Especially at low pH, the adsorption of arsenate into aluminum hydroxide is much better than under alkaline conditions.

Stabilizing process waste residuals

As environmental regulations become increasingly stringent, the cost for handling and disposal of water treatment process waste residuals is becoming an increasingly important issue. For a technology to be viable, the volume of the final process waste that leaves the plant must be small and the As leachability must be minimal. Determining the proper amount of adsorbent/co-precipitant necessary for removal may be quite different from the amount required to ensure a stable and disposable end product.

Fig. A-3 indicates that as the amount of Fe or Al added to the treatment process increases, the As leached from the waste residual decreases in both the TCLP and WET. The extracted concentration of As decreased with increasing Al or Fe molar ratio using both extraction methods. However, when applied by TCLP, this easily passed the current regulation limit of 5 mg/L for both hydroxides through all molar ratios. In comparison, although increasing the Al or Fe:As molar ratio from 5 to 15 resulted in a 85% and 96% decrease, respectively, WET was unable to satisfy this limit. Only an Fe:As molar ratio of 20 extracted sufficient As to reach a level of 4.85 mg/L As, which passes the WET limit of 5 mg/L for As. The increased stability of arsenic on $Al(OH)_3$ or $Fe(OH)_3$ by increased molar ratio is due to the enforced interfacial structure of inner-sphere surface complex between arsenic ion and iron ion (Phenrat et al., 2008). A similar trend was observed for the TCLP test, where residuals formed even at relatively lower Fe additions (Fe/As of 5) easily passed the TCLP limit. It is evident that the WET is a much more stringent extraction procedure (Mohamed et al., 1991) and therefore this was used for the remainder of this study as a means to compare the different parameters in sludge stabilization.

Effect of pH on Stabilization

In order to determine the stabilization from waste residual at different pH, a test at different pH was carried out with 10 molar ratio of $AlCl_3$ and a wet aging time of 20 days. Fig. A-4 shows the extracted concentration of As from waste residue with WET method as a function of pH. According to Fig. A-4, the extracted As concentration from condensed waste increased with increasing solution pH. It was observed that at pH values ranging from 7 to 10 the concentration of As was at least two times higher than that under acidic conditions. This result can be explained in terms of a discussion on the desorption of arsenic from water treatment by metal oxide adsorbent by Ghosh et al (2004) over a pH range of 7-10. When pH increases, protons from the adsorbent surface move to decreasing proton solution, which results in a more negative charge on the surface. As a result, arsenic desorption can start. Also, the arsenic species under alkaline conditions, which exist as $H_2AsO_4^-$ or $HAsO_4^{2-}$, are increasingly repelled and desorbed as the surface negativity increases. The release of arsenic reached a minimum in the pH range between 5 and 7 and increased dramatically when pH increased from 7 to 11 (Jing et al., 2005a). Christensen et al (2001) reported that the increase in arsenate desorption at high pH is of particular significance in mature landfills, where the pH ranges from 7.5 to 9.0.

Calcium addition

Calcium is often used in water treatment in the form of lime (CaO) and hydrated lime ($Ca(OH)_2$). Dutré and Vandecasteele (1995) observed that arsenates chemically bond with hydrated lime to form precipitates:

$$2H_3AsO_4 + 3Ca(OH)_{2(aq)} \rightarrow Ca_3(AsO_4)_{2(s)} + 6H_2O \quad \text{(A-1)}$$

The co-precipitation of Fe(III), As(V), and Ca(II) significantly lowers the dissolved arsenate concentration in neutral-to-alkaline pH range conditions (Emett and Kheo, 1994). Calcium as $Ca(OH)_2$ was added at 0, 30, 90, 150, and 210 mM Ca (Ca/Fe molar ratios of 0, 0.5, 1.5, 2.5, and 3.5) to the treatment process, where an Fe/As molar ratio of 15 was used. Fig. A-5 shows that the addition of calcium, in a particular range, will further stabilize the ferric residual according to the California WET. The addition of Ca at a Ca:Fe molar ratio of 1.5 (6.67 g/L $Ca(OH)_2$) decreased the leachable arsenic by 80%. Furthermore, using a Ca:Fe of 1.5 reduced the leachability so that the solid residual passes the WET test limit of 5 mg/L As. This reduced extraction concentration of As can be attributed to the effect of calcium, which has been reported to decrease the mobility of As(V) from ferric media (Bothe and Brown, 1999; Parks et al., 2003; Jing et al., 2003; Jing et al., 2005b). A similar trend was observed when the TCLP was applied to the Ca amended solid residuals in Fig. A-6, indicating a decrease in the amount of As leached when 30 and 90 mM Ca (Ca/Fe 0.5 and 1.5) was added. The improved effect on arsenic stability was obtained using iron hydroxide with cement (EPA, 1992). This may be because some arsenic was incorporated in the cementitious reaction products such as calcium silicate hydrate that have not been completely dissolved in the acid digestion process. Parks (2001) found that the addition of lime to sludge produced from coagulation treatment of water with ferric chloride and aluminum sulfate could reduce the release of arsenic into the water. Due to new formation between calcium and arsenate with different molar ratios of $Ca(OH)_2$ to arsenic, Bothe (1999) detected $Ca_4(OH)_2(AsO_4)_2 \cdot 4H_2O$, $Ca_5(AsO_4)_3OH$, and $Ca_3(AsO_4)_2 \cdot 3^2/_3H_2O$ minerals by scanning electron microscope (SEM) and X-ray diffraction (XRD).

As Ca addition increased (150-210 mM), more leachable As was observed. Applying mass balance it was determined that Ca constituted 2% and 8% of the total weight of the solid formed at additions of 90 and 210 mM, respectively. This is different from the results of a former study by Jing et al (2003). The sludge samples prepared by $FeCl_3$ had similar leaching concentration of arsenic, although the C:S (cement: sludge ratios) varied from 2.5 to 20. However, it is possible that increasing the total amount of Ca in the solid formed would increase the solubility of the residual, thus releasing more As during extraction tests because of the crystallized $Ca(OH)_2$. Phenrat et al (2005) concluded that calcium ion saturation in pore fluid from both hydration and addition of powder of hydrated lime as an additive seems highly beneficial for arsenic immobilization by reacting with arsenic to form calcium–arsenic compounds, which are solubility limiting phases. In contrast, crystallized $Ca(OH)_2$ was found to be inefficient in binding arsenic by both sorption and lattice inclusion.

Studies have indicated that the WET and TCLP are not representative of the wide range of possible environments in a landfill (Ghosh et al., 2004). To further investigate the impact of Ca addition on leaching, extraction tests were performed with a landfill leachate. The leachate came from a municipal/industrial landfill in the northeast United States. The leachate contained an initial As concentration of 170 µg/L and a pH of 5.7. Fig. A-7 indicates a very different leaching profile than that assumed by either WET or TCLP. No As above background levels was leached when the residuals were prepared without Ca addition. However, 150 µg/L of As was leached during the test when Ca/Fe molar ratios of 1.5 and 3.5 were used.

Sludge Production

Disposal of the waste residuals produced can potentially be the most costly part of the whole water treatment process (Frey et al., 1998). Disposal costs are based on the mass of waste produced, therefore the total sludge (air-dry weight, kg) to be disposed in a year were calculated and the results are presented in Table A-1. These calculations were based upon a 0.1 MGD treatment flow to the polymeric ligand exchange resin, and raw water As concentrations of 94 μg/L. As expected, with increasing Fe addition the amount of sludge produced also increased. In contrast, it was observed that the addition of Ca (at constant Fe/As) decreased the mass of sludge produced. Addition of 90 mM Ca reduced the final mass of sludge produced by ~20%. These results are counterintuitive since the mass of total additions (Fe + Ca) increased. In order to investigate these results a total analysis was performed on all contaminants and additions made for a 100 mL batch treated with no Ca and one with 90 mM Ca (Ca/Fe 1.5) (data not shown). The Fe/As molar ratio was kept constant at 15. It was found that the residuals formed with the calcium addition contained less Cl^- and SO_4^{2-}, which contributed to the reduction in mass produced.

Conclusions

The treatment of spent regeneration brine by aluminum and ferric chloride was optimized for pH and Al or Fe additions similar to those used for drinking water treatment. The most efficient removal was achieved in the pH range 7-6.5 for both. As removal increased with Al/Fe addition and nearly 100% removal was observed using a Al/Fe:As molar ratio of 5 or greater at pH 6.

Both TCLP and WET indicated that increased Al or Fe addition greatly decreased leachable As. The resultant waste sludge passed the TCLP when brine was treated at a Al/Fe:As molar ratio of

5, and passed the WET when treated at a Fe:As of 20 both at a treatment pH of 6. The WET was also passed at a Fe/As of 15 when 6.67 g/L $Ca(OH)_2$ was added simultaneously with the $FeCl_3$. The decrease in leached As with a certain range of Ca addition observed in the WET and TCLP was not observed when an actual landfill leachate was used.

It was found that using a $Ca(OH)_2$ addition of 90 mM as Ca not only decreased leachable As in the WET but also decreased overall process costs. Employing calcium hydroxide addition with ferric chloride to pass the WET decreased the mass of sludge produced by 20%.

References

An, B., Steinwinder, T., Zhao, D., 2005. Selective removal of arsenate from drinking water using a polymeric ligand exchanger. Water Res. 39, 4993-5004.

Anderson, M.A., Ferguson, J.F., Gavis, J., 1976. Arsenate adsorption on amorphous aluminum hydroxide. J. Colloid Interf. Sci. 54, 391-399.

Bothe, J.V., Brown, P.W., 1999. Arsenic immobilization by calcium arsenate formation. Environ. Sci. Technol. 33, 3806-3811.

California Code of Regulations. 1985. California Waste Extraction Test. Title 22, Division 30, 85, No. 2, 1800.78-1899.82.

Cheng, R., Liang, S., Wang, H., Beuhler, M., 1994. Enhanced coagulation for arsenic removal. J. AWWA 86 (9), 79.

Christensen, T., Kjeldsen, P., Bjeng, P., Jensen, D., Christensen, J., Braun, A., 2001. Biogeochemistry of landfill leachate plumes, Appl. Geochem. **16,** 659–718.

Dambies, L., 2004. Existing and prospective sorption technologies for the removal of arsenic in water. Separ. Sci. Technol. 39 (3), 603-627.

Driehaus, W., Jekel, M., Hildebrandt, U., 1998. Granular ferric hydroxide; a new adsorbent for the removal of arsenic from natural water. J. Water SRT-Aqua 47(1), 30-35.

Dutré, V., Vandecasteele, C., 1995. Solidification/stabilization of arsenic-containing waste: Leach tests and behavior of arsenic in leachate, Waste Manag. **15**, 55–62.

Dzombak, David A., Morel, Francois M. M., 1990. Surface Complexation Modeling: Hydrous Ferric Oxide. John Wiley & Sons, Inc. New York, NY.

Emett, M.T., Khoe, G.H., 1994. In: G. Warren, Editor, Environmental stability of arsenic bearing hydrous iron oxide, Warrendale, PA, TMS. 153–166.

EPA. 1992. Test methods for evaluating waste, physical/chemical Methods, 3rd Edition, SW-846 Method 1311, U.S. Government Printing Office, Washington, D.C.

Frey, M.M., Owen, D.M., Chowdhury, Z.K., Raucher, R.S., Edwards, M.A., 1998. Cost to utilities of a lower MCL for arsenic. J. AWWA 90 (3), 89-102.

Ghosh, A., Mukiibi, M., Ela, W., 2004. TCLP underestimates leaching of arsenic from solid residuals under landfill conditions. Environ. Sci. Technol. 38 (17), 4677- 4682.

Ghurye, G., Clifford, D., Tripp, A., 2004. Iron coagulation and direct microfiltration to remove arsenic from groundwater. J. AWWA. 96:4 143-152.

Hering, J.G., Chen, P., Wilkie, J.A., Elimelech, M., Liang, S., 1996. Arsenic removal by ferric chloride. J. AWWA 88 (4), 155-168.

Jing, C., Korfiatis, G., Meng, X., 2003. Immobilization mechanisms of arsenate in iron hydroxide sludge stabilized with cement. Environ. Sci. Technol. 37, 5050-5056.

Jing, C., Liu, S., Manish, P., Meng, X., 2005a. Arsenic leachability in water treatment adsorbents. Environ. Sci. Technol. 13, 5481-5487.

Jing,C., Liu,S., Meng,X., 2005b. Arsenic leachability and speciation in cement immobilized water treatment sludge. Chemosphere. 59, 1241-1247.

Lackovic, J., Nikolaidis, N., Chheda, P., Carley, R., Patton, E., 1997. Evaluation of batch leaching procedures for estimating metal mobility in glaciated soils. Ground Water Monit. Remediat. 17, 231-240.

McNeill, L.S., Edwards, M., 1997. Predicting As removal during metal hydroxide precipitation. J. AWWA 89 (1), 75-86.

Meng, X., Korfiatis, G., Jing, C., Christodoulatos, C., 2001. Redox transformations of arsenic in water treatment sludge during aging and TCLP extraction. Environ. Sci. Technol. 35, 3476-3481.

Mohamed, F., Cheng, I., Huang, R., Santos, E., 1991. Chemical fixation of sewage-sludge derived ash. J. Environ. Sci. Health Part A – Environ. Sci. Eng. Toxic Hazard Subst. Control 26, 353-371

NRC, 2001.Arsenic in drinking water: National research council, National Academy Press, Washington, DC.

Palfy, P., Vircikova, E., Molnar, L., 1999. Processing of arsenic waste by precipitation and solidification. Waste Management 19, 55-59.

Parks, J.L., 2001. M.S Thesis, Virginia Polytechnic Institute and State University, Blacksburg, VA.

Parks, J.L., Novak, J., Macphee, M., Itle, C., Edwards, M., 2003. Effect of Ca on As release from ferric and alum residuals. J. AWWA. 95:6, 108-118.

Pierce, M.L., Moore, C.B., 1982. Adsorption of arsenite and arsenate on amorphous iron hydroxide. Water Res. 16, 1247-1253.

Phenrat, T., Marhaba, T.F., Rachakornkij, M., 2008. Leaching behaviors of arsenic from arsenic-iron hydroxides sludge during TCLP. J. Environ. Eng. ASCE, 671-682.

Phenrat, T., Marhaba, T.F., Rachakornkij, M., 2005. A SEM and X-ray study for investigation of solidified/stabilized arsenic-iron hydroxide sludge. J. Hazard Matt. 185-195.

Robins, R.G., 1988. Arsenic Hydrometallurgy. Arsenic Metallurgy Fundamentals and Applications. R.G. Reddy, J.L. Hendrix, P.B. Queneau (Editors). TMS, Arizona, 215-247.

Yavuz, C.T., Mayo, J.T., Yu, W.W., Prakash, A., Falkner, J.C., Yean, S., Cong, L., Shipley, H.J., Kan., A., Tomson, M., Natelson, D., Colvin, V.L., 2006. Low-field magnetic separation of monodisperse Fe_3O_4 nanocrystals. Science, 314, 964-967.

Table A-1. Sludge mass produced under different $FeCl_3$ and $Ca(OH)_2$ additions

$FeCl_3$ (g/L)	Fe/As	$Ca(OH)_2$ (g/L)	Sludge Produced (g/L)	Sludge Disposed (kg/yr)
3.25	5	0	6.6	234.4
9.73	15	0	15.2	539.8
9.73	15	6.67	12	427.6
12.96	20	0	18.6	660.5

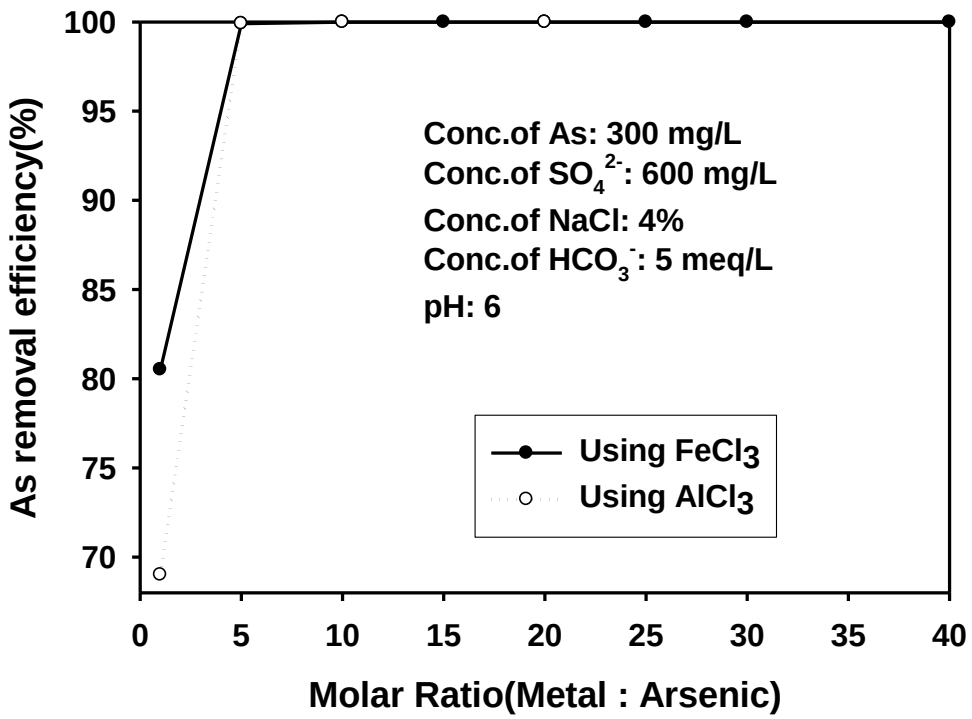

Fig. A-1. Arsenic removal efficiency from simulated brine solution consisting 300 mg/L as As using $AlCl_3$ and $FeCl_3$ at different molar ratios.

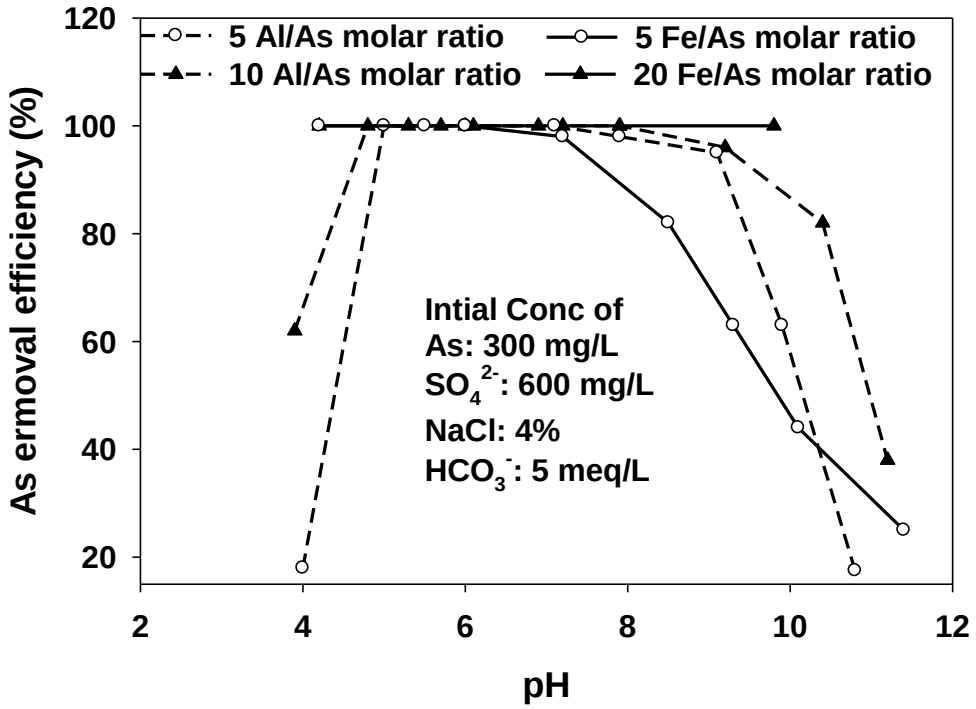

Fig. A-2. Arsenic removal efficiency as a function of pH using $AlCl_3$ and $FeCl_3$.

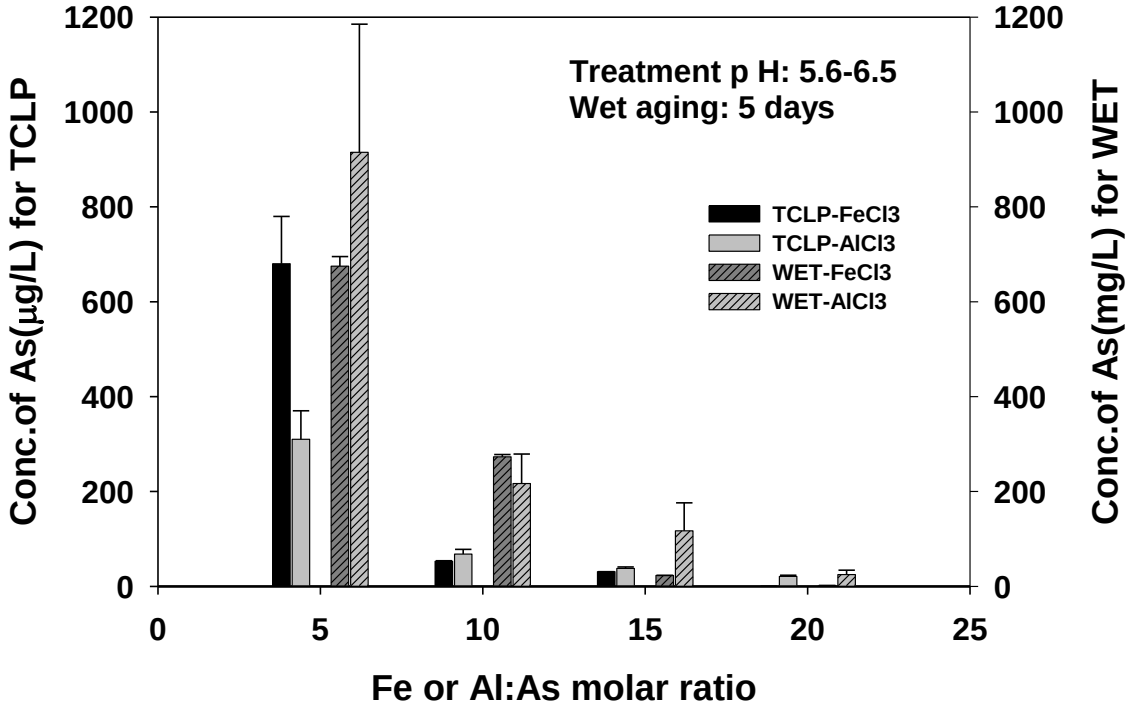

Fig. A-3. TCLP (left side) and WET (right side) extraction tests from simulated brine solution.

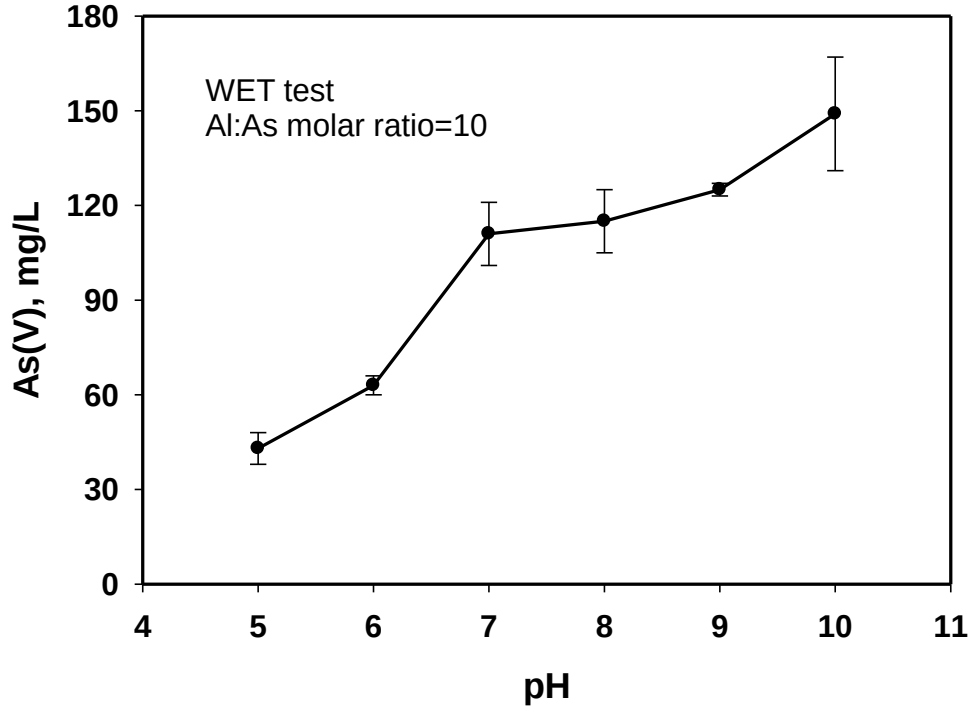

Fig. A-4. Extractable As concentration based on WET method as a function of brine treatment pH.

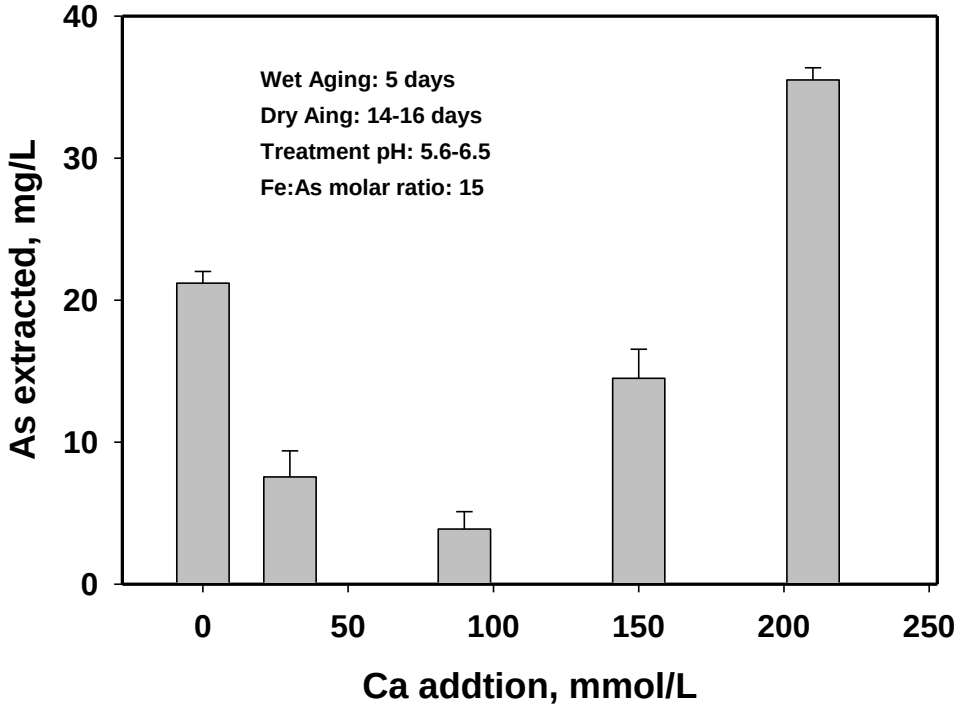

Fig. A-5. Extractable As concentration based on WET method using different concentrations at Fe:As molar ratio of 15

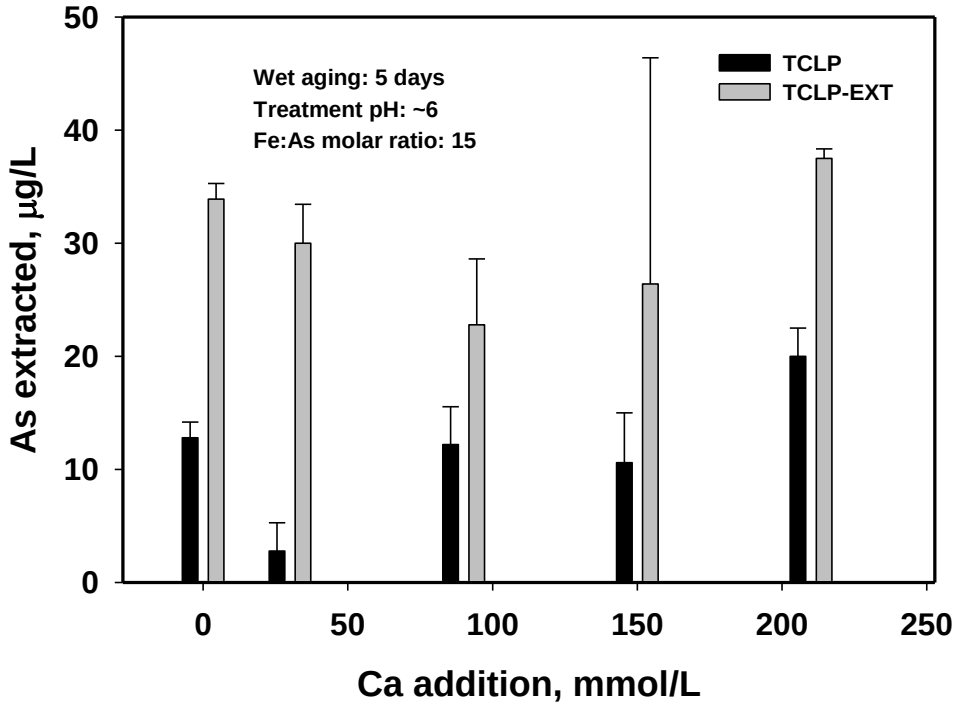

Fig. A-6. Extractable As concentration based on TCLP method using different concentrations at Fe:As molar ratio of 15.

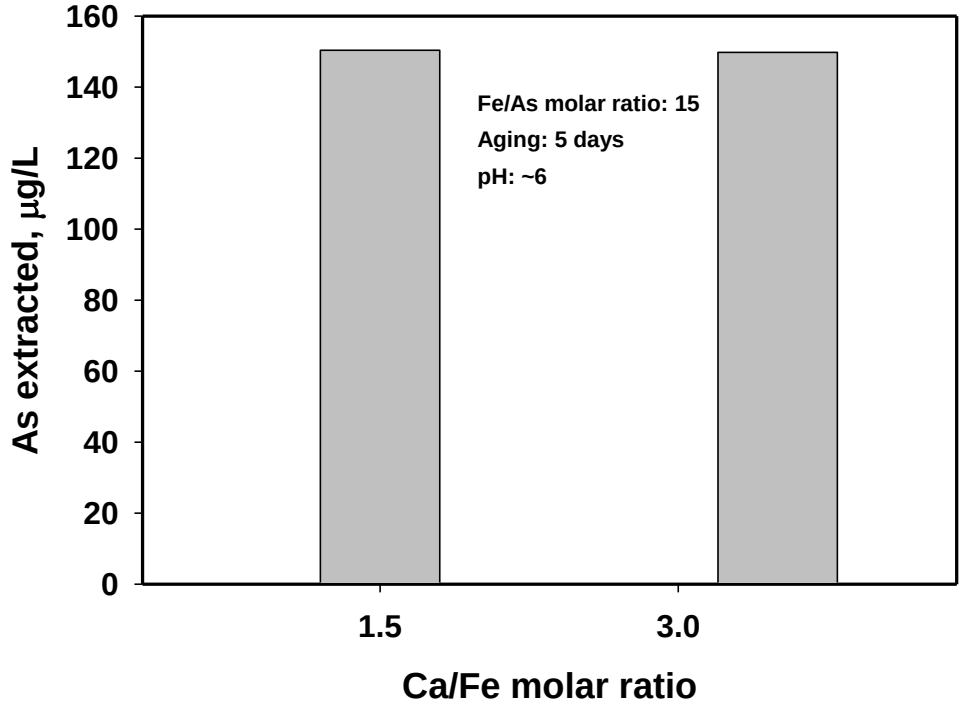

Fig. A-7. Calcium Effect on Extractable As Using a Landfill Leachate.